Doctoral Dissertation

Fluxless soldering under a formic acid atmosphere using Sn-3.0Ag-0.5Cu solder

Siliang He

January 2020

Graduate School of Engineering
Osaka University

Supervisor

Professor Hiroshi Nishikawa, Ph. D.
Joining and Welding Research Institute
Osaka University

Doctoral Committee

Professor Hiroshi Nishikawa, Ph. D.
Joining and Welding Research Institute
Osaka University

Professor Soshu Kirihara, Ph. D.
Joining and Welding Research Institute
Osaka University

Associate Professor Hiraoki Muta, Ph. D.
Division of Sustainable Energy and Environmental Engineering, Graduate School of Engineering
Osaka University

Contents

List of figures v

List of tables xi

Chapter 1 1

Research background 1

1.1 Electronic packaging 1

1.2 Lead-Free Soldering Processes Using for Electronic Packaging 8

1.3 Fluxless Soldering Processes 12

1.3.1 Role of Flux in Wetting during Soldering Process 12

1.3.2 Problems in Soldering Process Using Flux 15

1.3.3 Fluxless Soldering Technology Dealing with Oxides 18

1.4 Research Motivation 22

1.5 Purpose and Scope of This Study 23

Reference 24

Chapter 2 38

In-situ observation of fluxless soldering of Sn-3.0Ag-0.5Cu/Cu under a formic acid atmosphere 38

2.1 Introduction 38

2.2 Experimental 39

2.2.1 Wettability test 39

2.2.2 Soldering process 42

2.3 Results and discussion 42

2.3.1 Wettability test 42

2.3.2 Interfacial reaction 46

2.4 Conclusion 49

Reference 51

Chapter 3 55

Effect of Thermal Aging on the Impact Strength of Sn-3.0Ag-0.5Cu Solder Bumps Soldered on Cu under a Formic Acid Atmosphere....55

3.1 Introduction 55

3.2 Experimental 56

3.2.1 Soldering and Thermal Aging Methods 56

3.2.2 Impact Test 57

3.3 Results and Discussion.....58

3.3.1 Microstructure after Thermal Aging.....58

3.3.2 Impact strength and fracture surface before and after thermal aging 61

3.4 Conclusion.....68

Reference.....69

Chapter 4 70

Thermal Effect on Sn Steaming Phenomenon Under Formic Acid Atmosphere.....70

4.1 Introduction 70

4.2 Experimental 71

4.3 Results and discussion.....73

4.3.1 Effect of peak temperature on Sn steaming phenomenon under FA atmosphere.....73

4.3.2 Effect of heating time on Sn steaming phenomenon under FA atmosphere81

4.4 Conclusion.....82

Reference.....83

Chapter 5 84

Wettability, Interfacial Reaction and Impact Strength of Sn-3.0Ag-0.5Cu Solder/ENIG Substrate by Fluxless Soldering under Formic Acid Atmosphere.....84

5.1 Introduction 84

5.2 Experimental 85

5.2.1 Wettability test.....85

5.2.2 Sn steaming phenomenon.....87

5.2.3 Interfacial reactions and impact test 87

5.3 Results and discussion.....90

5.3.1 Wettability test.....90

5.3.2 Interfacial reaction.....95

5.3.3 Impact strength 98

5.4 Conclusion.....101

Reference.....102

Chapter 6 106

Conclusion 106

6.1 Summary 106

6.2 Environmental assessment on fluxless soldering under a FA atmosphere.....109

6.3 Future work 110

6.3.1 Effect of FA on joint long-term reliability 110

6.3.2 improvement of a suitable fluxless soldering process without Sn steaming for realistic application.....111

6.3.3 Improvement of wetting rate of solder on Cu substrate under FA atmosphere 111

Reference.....113

Research achievement 117

I List of publication.....117

i Peer-reviewed journal articles 117
ii Conference Proceedings 119
iii Domestic conference proceedings 120
II List of conference 120
Acknowledge..... 121

List of figures

Fig. 1.1 Various integration techniques: (a) Dual in-line package[3], (b) Leadless ceramic chip carrier[4], (c) Quad flat package[5], (d) Pin grid array[6], (e) Ball grid array[7], (f) Chip size package[8]. 3

Fig. 1.2 Integrated microsystem in 2D and in 3D.[1] 3

Fig. 1.3 Historical progression of integration technologies from 2D to 3D[1]. 4

Fig. 1.4 Interconnect lengths in different technologies[1]. 5

Fig. 1.5 Intrinsic gate and interconnect delays as a function of minimum feature size[13]. 6

Fig. 1.6 Schematic illustration of different options for IC-stacking[1]. 7

Fig. 1.7 Illustration of different 3D-packaging technologies: (a) wire-bonded die-stack, (b) BGA-stack, (c) folded–stack using chip-on-flex, and (d) ultra-thin package stack.[23] 8

Fig. 1.8 Historical trend in proportion of lead-free solder reported by IPC[43]. 10

Fig. 1.9 Illustrations of representative (a) single die flip chip package and (b) 3D chip stack lidless modules with select conceptual heat flow paths shown[53]. 11

Fig. 1.10 Schematic image of a solder/substrate interface[73]. 13

Fig. 1.11 Liquid sessile drop on a solid substrate. 13

Fig. 1.12 Different wetting of liquid solder drop on a solid base metal substrate. 14

Fig. 1.13 Molten flux converts oxides into salts to expose fresh solder and fresh base metal [73]. 15

Fig. 1.14 SEM image of solder with flux residue after soldering and after cleaning. . 16

Fig. 1.15 Daily global mean total ozone present in Dobson units (satellite data)[99]. 17

Fig. 1.16 Dermatitis from the soldering flux: (a) Acute dermatitis over the ulnar border of the forearm due to the irritant effect of flux, resulting from contamination of workbench[100]; (b) Dermatitis on the forearm due to the irritant effect of flux dust, resulting from clean-up of a flux-spraying unit[102]. 18

Fig. 1.17 Schematic image of removement of oxides on solder surface by plasma....19

Fig. 1.18 Schematic illustration of VUV irradiation system[120].....20

Fig. 1.19 Schematic diagram of hydrogen radial treatment[121].....20

Fig. 1.20 review of different reducing process gases with their advantages and disadvantages[79]. 21

Fig. 2.1 Schematic diagram of (a) Cu substrate using for wettability test and (b) FR-4 substrate with Cu pads for soldering process.....40

Fig. 2.2 Schematic diagram of heating equipment for wettability test.....40

Fig. 2.3 Heating process for soldering using liquid RMA flux. 41

Fig. 2.4 Schematic graph of (a) typical three-dimensional scan result of solder surface forming an angle with substrate surface and (b) sectional view of the section in (a) using three-dimensional laser scanning confocal microscope.....42

Fig. 2.5 Schematic of a sessile-drop contact angle system.....43

Fig. 2.6 (a) In situ observation and (b) the statistical data of spreading area of FA and RMA solders wetting Cu substrates.....47

Fig. 2.7 Effect of peak heating temperature on spreading area of FA and RMA solders on Cu substrate.....47

Fig. 2.8 OM image of residues on Cu substrate at 250 °C heating temperature using FA and RMA solders: (a) 2 min using FA solder; (b) 5 min using FA solder; (c) 10 min using FA solder; (d) 2 min using RMA solder. 48

Fig. 2.9 Cross-sectional microstructure of as-reflowed solder bumps on Cu substrate: (a) FA solder and (b) RMA solder.....49

Fig. 2.10 Cross-sectional SEM image of FA solder bumps.....49

Fig. 2.11 Effect of (a) peak heating time and (b) peak heating temperature on pore formation.....50

Fig. 3.1 Schematic experimental setup of soldering with Cu pads.....56

Fig. 3.2 Heating profile of both soldering under a formic acid atmosphere and using liquid flux. 57

Fig. 3.3 Schematic diagram of (a) high-speed impact test and (b) typical load-displacement curve of impact test. 57

Fig. 3.4 Cross sections of solder bumps on Cu pad using formic acid atmosphere and liquid flux: a), b) as-reflowed solder bumps; c), d) 168 h aged solder bumps; e). f) 1008 h aged solder bumps. 59

Fig. 3.5 EPMA mapping analysis results of the interface between solder and substrate under a formic acid atmosphere and using liquid flux. 60

Fig. 3.6 Pores formation near the interface under a formic acid atmosphere, after soldering and after thermal aging. 60

Fig. 3.7 Effect of aging time at 150 °C on the intermetallic compound thickness at the solder/Cu pad interface. 61

Fig. 3.8 Effect of aging time on the impact strength of solder bumps. 63

Fig. 3.9 EPMA mapping analysis results of fracture surfaces of as-soldered bumps using formic acid atmosphere and the liquid flux in an impact test. 63

Fig. 3.10 Effect of pores on fracture position. 63

Fig. 3.11 The load-displacement curves of as-soldered bumps using formic acid atmosphere and liquid flux in a high speed impact test. 64

Fig. 3.12 EPMA mapping analysis results of fracture surfaces of thermally aged bumps using FA atmosphere and the liquid flux in an impact test. 65

Fig. 3.13 The top view of the impact fracture surfaces for the 1008 h aged solder bumps. (a, b) solder bump under a formic acid atmosphere; (c, d) solder bump using the RMA liquid flux. 66

Fig. 3.14 The load-displacement curves of bumps after 1008 h thermal aging using formic acid atmosphere and liquid flux in high-speed impact test. 67

Fig. 3.15 Schematic diagram of fracture mode of solder bumps under a FA atmosphere and using liquid flux. 68

Fig. 4.1 Sample for Sn steaming experiment: (a) sample image; (b) schematic diagram. 72

Fig. 4.2 Schematic view of heating equipment for the Sn steaming experiment. 72

Fig. 4.3 Heating process as reference using liquid RMA flux and pure N_2.....73

Fig. 4.4 Sn residues confirmed after a fluxless soldering process under a FA atmosphere: (a) OM image of solder ball; (b) SEM image of solder ball; (c) distribution of Cu element detected by EPMA; (d) distribution of Sn element detected by EPMA.....74

Fig. 4.5 EMPA mapping results of Sn element on Cu pads at various temperature heating for 600 s: (a) heating at 130 ℃ under a FA atmosphere; (c) heating at 170 ℃ under a FA atmosphere; (d) heating at 210 ℃ under a FA atmosphere; (e) heating at 250 ℃ under a FA atmosphere; (f) heating at 290 ℃ under a FA atmosphere; (g) heating at 250 ℃ using RMA flux; (h) heating at 250 ℃ under N_2 atmosphere. 75

Fig. 4.6 Diagram of Sn steaming hypothesis. 76

Fig. 4.7 EMPA analysis for C element on Cu pads: (a) SEM image of Cu pad using RMA flux; (b) EPMA mapping result of C element on Cu pad using RMA flux; (c) SEM image of Cu pad under N_2 atmosphere; (d) EPMA mapping result of C element on Cu pad under N_2 atmosphere; (e) SEM image of Cu pad under FA atmosphere; (f) EPMA mapping result of C element on Cu pad under a FA atmosphere.....77

Fig. 4.8 Morphologies of residues on Cu pads: (a) SEM image of Cu pad untreated; (b) SEM image of Cu pad under a FA atmosphere at 130 ℃; (c) SEM image of Cu pad under a FA atmosphere at 170 ℃; (d) SEM image of Cu pad under a FA atmosphere at 210 ℃; (e) SEM image of Cu pad under a FA atmosphere at 250 ℃; (f) SEM image of Cu pad under a FA atmosphere at 290 ℃; (g) SEM image of Cu pad using RMA flux; (h) SEM image of Cu pad under N_2 atmosphere. 78

Fig. 4.9 XRD pattern of Cu pad under a FA atmosphere after Sn steaming experiment. 79

Fig. 4.10 Effect of Sn steaming phenomenon on wettability.....80

Fig. 4.11 EMPA mapping results of Sn element on Cu pads under a FA atmosphere heating at 250 °C for various heating times: (a) 60 s; (b) 600 s; (c) 3600 s. 81

Fig. 4.12 Morphologies of residues on Cu pads at 250 °C for various heating times: (a) Cu pads untreated; (b) SEM image of Cu pad heating for 60 s; (c) SEM image of Cu pad heating for 600 s; (d) SEM image of Cu pad heating for 3600 s. 82

Fig. 5.1 Schematic diagram of (a) ENIG pads using for wettability test.....86

Fig. 5.2 Sample for Sn steaming experiment: (a) sample image; (b) schematic image. 88

Fig. 5.3 Schematic view of the Sn steaming experiment.....88

Fig. 5.4 Schematic diagram of Cu substrate with ENIG finish using for the soldering process.....89

Fig. 5.5 Soldering process of RMA solder. 89

Fig. 5.6 Schematic diagram of a high-speed impact test. 90

Fig. 5.7 Spreading area of solders on ENIG pad: (a) the average spreading areas of solders under formic acid atmosphere at 250 °C, 270 °C and 290 °C for 2 mins, and that of solder using RMA flux was at 250 °C; (b) the tendency of the spreading of solder under formic acid atmosphere and solder using RMA flux of reflow at 250 °C.....91

Fig. 5.8 Diagram of Sn steaming hypothesis: (a) SEM image of ENIG pad under a FA atmosphere heating at 250 °C for 30 min; (b) EPMA mapping results of Sn steaming experiment; (c) the process of Sn residues on the ENIG substrate via Sn formate steaming hypothesis; (d) SEM image of ENIG pad without Sn residues; (e) SEM image of IMC in the area of Sn residues. 93

Fig. 5.9 Effect of Sn steaming phenomenon on wettability.....94

Fig. 5.10 Tendency of the spreading of FA-exposed solder on ENIG substrate and Cu substrate reflowed at 250 °C. 95

Fig. 5.11 Cross-sectional SEM image of solder bumps on ENIG substrate for FA soldering and RMA soldering: (a), (b)as -reflowed solder bumps; (c), (d) thermally aged

solder bumps for 168 h; thermally aged solder bumps for 504 h; thermally aged solder bumps for 1008 h. 96

Fig. 5.12 Statistics of IMC thickness of solder bumps for FA soldering and RMA soldering.....97

Fig. 5.13 Effect of aging time on the impact strength of FA-exposed and RMA solder bumps.....98

Fig. 5.14 EPMA mapping analysis results of the fracture surface of as-reflowed and 168, 504, and 1008 h aged FA-exposed and RMA solders in an impact test.....99

Fig. 5.15 The impact strength of solder bumps after soldering by a fluxless soldering process heating at 250 °C for 2 min under a FA atmosphere and thermal aging at 150 °C for 168, 504, and 1008 h fabricated using Cu substrate and ENIG substrate.....102

List of tables

Table 2.1 Summary of heating processes using formic acid atmosphere.....41

Table 2.2 Summary of contact angle results.....44

Table 3.1 EPMA point analysis results of selected points in **Fig. 3.12**.....67

Table 4.1 Summary of heating processes under a FA atmosphere. 72

Table 5.1 Summary of FA-exposed solder heating processes for wettability test.....86

Table 6.1 Environmental assessment on the soldering process using flux and fluxless soldering under a FA atmosphere. 112

Chapter 1

Research background

1.1 Electronic packaging

In recent years, with the popularity of consumer electronics such as smartphones and smart wearable devices, humans have entered the digital age. In turn, the demand for electronic products has been increasing, and the electronics industry has been the largest industry in the world since 1996[1, 2]. It is the most dynamic, fascinating, and important area of manufacturing. IC design, wafer fabrication, wafer probe, and electronic packaging (including test) are the main processes for the manufacturing of electronic devices. Electronic packaging is a comprehensive technology that combines electronic components that make up an electronic circuit. In detail, electronic packaging refers to the process of manufacturing electronic components such as chips, ceramics, metal, and organic materials into circuit boards, and finally assembling them into electronic

products.

Four significant functions were provided by electronic packaging:

1. Signal distribution, providing I/O connection to other components in the system.
2. Power distribution, delivering electrical power to require area on the chip.
3. Heat dissipation (cooling), removing generated heat and maintain the operational temperature of the electronic component.
4. Protection, protecting components and interconnections, ensuring reliable performance over using life.

Since the invention of the first transistor by Bell Labs of the AT&T in 1947, it has entered the era of microelectronic packaging. In the 1950s, the three-lead transistor outline (TO) was utilized extensively and later developed into ceramic plastic packaging. The development of microelectronics, packaging technology evolved significantly. In the mid-1960s, the rapid development of integrated circuits from small-scale integration (SSI) to medium-sized integration (MSI) resulted in the emergence of the dual in-line package (DIP). DIP is a package type which pins are perpendicular to the body (see **Fig. 1.1(a)**). This structure provided better thermal and electrical conductivity, was promoted soon. Large-scale integration (LSI) appeared in the 1970s, the degree of integration had been greatly improved, and innovative packaging technology was required. In the 1980s, with the replacement from DIP to surface-mounted technology (SMT), a revolution in electronic packaging technology was coming. Various surface mounted component/device (SMC/SMD) adapted to SMT were developed, such as leadless ceramic chip carrier (LCCC) (see **Fig. 1.1(b)**), plastic leaded chip carrier (PLCC), quad flat package (QFP) (see **Fig. 1.1(c)**), and plastic quad flat package (PQFP). Among them, PQFP had been extensively used because of its high packing density, small pitch, and low cost. In the 1990s, as ICs continued to shrink in size and integration increased, LSI developed to very-large-scale integration (VLSI). VLSI has hundreds of thousands of pins, lead the microelectronic package developed from peripheral type to array type, such as pin grid array (PGA), as shown in **Fig. 1.1(d)**.

PGA was not so suitable to SMT, it is challenging to achieve industrial-scale production. Combining the advantages of QFP and PGA, ball grid array (BGA) packaging technology (see **Fig. 1.1(e)**) was developed. The electronic industry experienced an explosion by BGA design, and the packaging technology had accommodated the development of the chip. Since then, the BGA packaging has been considered as a standard for high-density and high I/O ICs. Lately, chip size package (CSP) was emerged to solve the excessive chip package area, as shown in **Fig. 1.1(f)**.

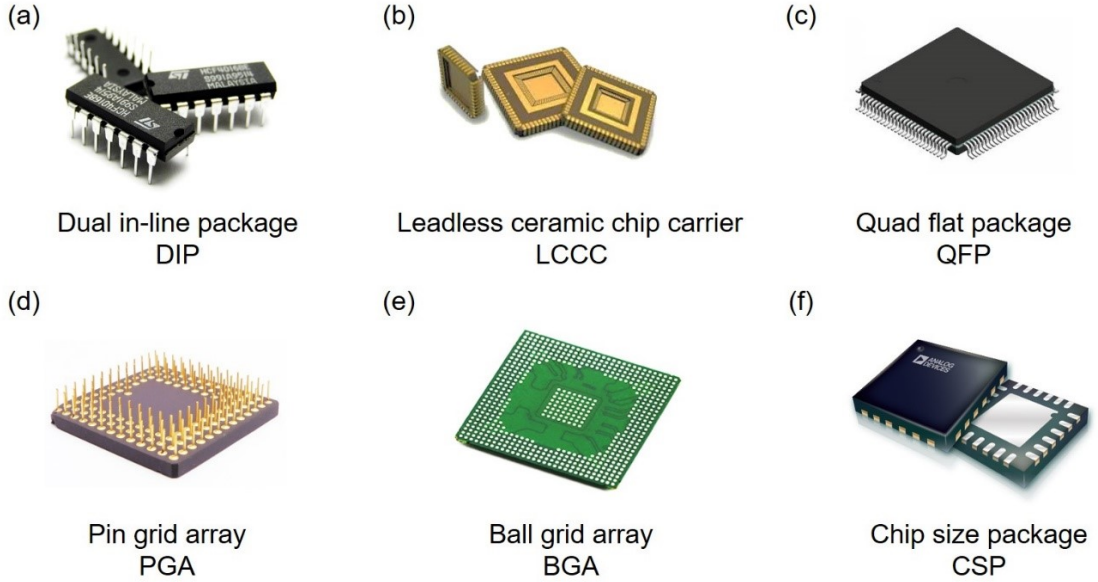

Fig. 1.1 *Various integration techniques: (a) Dual in-line package[3], (b) Leadless ceramic chip carrier[4], (c) Quad flat package[5], (d) Pin grid array[6], (e) Ball grid array[7], (f) Chip size package[8].*

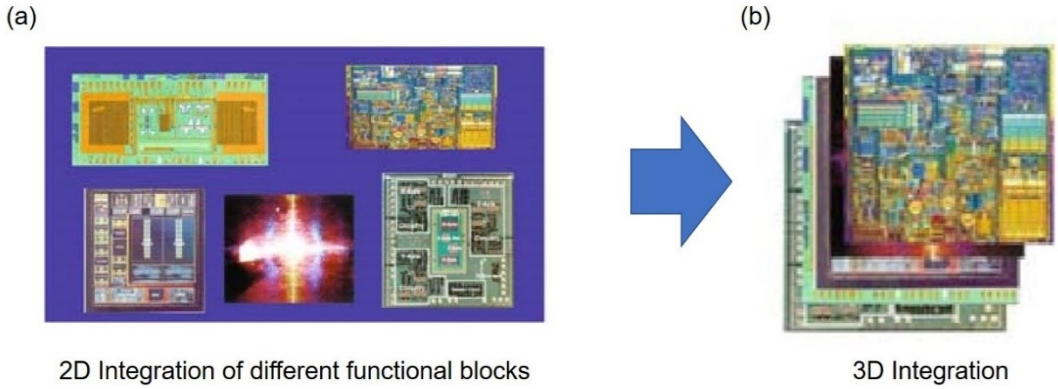

Fig. 1.2 *Integrated microsystem in 2D and in 3D.[1]*

It was found that electronic packaging has been moving toward high density, multi-pin, and miniaturization by reviewing the developed history of electronic packaging. Hence, the next generation of integrated micro-system technologies can only keep up with the functionality and performance demands by using third dimension. A schematic graph of two integrated microsystem instances with individual functional blocks integrated function modules, as shown in **Fig. 1.2**. Traditionally, these different functional blocks are integrated on a printed wiring board (PWB) or done in two-dimension (2D) package (see **Fig. 1.2 (a)**). In a 3D structure, these functional blocks can be stacked vertically, and each block can be a separate layer in the stack. Each layer is capable to connect together via vertical interlayer interconnects (see **Fig. 1.2(b)**). If integration is done in 3D, the spatial size of the microsystem can be greatly reduced. In other words, the dimensions of the X and Y directions in the 2D integration is reduced significantly, with the limited increase of dimension in the Z direction.

Fig. 1.3 shows the historical progression into 3D integration. One measurement of circuit density is Silicon Packaging Efficiency (SPE), which is the ratio of total silicon area to the total area of circuitry, as follow[9]:

$$Silicon\ Packaging\ Efficiency\ (SPE) = \frac{Area\ of\ Silicon}{Total\ Substrate\ (board\ )Area} \quad (1)$$

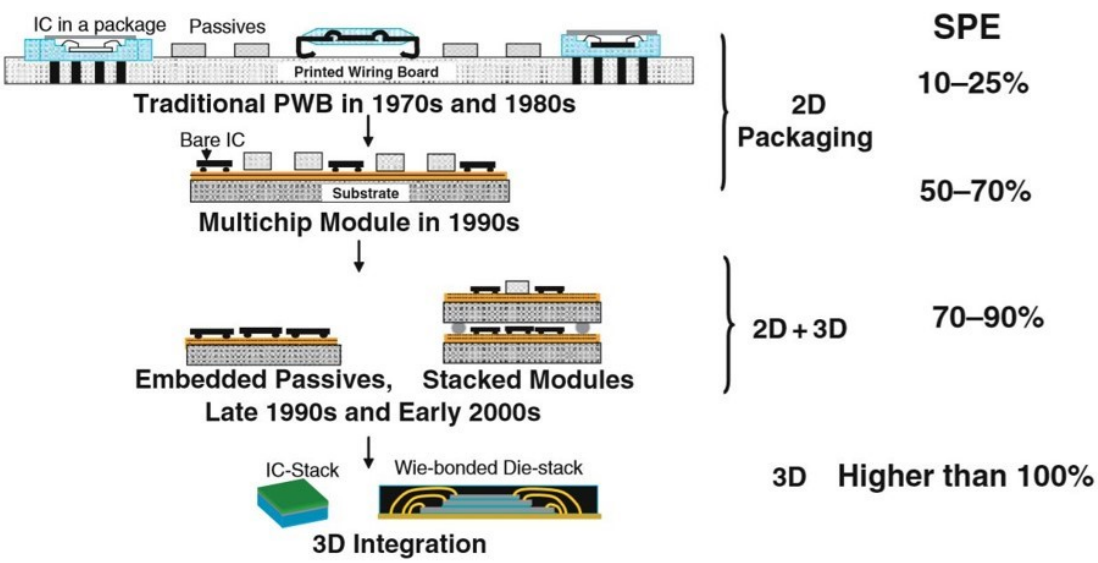

Fig. 1.3 *Historical progression of integration technologies from 2D to 3D[1].*

A typical SPE value for a traditional circuit board is between 10% and 25%. In the next generation of packaging technologies, such as multichip modules, the SPE reaches 50 – 70%. A higher SPE is obtained via 2D integration combining with 3D integration. As shown in **Fig. 1.3**, a fully 3D integration is capable provide a SPE over 100%. Therefore, 3D integration allows a higher density of integration, offers several practical advantages over 2D technologies, for example, form-factor, cost, and performance. System performance is much better in 3D integration than 2D integration because of much shorter vertical interconnections in 3D integration[10-12]. **Fig. 1.4** shows the schematic diagram of interconnection lengths in different technologies. The lower interconnect time delays, cross-talk and power dissipation by shorter interconnects develop the performance in ICs.

By packing more transistors in a single chip, the IC industry has met the demand for high performance and miniaturization of electronic products. In IC manufacturing, this is achieved by scaling or reducing the feature size. As the feature size reduces, the intrinsic gate delay decreases (see **Fig. 1.5**). However, scaling increases interconnects length to accommodate increasing transistor[7, 11]. **Fig. 1.5** shows the effect of interconnect length on interconnect delay. It was found interconnect delay increases with increasing the interconnect length[7, 11, 13, 14]. Therefore, when using 3D integration design, shorter interconnect lengths and higher pitch results in lower time delays.

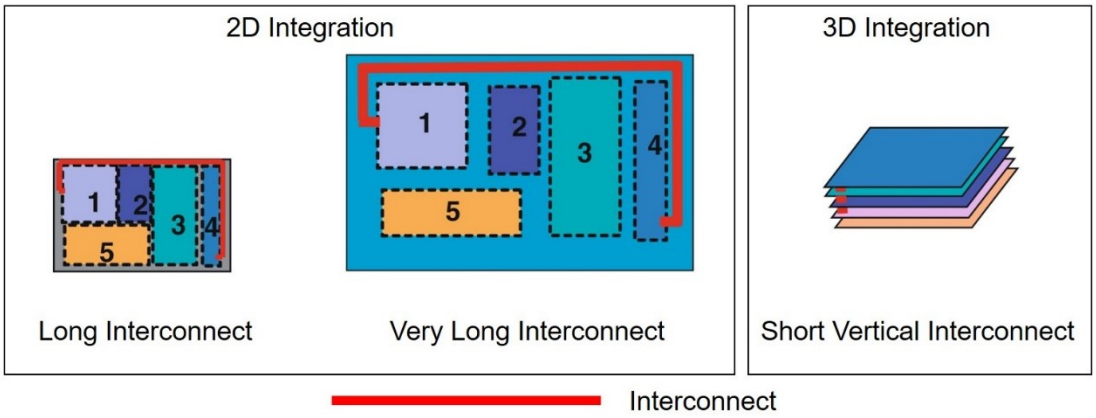

Fig. 1.4 *Interconnect lengths in different technologies[1].*

3D integration technology can be grouped into three categories, namely 3D on-chip integration, 3D IC-stacking, and 3D packaging. These three technologies will be described next in more detail.

First, 3D on-chip integration. This technology is a vertical extension of IC technology using for 3D integration, where active silicon layers are built-up sequentially and separated from each other with interlayer dielectric. However, major technical challenges and research and design (R & D) issues are still being addressed at the leading universities.

Secondly, 3D IC-stacking using thru-Si vias (TSVs). In this technology, each IC wafer design is first fabricated independently. Then the wafers or ICs are bonded and electrical interconnection between ICs is made using thru-Si vias. In 3D-stacking, a better performance reaches because 3D silicon layers are connected with very short vertical interconnects as mentioned before. The IC-stacking process can be implemented in wafer-to-wafer[15], chip-to-wafer[16, 17], and chip-to-chip[18] levels, as illustrated in **Fig .1.6.** Due to the potential for cost reduction, most world-wide R & D is concentrated on wafer-level process[1].

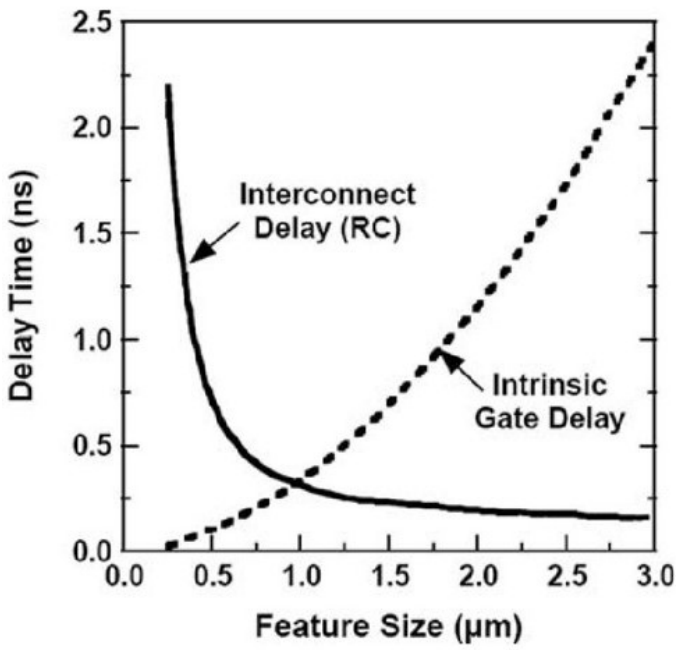

Fig. 1.5 *Intrinsic gate and interconnect delays as a function of minimum feature size[13].*

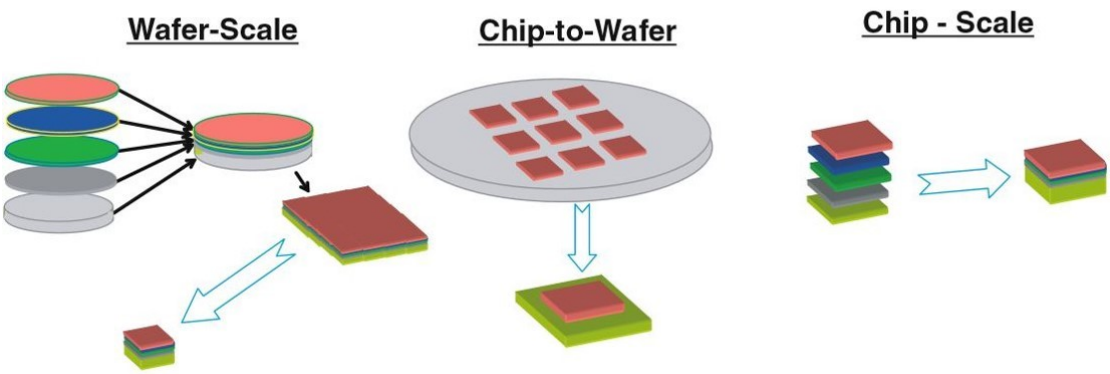

Fig. 1.6 *Schematic illustration of different options for IC-stacking[1].*

Last but not least, 3D packaging. 3D packaging provides the simplest way to make an integrated microsystem by stacking the packaged ICs in 3D structures. As the most mature 3D integration technology, 3D packaging includes many different technologies, most of which are extensions to 3D the existing single-chip packaging technology to 3D. Due to this, the implementation of 3D packaging has been easier, more cost-effective and higher yield. As a result, 3D packaging is widely used in consumer electronics such as smartphones, digital cameras, and laptop computers. Different 3D packaging techniques can be further subdivided into four major types, as shown in **Fig. 1.7**. These are wire-bonded die-stack[19], BGA-stack[20], folded–stack using chip-on-flex[21], and ultra-thin package stack[22]. The first two types, wire-bonded die-stack and BGA-stack, are the most commonly used 3D packaging technologies.

Since 3D packaging is already used in many applications, many issues have already been resolved. However, two main issues still remain, namely thermal management and cost. Each specific 3D-packaging technology has to be individually evaluated for thermal issues and solutions. Use of heat spreaders and heat sinks can be extended to 3D in a few cases[1]. Some systems may require exotic heat dissipation apparatus. Although 3D-packaging is the lowest cost 3D integration category, there is still a push to further lower the cost in the consumer product applications market[1]. These demands are a driving force to develop the advanced materials and emerging processes for 3D packaging.

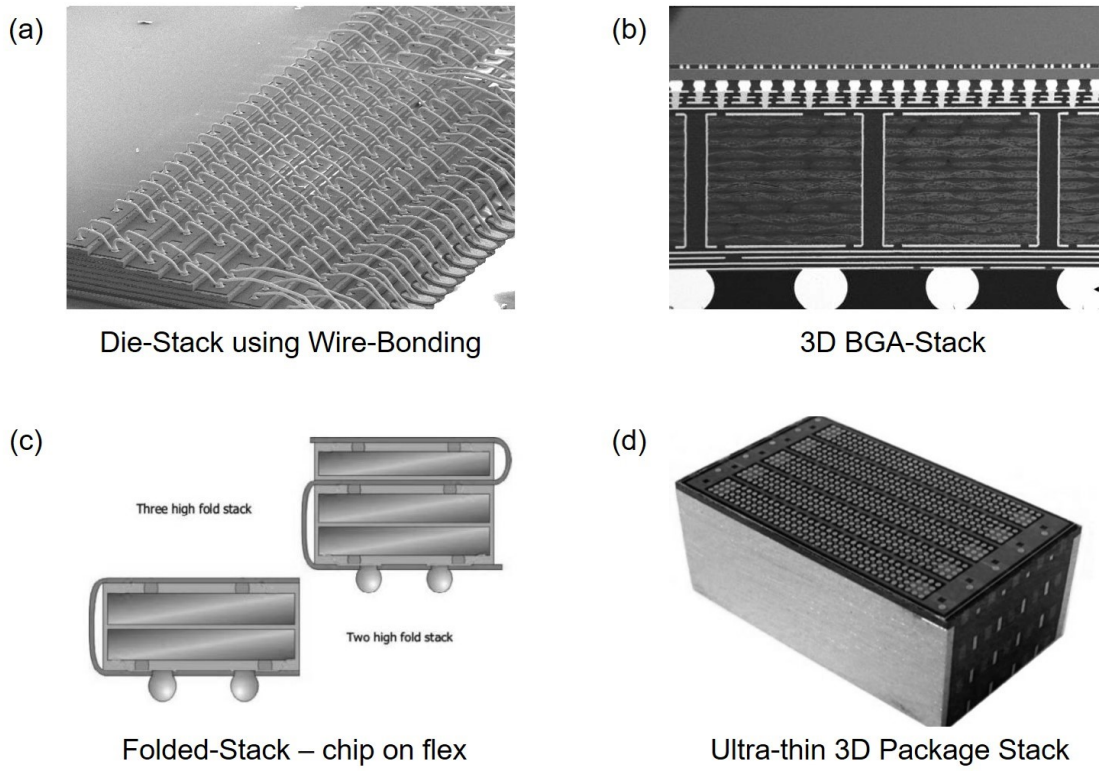

Fig. 1.7 *Illustration of different 3D-packaging technologies: (a) wire-bonded die-stack, (b) BGA-stack, (c) folded–stack using chip-on-flex, and (d) ultra-thin package stack.[23]*

1.2 Lead-Free Soldering Processes Using for Electronic Packaging

Soldering process has been used in industries for several decades[24, 25]. When temperature reach the melting temperature, the solder turns into molten phase, then the molten solder reacts the base metal to ignite the bonding. Hence, in order to reduce the cost and complexity of soldering process, decreasing the soldering temperature is necessary. To have low soldering temperature, solders need to have low melting temperature. Thus, solder alloys always contain an element that has low melting temperature such as tin (Sn), indium (In), lead (Pb), and bismuth (Bi). Among them, Lead-containing solders (Sn–Pb) have been widely used as low temperature joining alloys because of their good combination of process attributes, convenient material properties and low cost[26-30]. However, the electronic industry is moving toward green manufacturing as a global trend in 1990s[1, 31-33]. In 1998, the European Commission introduced two draft proposals called the Waste Electrical and Electronic

Equipment (WEEE) and Reduction of Hazardous Substances (ROHS) directives. The primary objective of these complementary proposals is to minimize the risks and impacts that the production, use, treatment, and disposal of waste electrical and electronic equipment have on human health and the environment. Additionally, the directives are intended to prevent uncontrolled disposal of electrical and electronic equipment and to foster the development of reuse and recycling methods in order to reduce the amount of waste for disposal. In short, they aim for "green" products.

In the area of soldering, mainly driven by European RoHS, lead was banned effective July 1, 2006 except in some exempt items[31, 32, 34, 35]. This European legislation is followed by China RoHS which has similar list of banned materials[36]. In Japan, the legislative activities dealt with the reclamation and recycling of electronics[37]. Although not specifically aiming at lead, this legislation effectively drove Japanese industry toward lead-free soldering process. These directives have led to the trend of lead-free, which has effectively promoted the development of lead-free soldering in other countries in the world. **Fig. 1.8** shows the lead-free soldering implementation status from 2004 to 2015 by IPC.

Among the numerous lead-free solder options available, the following families are of particular interest and are the prevailing choices of industry: eutectic Sn-Ag, eutectic Sn-Cu, eutectic Sn-Bi, eutectic Sn-Ag-Cu, and their modifications[29].

The eutectic composition for the Sn-Ag occurs at Sn-3.5 wt.% Ag and the eutectic temperature is 221 °C[38]. The solidified microstructure of the binary eutectic Sn-3.5 wt.% Ag as consisting of a β-Sn phase with dendritic globules and inter-dendritic regions with a eutectic dispersion of Ag_3Sn precipitates within a b-Sn matrix[39]. The development trend of this solder is to reduce the content of Ag[40].

The Sn-Cu binary alloy has a eutectic composition of Sn-0.7 wt.% Cu and a eutectic temperature of 227 °C[41]. Sn-0.7Cu solder is lower in tensile strength but higher in elongation than Sn-Pb solder, reflecting the softness and ductility of Sn-Cu solder[33]. And the wettability of Sn-0.7Cu solder is lower than Sn-Pb solder[42].

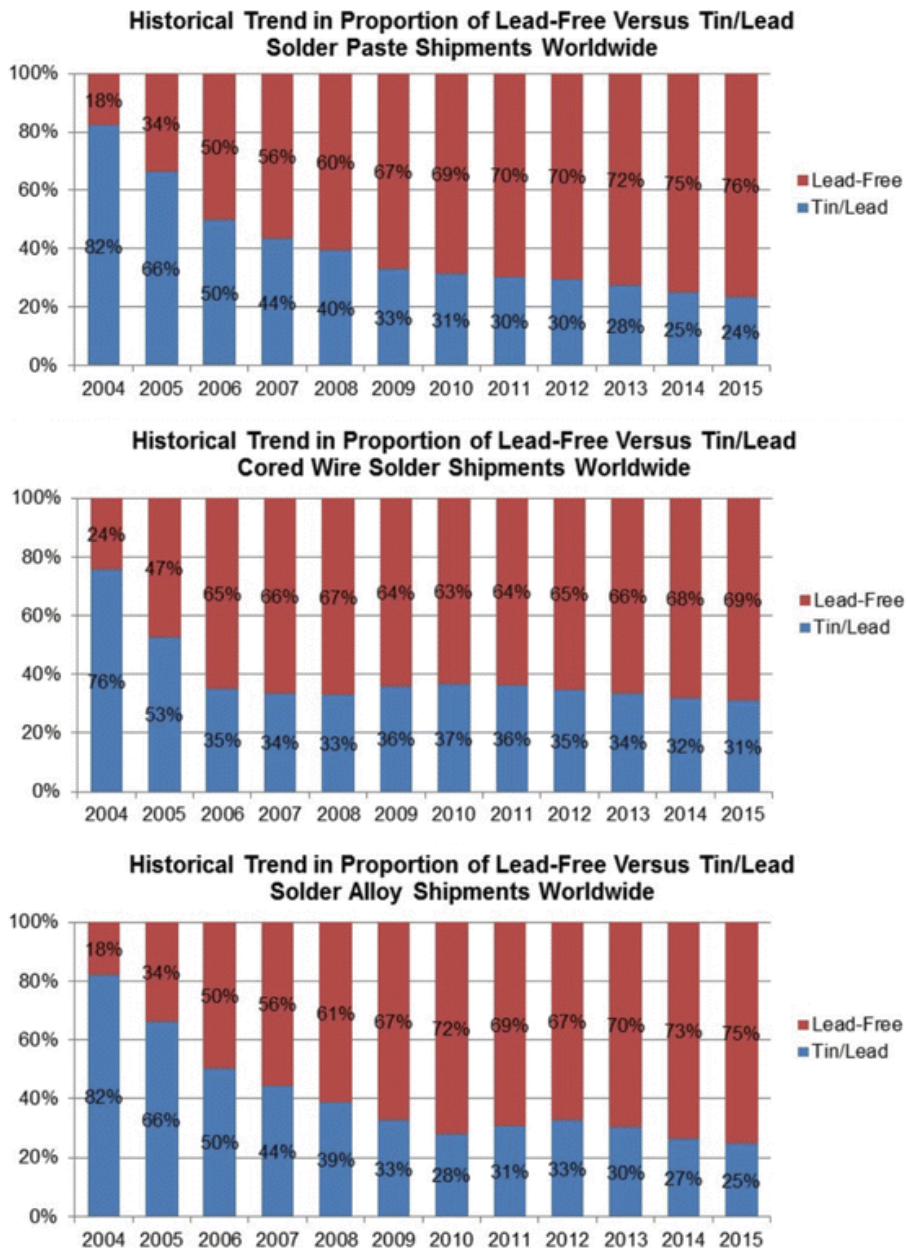

Fig. 1.8 *Historical trend in proportion of lead-free solder reported by IPC[43].*

Sn-Bi alloy shows promise as Pb-free solder. The addition of 58 wt.% Bi into Sn form a eutectic with a relatively low melting temperature of 138 °C[44]. Sn-58Bi solder has fracture strength approaching that of Sn-Pb solder at room temperature[45]. However, Sn-Bi solder is more sensitive than Sn-Pb solder to strain rate[46]. That means, its elongation decreases more rapidly with increasing strain rate. The increased elongation at low strain rates after aging resulted in ductile failure in solder, versus a brittle fracture at high strain rate[47].

The eutectic and near eutectic Sn-Ag-Cu alloys are the most prevailing alloy family for electronic soldering[29, 32]. The melting temperatures of the series solders were about 217 °C[48]. These series solders show relatively slow creep rate, promising joint strength and ductility. The wetting performance of Sn-Ag-Cu solders were better than both Sn-Cu solder and Sn-Ag solder[49-51]. Lee also reported that the wetting ability decreased in the following order: eutectic Sn-Pb > Sn-Ag-Cu > Sn-Ag > Sn-Cu when an un-activated flux was used[52]. Hence, from among the Pb-free solders, eutectic and near eutectic Sn-Ag-Cu alloys have been considered as the primary candidates to replace the Sn-Pb solder.

At present, the most advanced electronic packaging technique is 3D packaging, which is the solution of high-level integration and miniaturization. **Fig. 1.9** shows a simple structure of 3D packaging by heating flow. The Pb free solders as the interconnection materials also play an important role in 3D packaging technology.

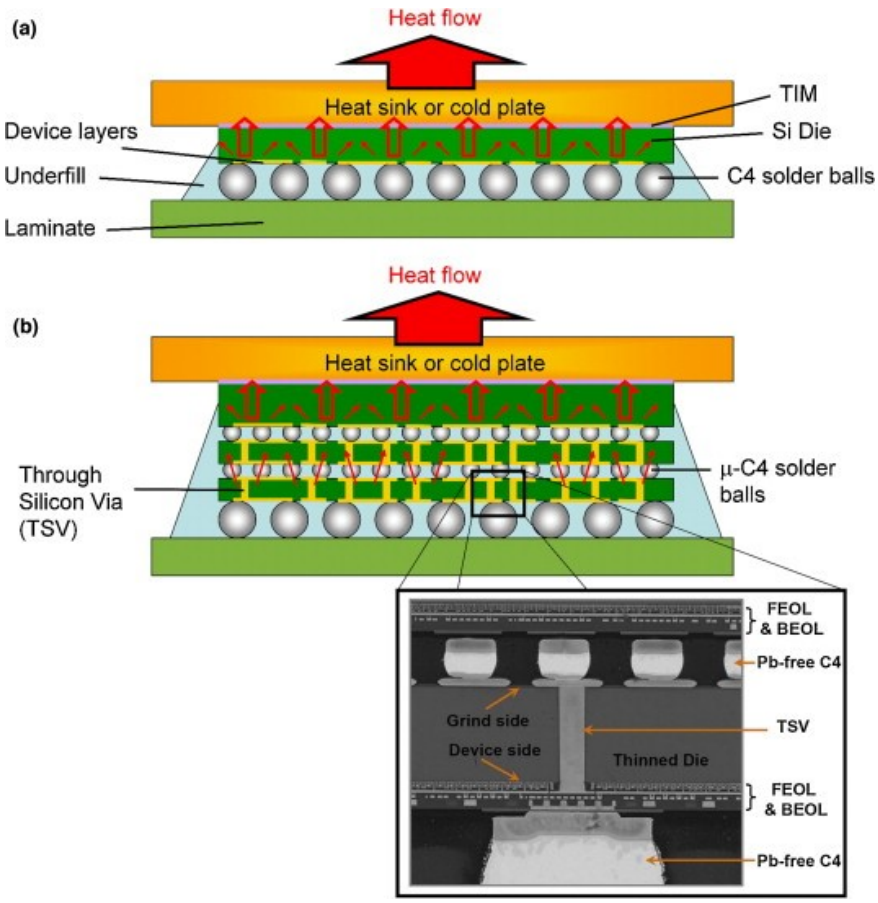

Fig. 1.9 *Illustrations of representative (a) single die flip chip package and (b) 3D chip stack lidless modules with select conceptual heat flow paths shown[53].*

1.3 Fluxless Soldering Processes

1.3.1 Role of Flux in Wetting during Soldering Process

To form a proper metallurgical bond between the solder and the base metal, good wetting is necessary[54-57]. Wetting a liquid on a solid is a surface phenomenon in which the surface of the solid is covered by the liquid on placing it over the surface[58]. Wetting or spreading can be broadly classified into two categories: non-reactive wetting and reactive wetting. A liquid spreading on a substrate with no reaction/absorption of the liquid by substrate material is known as non-reactive[59]. On the other hand, the wetting process influenced by reaction between the spreading liquid and substrate material is known as reactive wetting[60, 61]. A spreading of solder on base metal substrate is an example of reactive wetting[58, 62, 63]. Wettability is an essential characteristic of a soldering process for bonding in electronics because it ensures that the chemical reaction at the interface between solder and base metal has happened and the joint was created[30, 64, 65]. Consider Sn-based Pb-free solder on Cu substrate as an example. During the soldering process, when the temperature reaches the melting temperature of solder, the Sn in the molten solder reacts with Cu to form Cu_6Sn_5 intermetallic compound (IMC) at the interface, often known as a reactive wetting action, as shown in **Fig. 1.10**. Degree or extent of wetting and the rate of wetting are two important parameters to characterize the wettability of a solder on a solid base metal[58, 66]. In soldering process, the degree of wetting is generally indicated by the contact angle formed at the interface between solid base metal substrate and liquid molten solder[67-70]. When a solder is set on a base metal surface, it will spread to some extent on the surface and then forms an angle with it, as shown in the **Fig. 1.11**. The angle between the tangent drawn at the triple point between the three phases (solid, liquid and vapor) and the substrate surface is known as contact angle[71]. Under equilibrium conditions this angle is decided by the surface and interfacial energies according to Young's equation[72].

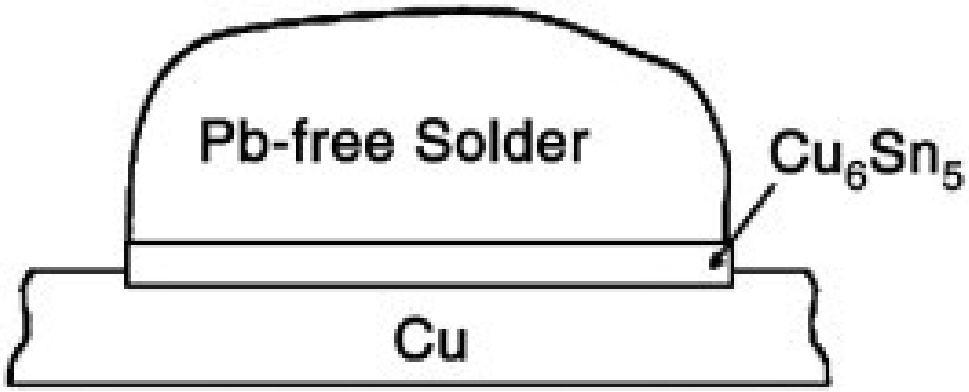

Fig. 1.10 *Schematic image of a solder/substrate interface[73].*

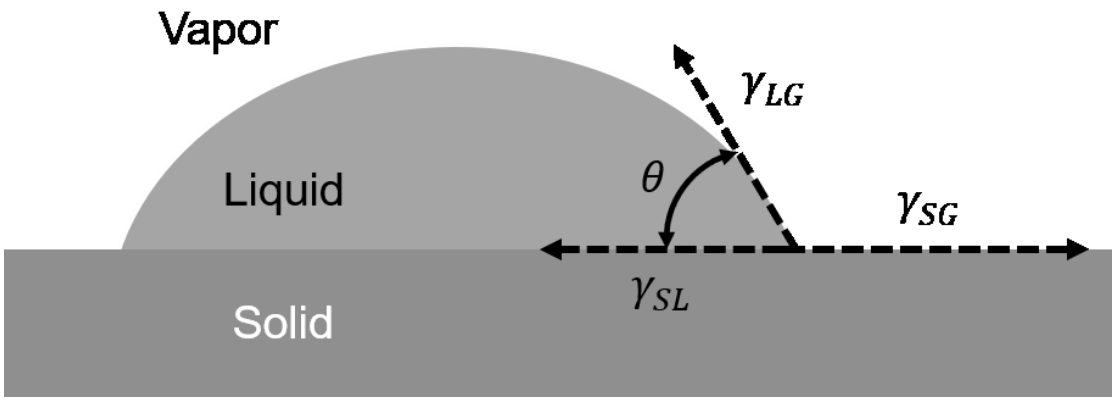

Fig. 1.11 *Liquid sessile drop on a solid substrate.*

$$\gamma_{SG} - \gamma_{SL} - \gamma_{LG}\cos\theta = 0 \qquad (2)$$

Where γ_{SG} is the surface tension at the interface of the solid and vapor phases, γ_{SL} is the surface tension at the solid and liquid phases, γ_{LG} is the surface tension at the liquid and vapor phases, and θ is the contact angle. **Fig. 1.12** schematically shows a liquid solder drop on a solid base metal substrate from complete wetting (θ= 0°) to total non-wetting condition (θ= 180°).

Since the wetting of a solder on base metal substrate is a reactive wetting[74]. The bonding of solder and substrate is the chemical reaction that forms an IMC, the soldering environment have to protect this chemical reaction. However, both the solder and the base metal have oxides on their surfaces[75-77]. The melting temperature of these oxide layers are much higher than the soldering temperature[78, 79]. The

breakdown of oxide layers of solder and base metal is vital to achieve true wetting in soldering process since the oxide layers on the substrate surface or spreading solder will alter the interfacial properties and prevent the molten solder to react with the base metal[80]. To overcome the negative effects of oxide layers, fluxes are generally used[81, 82]. The flux is used in soldering process to provide an oxide-free surface and to keep the surface clean, breaking existing oxides and protecting the cleaned surfaces against re-oxidation[83, 84]. There are many literatures that suggest fluxes improve wetting[82, 85, 86]. **Fig. 1.13** shows the role of flux playing in the wetting during soldering process. Since the wettability of lead-free solder when an un-activated flux was used, as we mentioned in **Section 1.2**, the rosin mild-activated flux has been used for lead-free solder to improve wetting[87].

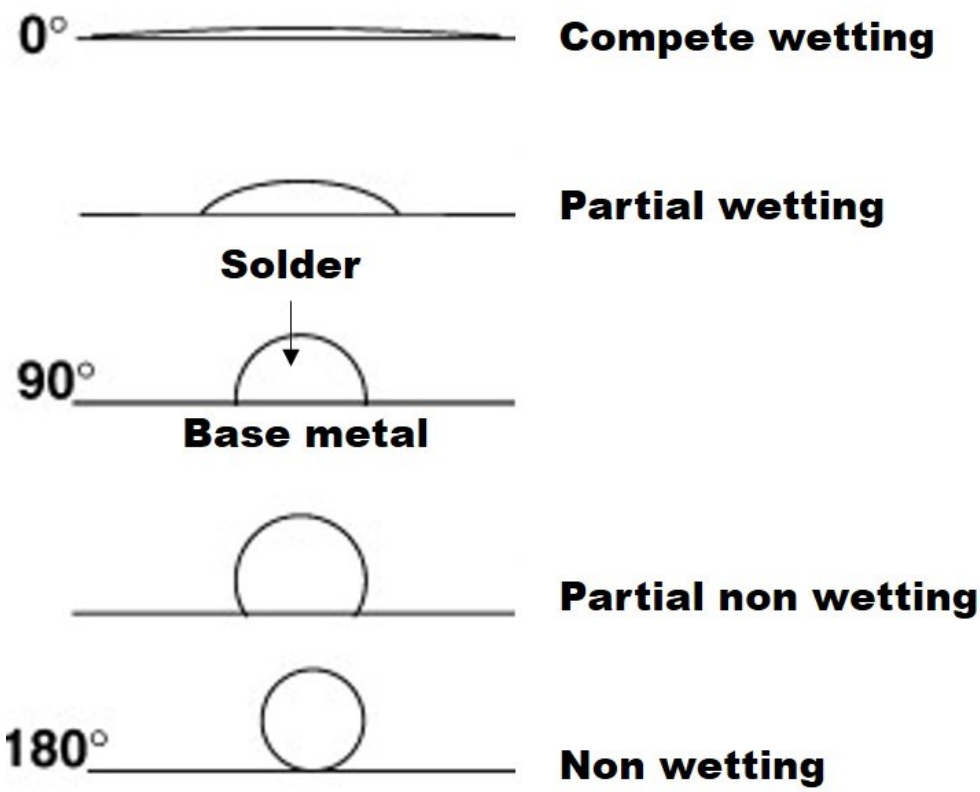

Fig. 1.12 *Different wetting of liquid solder drop on a solid base metal substrate.*

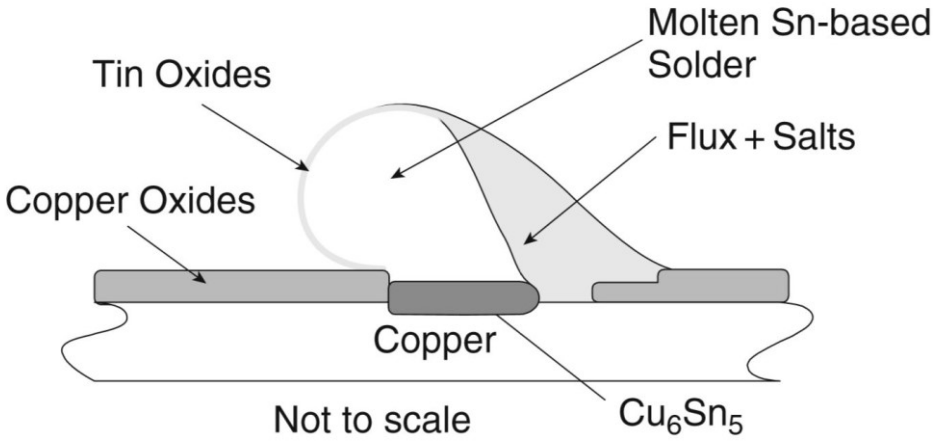

Fig. 1.13 *Molten flux converts oxides into salts to expose fresh solder and fresh base metal [73].*

1.3.2 Problems in Soldering Process Using Flux

The key of a successful soldering is to remove or convert the oxides on the surface of solder and base metal substrate. Fluxes are used commonly to keep the surfaces clean, as explained in the **Section 1.3.1**. The organic flux containing rosin has been widely used in industry. Such a flux generally contains 40–60 wt.% rosin, 7–10 wt.% thickeners, 5–10 wt.% viscosity agents, about 2 wt.% activators and different solvents as a balance[58]. Although these fluxes are generally not electrically conductive, they are corrosive in nature[88, 89]. The residues of fluxes at the interface between solder and base metal or in the solder paste become voids easily[90], the voids may cause long term reliability problems. For optoelectronic products such as light emitting diodes (LEDs), the organic fluxes residue affects the optical efficiency[91]. Hence, cleaning process is necessary after using fluxes. However, the use of halogenated solvents (such as chlorofluorocarbons) for removing rosin-based liquid fluxes are hazardous and harmful to the ozone layer[92]. Chlorofluorocarbons (CFCs) are now believed to be major contributors to the seasonal ozone depletion over the Antarctic continent[92, 93]. The ozone layer in the stratosphere is essential for the protection of creature on Earth. Ozone absorbs most of the harmful UV insolation[94]. Without it human beings would

suffer very high rates of incidence of skin cancers, eye disorders and suppression of the immune systems; reductions in the yields of major agricultural crops; lower rates of productivity of phytoplankton, with possible implications for the aquatic food chain; and substantial losses at the larval stage of many fish (e.g. anchovies), shrimps and crabs[95]. The principal chemical reaction, involving the chlorine and ozone could be described as follow[96-98]:

$$Cl + O_3 \rightarrow ClO + O_2 \quad (2)$$

Hence, the CFCs can lead to a net destruction of ozone by the radical reaction. Because of their chemical stabilities, man-made CFCs difficultly decompose in the atmosphere covered Earth[93]. What's worse, CFCs cannot remove by 'rain-out' because it is difficult to dissolve in water[98]. And using only ethanol, which is common agent to clean organic residues, is difficult to remove the flux residues completely, as shown in **Fig. 1.14**. As the cleaning process of flux used for many years, considering about the impact of environment, limitation of usage of flux is necessary. **Fig. 1.15** shows the results of measurements of the total amount of ozone present as indicated by the ozone-mapping spectrometer on the Nimbus 7 satellite from 1979 to1986[99].

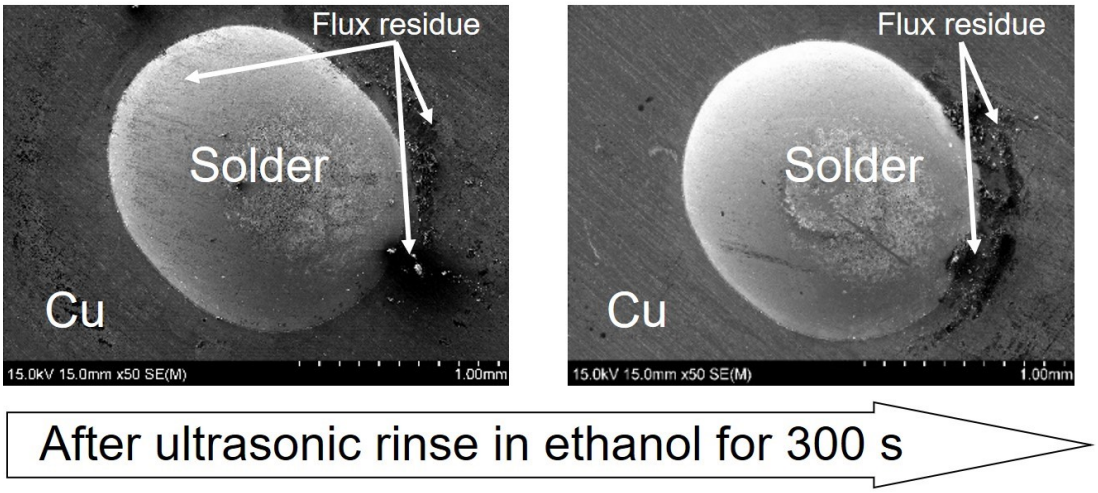

Fig. 1.14 *SEM image of solder with flux residue after soldering and after cleaning.*

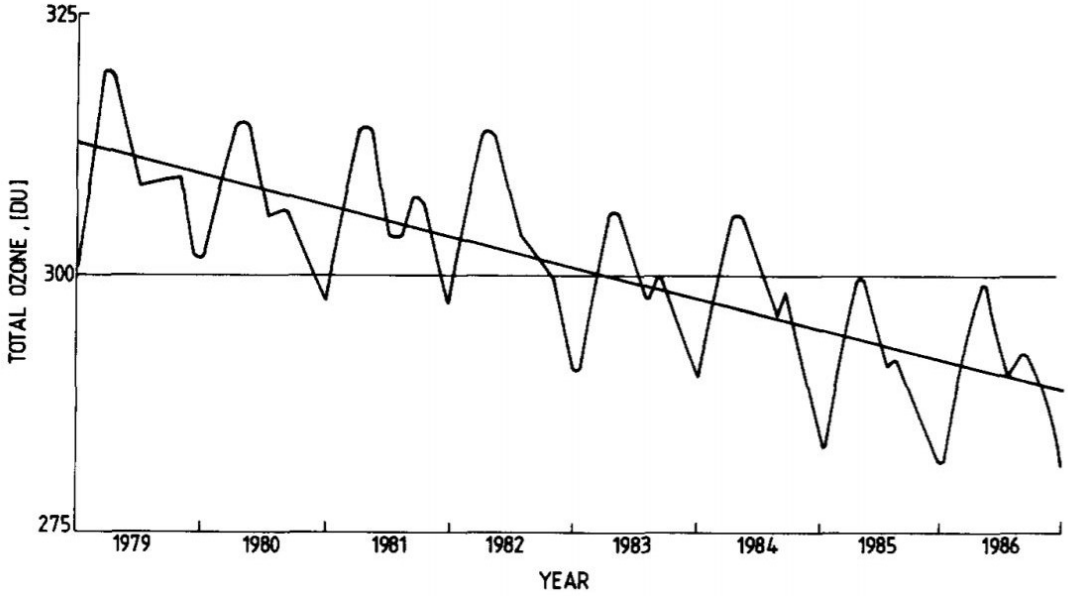

Fig. 1.15 *Daily global mean total ozone present in Dobson units (satellite data)[99].*

Flux is also harmful to health of human beings. C. L. Goh[100] has reported occupational dermatitis among workers in the electronics industry from soldering flux. With the expansion of the electronic industry, the demand for PCBs will increase and so will workers' exposure to soldering flux. Allergic contact dermatitis from colophony, hydrazine and aminoethyl ethanolamine in fluxes has been reported among electricians[80, 101, 102]. **Fig. 1.16** shows the workers had irritant contact dermatitis from the soldering flux. Rosin- and hydrazine-containing fluxes are seldom used in the soldering of PCBs as they tend to leave more corrosive residues and are difficult to clean. Occupational allergic contact dermatitis from aminoethyl ethanolamine has been reported[102, 103]. And the acids in flux used to reduce the oxides of metal is also corrosive and toxicant[89, 104].

In order to decrease the impact to environment, water soluble fluxes (non-rosin) are developed used for soldering PCBs in electronics factories[105, 106]. The advantage of this flux is that residues, which may cause serious corrosions after soldering, are water soluble and PCBs soldered with these fluxes can easily be cleaned after soldering. This cleaning process would consume water, obviously.

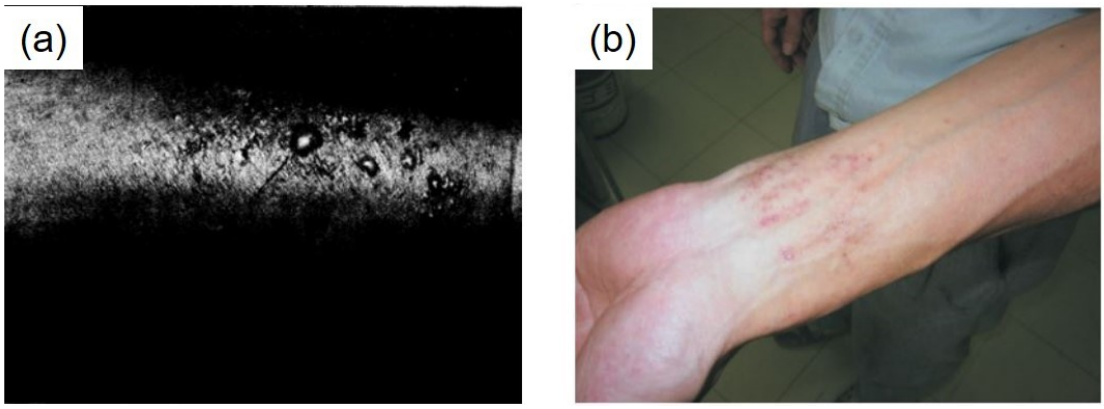

Fig. 1.16 *Dermatitis from the soldering flux: (a) Acute dermatitis over the ulnar border of the forearm due to the irritant effect of flux, resulting from contamination of workbench[100]; (b) Dermatitis on the forearm due to the irritant effect of flux dust, resulting from clean-up of a flux-spraying unit[102].*

Furthermore, in most advanced 3D packaging, the increased solder bump density and reduced chip to substrate gap and intercomponent space hinder the flux cleaning process. No-clean fluxes have been developed recently, but Dušek et al. reported that they cause flux residue spattering problems on in-circuit testing pads[107-109].

1.3.3 Fluxless Soldering Technology Dealing with Oxides

The soldering process without the use of fluxes is called fluxless soldering process[1]. The present tendency is to go for fluxless soldering[27, 88, 110-116] because the problems of flux which was discussed in **Section 1.3.2**. In soldering process, in order to achieve a stable bonding, the flux is used to break down the oxide layers on the surface of solder and base metal substrate, as we mentioned in **Section 1.3.1**. Thus, fluxless soldering processes are considered dealing with oxides easily. We try to review the fluxless soldering processes dealing with oxides of metals reported. In 1990, a fluxless soldering process using fluorine treatment was developed, which is called Plasma Assisted Dry Soldering (PADS)[117, 118]. In PADS, Radio Frequency (RF) generated plasma disassociates innocuous fluorine containing source gases (CF4 or SF6)

to produce the reactive radical atomic fluorine, as illustrate in **Fig. 1.17**. When solder is treated with the atomic fluorine, the following reaction will happen:

$$SnO_x + yF \rightarrow SnO_xF_y \quad (3)$$

The resulting SnO_xF_y can be easily dissolved in the molten solder and thus the oxide of solder is capable to be removed. After the atomic fluorine treatment, the solders can store in air for several days. However, there are some potential problems using PADS: (a) fluorine can etch SiO_2 and SiN[119]; (b) the RF source may damage the IC chip[120].

K. Sakuma et.al developed a vacuum ultraviolet (VUV) surface treatment process to remove the oxides on the metal prior to bonding, offering simplicity, low cost, and high productivity[120]. A schematic illustration of the VUV surface treatment system is shown in **Fig. 1.18**. Although there was a significant reduction in the organic contaminants on the bonding surfaces of the solder-Cu bumps by using VUV treatment, the oxides was not capable to remove completely[121].

A hydrogen radical treatment was technology developed since 2011[121]. The organic compounds, contaminants, and oxide films were able to remove effectively via hydrogen radical treatment. **Fig 1.19** shows a schematic diagram of hydrogen radical treatment. The oxide film of the solder is removed and prevented from re-oxidation by using hydrogen radical treatment. However, the cost of this treatment is very high.

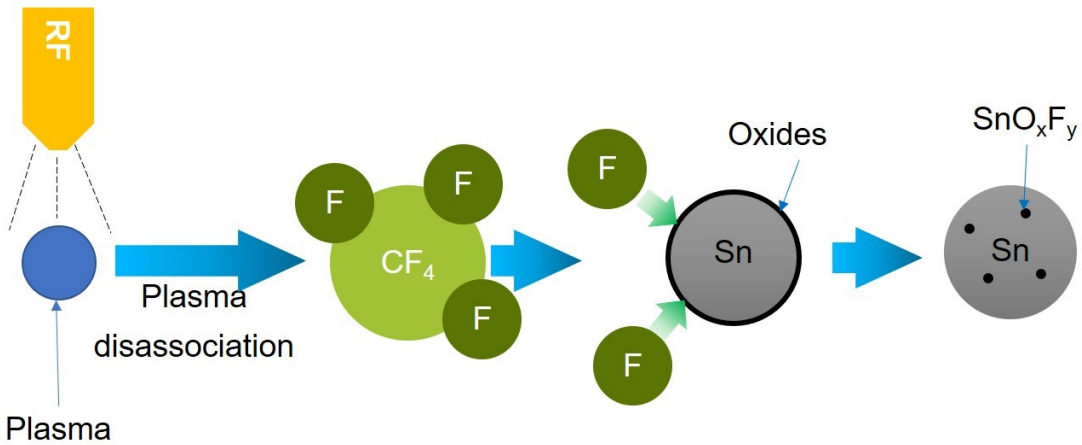

Fig. 1.17 *Schematic image of removement of oxides on solder surface by plasma.*

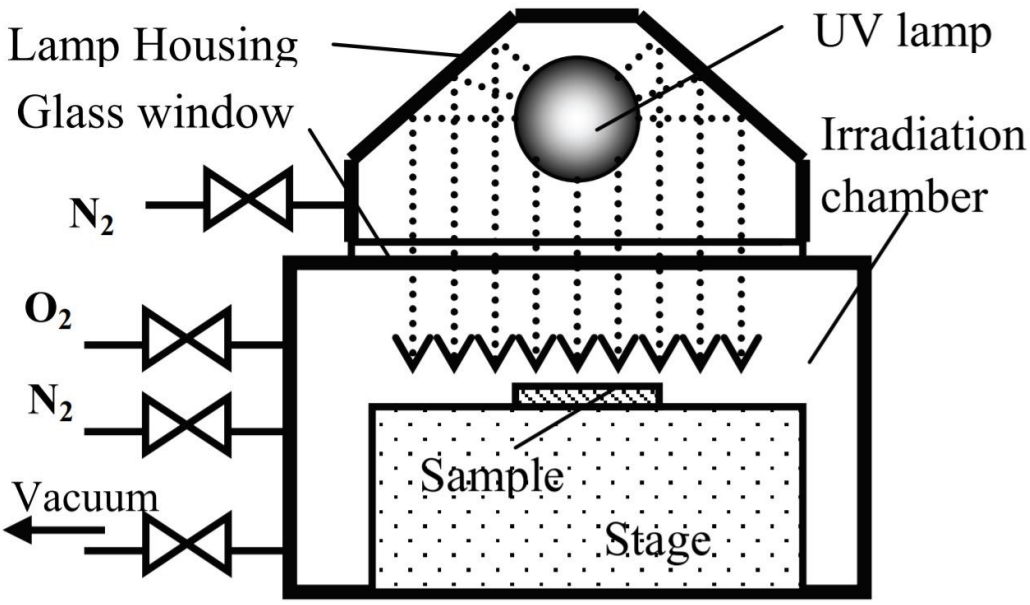

Fig. 1.18 *Schematic illustration of VUV irradiation system[120].*

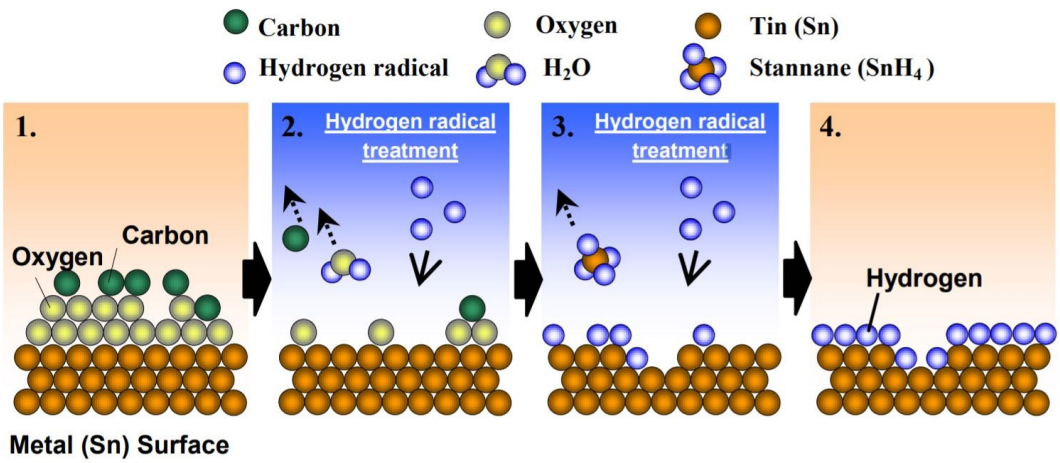

Fig. 1.19 *Schematic diagram of hydrogen radial treatment[121].*

Among the fluxless soldering processes, the soldering under a reducing atmosphere, such as hydrogen and formic acid, has been wildly applied to remove the oxides[78, 79, 88, 116, 121-127]. However, for most solders, achieving efficient reduction using pure

hydrogen requires temperatures of over 300 °C[113, 127, 128], which is not suitable for surface mount devices. **Fig. 1.20** lists the advantages and disadvantages of the three most common reducing process gases: pure hydrogen, forming gas (N_2 with 5vol.% H_2) and N_2 enriched with gaseous formic acid.

The disadvantage of formic acid is harmful to health. However, within modern soldering systems using for electronic packaging, the handling of nitrogen enriched with formic acid is feasible and widely used in electronic manufacturing[91, 116, 122, 129]. Based on the previous studies, formic acid-containing atmospheres can be used effectively to reduce the oxide film on the surface of Sn-based solders. However, most publications on soldering under a formic acid atmosphere have focused only on the soldering results, such as the mechanical properties[79, 130, 131]. The motivations of this study were therefore focused on parameters of fluxless soldering under a formic acid atmosphere.

Reducing Process Gas	***Advantages***	***Disadvantages***
Forming Gas (95% N_2, 5% H_2)	• Non-toxic • Non-flammable (up to 5,5% H_2)	• Only slightly reducing effect • Only effective at soldering temperatures > 300°C
Pure H_2	• Strong reducing effect	• Explosion-proof system necessary • Only effective at soldering temperatures > 300°C
Formic Acid Vapor (ca. 95% N_2, 5% HCOOH)	• Strong reducing effect	• Respiratory and eye irritant vapors

Fig. 1.20 *review of different reducing process gases with their advantages and disadvantages[79].*

1.4 Research Motivation

Based on the previous studies[27, 73, 78, 79, 88, 110-113, 115-119, 121, 122, 127, 130, 132-145], the method of using formic acid atmosphere is believed to be a promising technique for fluxless soldering. The oxide films of conventional Sn-3.0Ag-0.5Cu are mostly composed of SnO and SnO_2[75]. Thus, the reaction of formic acid (HCOOH) atmosphere with solder (Sn) oxide can be described as follows[140]:

$$SnO + 2HCOOH \rightarrow Sn(HCOO)_2 + H_2O \quad (4)$$

$$SnO_2 + 2HCOOH \rightarrow Sn(HCOO)_2 + 2CO_2 + H_2 \quad (5)$$

At above 150 °C,

$$Sn(HCOO)_2 \rightarrow Sn + 2CO_2 + H_2 \quad (6)$$

Finally, formic acid becomes carbon dioxide and hydrogen in the reflow process.

The use of a formic acid-enriched nitrogen atmosphere has been widely reported to be suitable for the reflow soldering of electronic packaging. For example, Monta et al.[140] used a formic acid atmosphere to remove the native oxide of Sn-based solders on copper pillars. Hanss et al.[79] reported a residual-free solder process by applying a fluxless solder paste under a formic acid atmosphere. Formic acid atmospheres have also been used to reduce the solder oxide layer in a fluxless chip joint process[115]. Formic acid-containing atmospheres can be used effectively to reduce the oxide film on the surface of Sn-based solders. However, most publications on soldering under a formic acid atmosphere have focused only on the final contact angle results or mechanical properties[78, 79, 116]; not parametric studies, such as in situ observation of wetting of solder under formic acid atmosphere, effect of formic acid atmosphere on interfacial reaction, and the long term reliability of solder joint after fluxless soldering. These parametric studies are important for identifying the optimal processing conditions and essential for establishing a reliable fluxless soldering process under a formic acid atmosphere.

1.5 Purpose and Scope of This Study

The purpose of this study was to establish a reliable fluxless soldering process under a formic acid atmosphere using Sn-3.0Ag-0.5Cu solder for electronic packaging. Attempts were made to investigate the mechanism of formic acid atmosphere in fluxless soldering process. Three main issues, wetting behavior of solder under a formic acid, effect of formic acid atmosphere on interfacial reaction between solder and different substrates, and long-term reliability of solder bumps after fluxless soldering were the focusing points of this study.

In **Chapter 1**, a brief introduction of electronic packaging, lead free soldering process, role of flux in soldering were given. Various fluxless soldering technologies were listed and parametric studies about fluxless soldering under a formic acid atmosphere were proposed.

In **Chapter 2**, the effects of heating processes on the wetting behavior of Sn-Ag-Cu solder on a Cu pad under a formic acid atmosphere were observed in situ. The effect of formic acid on the interfacial reaction between the solder and Cu substrate was also confirmed.

In **Chapter 3**, the effect of pores formed at the interface between solder and Cu (mentioned in **Chapter 2**) on long term reliability was evaluated by conducting impact tests on solder bumps after soldering under a formic acid atmosphere and thermal aging in an oil bath. The different fracture modes of solder bumps soldered under a formic acid atmosphere and that soldered using flux were also discussed.

In **Chapter 4**, the thermal effect on Sn steaming phenomenon on Cu pads under a formic acid atmosphere, produced by series peak temperature and different holding times under a formic acid atmosphere, were investigated. Based on the results, methods for improving the Sn steaming phenomenon were proposed.

In **Chapter 5**, in order to further improve the wettability of solder under a formic acid atmosphere, the ENIG substrate was prepared. Sn-Ag-Cu solder balls were applied onto ENIG substrates under a formic acid atmosphere, and wettability of solder,

interfacial reactions between solder and substrate, and impact strength of the solder bumps before and after the thermal aging at 150 °C for 168, 512, and 1008 h were examined. The Sn steaming phenomenon during fluxless soldering process under a formic acid atmosphere (discussed in **Chapter 4**) was also confirmed.

In **Conclusion**, brief achievements and results of each chapter in this thesis were summarized.

Reference

[1] D. Lu, C. Wong, Materials for advanced packaging, Springer2009.

[2] J. Fujimoto, Proposal of Service-Oriented Products based on the Inverse Manufacturing Concept (1st Report)-Concept and Business Model, Proceedings of Electronics Goes Green 200+, 2000 (2000).

[3] R. Bowlby, The DIP may take its final bows: The dual-in-line package, the reigning IC package for several generations, is losing position to newcomers for packaging advanced chips, IEEE Spectrum 22(6) (1985) 37-42.

[4] P. Hall, Forces, moments, and displacements during thermal chamber cycling of leadless ceramic chip carriers soldered to printed boards, IEEE Transactions on Components, Hybrids, and Manufacturing Technology 7(4) (1984) 314-327.

[5] H. Iwanishi, A. Hirose, T. Imamura, K. Tateyama, I. Mori, K. Kobayashi, Properties of quad flat package joints using Sn-Zn-Bi solder with varying lead-plating materials, Journal of electronic materials 32(12) (2003) 1540-1546.

[6] L. Mahalingam, J. Andrews, J. Drye, Thermal studies on pin grid array packages for high density LSI and VLSI logic circuits, IEEE transactions on components, hybrids, and manufacturing technology 6(3) (1983) 246-256.

[7] M.T. Bohr, Interconnect scaling-the real limiter to high performance ULSI, Proceedings of International Electron Devices Meeting, IEEE, 1995, pp. 241-244.

[8] A. Badihi, Ultrathin wafer level chip size package, IEEE Transactions on Advanced Packaging 23(2) (2000) 212-214.

[9] G. Roelkens, D. Van Thourhout, R. Baets, High efficiency grating coupler between

silicon-on-insulator waveguides and perfectly vertical optical fibers, Optics letters 32(11) (2007) 1495-1497.

[10] S.J. Souri, K. Banerjee, K. Banerjee, A. Mehrotra, K.C. Saraswat, Multiple Si layer ICs: Motivation, performance analysis, and design implications, Proceedings of the 37th Annual Design Automation Conference, ACM, 2000, pp. 213-220.

[11] K. Banerjee, S.J. Souri, P. Kapur, K.C. Saraswat, 3-D ICs: A novel chip design for improving deep-submicrometer interconnect performance and systems-on-chip integration, Proceedings of the IEEE 89(5) (2001) 602-633.

[12] K.C. Saraswat, 3-D ICs: Motivation, performance analysis, technology and applications, 2010 17th IEEE International Symposium on the Physical and Failure Analysis of Integrated Circuits, IEEE, 2010, pp. 1-6.

[13] A.L.S. Loke, Process integration issues of low-permittivity dielectrics with copper for high-performance interconnects, Stanford University1999.

[14] A. Rahman, R. Reif, System-level performance evaluation of three-dimensional integrated circuits, IEEE Transactions on Very Large Scale Integration (VLSI) Systems 8(6) (2000) 671-678.

[15] C.-T. Ko, K.-N. Chen, Wafer-level bonding/stacking technology for 3D integration, Microelectronics reliability 50(4) (2010) 481-488.

[16] T. Fukushima, E. Iwata, Y. Ohara, A. Noriki, K. Inamura, K.-W. Lee, J. Bea, T. Tanaka, M. Koyanagi, Three-dimensional integration technology based on reconfigured wafer-to-wafer and multichip-to-wafer stacking using self-assembly method, 2009 IEEE International Electron Devices Meeting (IEDM), IEEE, 2009, pp. 1-4.

[17] A. Klumpp, R. Merkel, P. Ramm, J. Weber, R. Wieland, Vertical system integration by using inter-chip vias and solid-liquid interdiffusion bonding, Japanese Journal of Applied Physics 43(7A) (2004) L829.

[18] C. Ryu, D. Chung, J. Lee, K. Lee, T. Oh, J. Kim, High frequency electrical circuit model of chip-to-chip vertical via interconnection for 3-D chip stacking package, IEEE 14th Topical Meeting on Electrical Performance of Electronic Packaging, 2005., IEEE,

2005, pp. 151-154.

[19] I. Qin, O. Yauw, G. Schulze, A. Shah, B. Chylak, N. Wong, Advances in wire bonding technology for 3D die stacking and fan out wafer level package, 2017 IEEE 67th Electronic Components and Technology Conference (ECTC), IEEE, 2017, pp. 1309-1315.

[20] C.-C. Lee, C. Hung, C. Cheung, P.-F. Yang, C.-L. Kao, D.-L. Chen, M.-K. Shih, C.-L.C. Chien, Y.-H. Hsiao, L.-C. Chen, An overview of the development of a GPU with integrated HBM on silicon interposer, 2016 IEEE 66th Electronic Components and Technology Conference (ECTC), IEEE, 2016, pp. 1439-1444.

[21] W. Koh, System in package (SiP) technology applications, 2005 6th International Conference on Electronic Packaging Technology, IEEE, 2005, pp. 61-66.

[22] W. Ki, W. Lee, I. MoK, I. Lee, W. Do, M. Kolbehdari, A. Copia, S. Jayaraman, C. Zwenger, K. Lee, Chip stackable, ultra-thin, high-flexibility 3D FOWLP (3D SWIFT® Technology) for hetero-integrated advanced 3D WL-SiP, 2018 IEEE 68th Electronic Components and Technology Conference (ECTC), IEEE, 2018, pp. 580-586.

[23] R. Chanchani, 3D integration technologies–an overview, Materials for Advanced Packaging, Springer2009, pp. 1-50.

[24] N.-C. Lee, Reflow soldering processes, Elsevier2002.

[25] G. Humpston, D.M. Jacobson, Principles of soldering, ASM international2004.

[26] M. Schaefer, R.A. Fournelle, J. Liang, Theory for intermetallic phase growth between Cu and liquid Sn-Pb solder based on grain boundary diffusion control, Journal of Electronic Materials 27(11) (1998) 1167-1176.

[27] J.-H. Lee, D. Park, J.-T. Moon, Y.-H. Lee, D.-H. Shin, Y.-S. Kim, Characteristics of the Sn-Pb eutectic solder bump formed via fluxless laser reflow soldering, Journal of electronic materials 29(10) (2000) 1153-1159.

[28] M. Abtew, G. Selvaduray, Lead-free solders in microelectronics, Materials Science and Engineering: R: Reports 27(5-6) (2000) 95-141.

[29] S. Cheng, C.-M. Huang, M. Pecht, A review of lead-free solders for electronics

applications, Microelectronics Reliability 75 (2017) 77-95.

[30] E.E. Mhd Noor, N.F. Mhd Nasir, S.R.A. Idris, A review: lead free solder and its wettability properties, Soldering & Surface Mount Technology 28(3) (2016) 125-132.

[31] M. Harrison, J. Vincent, H. Steen, Lead-free reflow soldering for electronics assembly, Soldering & Surface Mount Technology 13(3) (2001) 21-38.

[32] H. Ma, J.C. Suhling, A review of mechanical properties of lead-free solders for electronic packaging, Journal of materials science 44(5) (2009) 1141-1158.

[33] Y. Li, K.-s. Moon, C. Wong, Electronics without lead, Science 308(5727) (2005) 1419-1420.

[34] N.-C. Lee, Lead-free soldering-where the world is going, Citeseer2000.

[35] J. Bath, Lead-free soldering, Springer Science & Business Media2007.

[36] X. Tong, J. Shi, Y. Zhou, Greening of supply chain in developing countries: Diffusion of lead (Pb)-free soldering in ICT manufacturers in China, Ecological Economics 83 (2012) 174-182.

[37] Y. Fukuda, M.G. Pecht, K. Fukuda, S. Fukuda, Lead-free soldering in the Japanese electronics industry, IEEE transactions on components and packaging technologies 26(3) (2003) 616-624.

[38] T. Lee, W. Choi, K. Tu, J. Jang, S. Kuo, J. Lin, D. Frear, K. Zeng, J. Kivilahti, Morphology, kinetics, and thermodynamics of solid-state aging of eutectic SnPb and Pb-free solders (Sn–3.5 Ag, Sn–3.8 Ag–0.7 Cu and Sn–0.7 Cu) on Cu, Journal of Materials Research 17(2) (2002) 291-301.

[39] M. McCormack, S. Jin, G. Kammlott, H. Chen, New Pb-free solder alloy with superior mechanical properties, Applied Physics Letters 63(1) (1993) 15-17.

[40] J. Shen, Y. Liu, H. Gao, C. Wei, Y. Yang, Formation of bulk Ag 3 Sn intermetallic compounds in Sn-Ag lead-free solders in solidification, Journal of electronic materials 34(12) (2005) 1591-1597.

[41] K.-S. Bae, S.-J. Kim, Microstructure and adhesion properties of Sn–0.7 Cu/Cu solder joints, Journal of materials research 17(4) (2002) 743-746.

[42] M. Rizvi, C. Bailey, Y. Chan, M. Islam, H. Lu, Effect of adding 0.3 wt% Ni into the Sn–0.7 wt% Cu solder: Part II. Growth of intermetallic layer with Cu during wetting and aging, Journal of Alloys and Compounds 438(1-2) (2007) 122-128.

[43] N.-C. Lee, Lead-Free Soldering, Materials for Advanced Packaging (2016) 199-236.

[44] S. Zhou, O. Mokhtari, M.G. Rafique, V.C. Shunmugasamy, B. Mansoor, H. Nishikawa, Improvement in the mechanical properties of eutectic Sn58Bi alloy by 0.5 and 1 wt% Zn addition before and after thermal aging, Journal of Alloys and Compounds 765 (2018) 1243-1252.

[45] J. Morris, J.F. Goldstein, Z. Mei, Microstructure and mechanical properties of Sn-In and Sn-Bi solders, JOM 45(7) (1993) 25-27.

[46] Z. Mei, J. Morris, Characterization of eutectic Sn-Bi solder joints, Journal of Electronic Materials 21(6) (1992) 599-607.

[47] J. Glazer, Metallurgy of low temperature Pb-free solders for electronic assembly, International Materials Reviews 40(2) (1995) 65-93.

[48] K. Kim, S. Huh, K. Suganuma, Effects of intermetallic compounds on properties of Sn–Ag–Cu lead-free soldered joints, Journal of Alloys and compounds 352(1-2) (2003) 226-236.

[49] J.-W. Yoon, B.-I. Noh, B.-K. Kim, C.-C. Shur, S.-B. Jung, Wettability and interfacial reactions of Sn–Ag–Cu/Cu and Sn–Ag–Ni/Cu solder joints, Journal of alloys and compounds 486(1-2) (2009) 142-147.

[50] T. Matsumoto, K. Nogi, Wetting in soldering and microelectronics, Annu. Rev. Mater. Res. 38 (2008) 251-273.

[51] M. Hosking, F.G. Yost, The mechanics of solder alloy wetting and spreading, Springer Science & Business Media2012.

[52] N.C. Lee, Lead-free soldering, Materials for Advanced Packaging, Springer2009, pp. 181-218.

[53] A.L. Moore, L. Shi, Emerging challenges and materials for thermal management

of electronics, Materials today 17(4) (2014) 163-174.

[54] P. Kim, K. Tu, Morphology of wetting reaction of eutectic SnPb solder on Au foils, Journal of Applied Physics 80(7) (1996) 3822-3827.

[55] K. Suganuma, K. Niihara, T. Shoutoku, Y. Nakamura, Wetting and interface microstructure between Sn–Zn binary alloys and Cu, Journal of Materials Research 13(10) (1998) 2859-2865.

[56] K. Tu, T. Lee, J. Jang, L. Li, D. Frear, K. Zeng, J. Kivilahti, Wetting reaction versus solid state aging of eutectic SnPb on Cu, Journal of Applied Physics 89(9) (2001) 4843-4849.

[57] O. Dezellus, F. Hodaj, N. Eustathopoulos, Progress in modelling of chemical-reaction limited wetting, Journal of the European Ceramic Society 23(15) (2003) 2797-2803.

[58] G. Kumar, K.N. Prabhu, Review of non-reactive and reactive wetting of liquids on surfaces, Advances in colloid and interface science 133(2) (2007) 61-89.

[59] K. Hermansson, U. Lindberg, B. Hok, G. Palmskog, Wetting properties of silicon surfaces, TRANSDUCERS'91: 1991 International Conference on Solid-State Sensors and Actuators. Digest of Technical Papers, IEEE, 1991, pp. 193-196.

[60] X. Zhou, J.T.M. De Hosson, Reactive wetting of liquid metals on ceramic substrates, Acta Materialia 44(2) (1996) 421-426.

[61] N. Eustathopoulos, Dynamics of wetting in reactive metal/ceramic systems, Acta Materialia 46(7) (1998) 2319-2327.

[62] H. Wang, F. Gao, X. Ma, Y. Qian, Reactive wetting of solders on Cu and Cu6Sn5/Cu3Sn/Cu substrates using wetting balance, Scripta materialia 55(9) (2006) 823-826.

[63] R. Voytovych, A. Koltsov, F. Hodaj, N. Eustathopoulos, Reactive vs non-reactive wetting of ZrB2 by azeotropic Au–Ni, Acta Materialia 55(18) (2007) 6316-6321.

[64] K. Wang, F. Wang, Y. Huang, K. Qi, Comprehensive Properties of a Novel Quaternary Sn-Bi-Sb-Ag Solder: Wettability, Interfacial Structure and Mechanical

Properties, Metals 9(7) (2019) 791.

[65] C.-Y. Ho, J.-G. Duh, Wetting kinetics and wettability enhancement of Pd added electrolytic Ni surface with molten Sn–3.0 Ag–0.5 Cu solder, Materials Letters 92 (2013) 278-280.

[66] D. Frear, Solder mechanics: a state of the art assessment, Tms1991.

[67] C.-T. Lin, K.-L. Lin, Contact angle of 63Sn–37Pb and Pb-free solder on Cu plating, Applied surface science 214(1-4) (2003) 243-258.

[68] Y. Plevachuk, W. Hoyer, I. Kaban, M. Köhler, R. Novakovic, Experimental study of density, surface tension, and contact angle of Sn–Sb-based alloys for high temperature soldering, Journal of materials science 45(8) (2010) 2051-2056.

[69] M.F. Arenas, V.L. Acoff, Contact angle measurements of Sn-Ag and Sn-Cu lead-free solders on copper substrates, Journal of Electronic Materials 33(12) (2004) 1452.

[70] O. Dezellus, F. Hodaj, N. Eustathopoulos, Chemical reaction-limited spreading: the triple line velocity versus contact angle relation, Acta Materialia 50(19) (2002) 4741-4753.

[71] B. He, J. Lee, N.A. Patankar, Contact angle hysteresis on rough hydrophobic surfaces, Colloids and Surfaces A: Physicochemical and Engineering Aspects 248(1-3) (2004) 101-104.

[72] N. Adam, Use of the term ‘Young's Equation’for contact angles, Nature 180(4590) (1957) 809-810.

[73] C.C. Lee, J. Kim, Fundamentals of fluxless soldering technology, Proceedings. International Symposium on Advanced Packaging Materials: Processes, Properties and Interfaces, 2005., IEEE, 2005, pp. 33-38.

[74] C. Liu, H. Kim, K. Tu, P. Totta, Dewetting of molten Sn on Au/Cu/Cr thin-film metallization, Applied physics letters 69(26) (1996) 4014-4016.

[75] S. Zhang, Y. Zhang, H. Wang, Effect of oxide thickness of solder powders on the coalescence of SnAgCu lead-free solder pastes, Journal of Alloys and Compounds 487(1-2) (2009) 682-686.

[76] M. Batzill, U. Diebold, The surface and materials science of tin oxide, Progress in surface science 79(2-4) (2005) 47-154.

[77] O. Mokhtari, F. Conti, S.K. Bhogaraju, M. Meier, H. Schweigart, U. Tetzlaff, G. Elger, Characterization of tin-oxides and tin-formate crystals obtained from SnAgCu solder alloy under formic acid vapor, New Journal of Chemistry (2019).

[78] A. Hanss, M. Hutter, J. Trodler, G. Elger, Solder process for fluxless solder paste applications, Electronic Components and Technology Conference (ECTC), 2016 IEEE 66th, IEEE, 2016, pp. 447-454.

[79] A. Hanss, G. Elger, Residual free solder process for fluxless solder pastes, Soldering & Surface Mount Technology 30(2) (2018) 118-128.

[80] I. Fawcett, A. Taylor, J. Pepys, Asthma due to inhaled chemical agents--fumes from'Multicore'soldering flux and colophony resin, Clinical Allergy 6(6) (1976) 577-585.

[81] C.T. Mathias, R.M. Adams, Allergic contact dermatitis from rosin used as soldering flux, Journal of the American Academy of Dermatology 10(3) (1984) 454-456.

[82] V. Lopez, A. Kennedy, Flux-assisted wetting and spreading of Al on TiC, Journal of colloid and interface science 298(1) (2006) 356-362.

[83] A. Siewiorek, A. Kudyba, N. Sobczak, M. Homa, Z. Huber, Z. Adamek, J. Wojewoda-Budka, Effects of PCB substrate surface finish and flux on solderability of lead-free SAC305 alloy, Journal of Materials Engineering and Performance 22(8) (2013) 2247-2252.

[84] G. Kumar, K.N. Prabhu, Wetting behavior of solders, Journal of ASTM International 7(5) (2010) 1-18.

[85] P. Baumli, J. Sychev, I. Budai, J. Szabo, G. Kaptay, Fabrication of carbon fiber reinforced aluminum matrix composites via a titanium-ion containing flux, Composites Part A: Applied Science and Manufacturing 44 (2013) 47-50.

[86] D. Peebles, H. Peebles, J. Ohlhausen, Kinetics of the isothermal spreading of tin

on the air-passivated copper surface in the absence of a fluxing agent, Colloids and Surfaces A: Physicochemical and Engineering Aspects 144(1-3) (1998) 89-114.

[87] F. Gao, K. Rajathurai, Q. Cui, G. Zhou, I. NkengforAcha, Z. Gu, Effect of surface oxide on the melting behavior of lead-free solder nanowires and nanorods, Applied Surface Science 258(19) (2012) 7507-7514.

[88] W. Lin, Y. Lee, Study of fluxless soldering using formic acid vapor, IEEE transactions on Advanced Packaging 22(4) (1999) 592-601.

[89] K.S. Hansen, M.S. Jellesen, P. Moller, P.J.S. Westermann, R. Ambat, Effect of solder flux residues on corrosion of electronics, 2009 Annual Reliability and Maintainability Symposium, IEEE, 2009, pp. 502-508.

[90] R. Diehm, M. Nowottnick, U. Pape, Reduction of voids in solder joints an alternative to vacuum soldering, Proc. of the IPC APEX EXPO, San Diego, CA 28 (2012).

[91] A. Hanss, M. Schmid, S.K. Bhogaraju, F. Conti, G. Elger, Process development and reliability of sintered high power chip size packages and flip chip LEDs, Electronics Packaging and iMAPS All Asia Conference (ICEP-IAAC), 2018 International Conference on, IEEE, 2018, pp. 479-484.

[92] Q.-B. Lu, L. Sanche, Effects of cosmic rays on atmospheric chlorofluorocarbon dissociation and ozone depletion, Physical Review Letters 87(7) (2001) 078501.

[93] O. Badr, S. Probert, P. O'Callaghan, Chlorofluorocarbons and the environment: scientific, economic, social and political issues, Applied energy 37(4) (1990) 247-327.

[94] M. Lippmann, Health effects of ozone a critical review, Japca 39(5) (1989) 672-695.

[95] F.R. De Gruijl, J. Longstreth, M. Norval, A.P. Cullen, H. Slaper, M.L. Kripke, Y. Takizawa, J.C. van der Leun, Health effects from stratospheric ozone depletion and interactions with climate change, Photochemical & Photobiological Sciences 2(1) (2003) 16-28.

[96] R.S. Stolarski, R.J. Cicerone, Stratospheric chlorine: a possible sink for ozone,

Canadian journal of Chemistry 52(8) (1974) 1610-1615.

[97] P.J. Crutzen, Chlorofluoromethanes: threats to the ozone layer, Reviews of Geophysics 17(7) (1979) 1824-1832.

[98] F.S. Rowland, Chlorofluorocarbons and the depletion of stratospheric ozone, American Scientist 77(1) (1989) 36-45.

[99] K.P. Bowman, Global trends in total ozone, Science 239(4835) (1988) 48-50.

[100] C. Goh, Occupational dermatitis from soldering flux among workers in the electronics industry, Contact Dermatitis 13(2) (1985) 85-90.

[101] K. Crow, R. Harman, H. Holden, Amine flux sensitization dermatitis in electricity cable jointers, British Journal of Dermatology 80(11) (1968) 701-710.

[102] K. YOKOTA, T. MINAMI, H. MICHITSUJI, T. FUJIO, S. YAMADA, Occupational dermatitis from soldering flux, Industrial health 42(3) (2004) 383-384.

[103] T. Mathias, Contact Allergy to Colophony in Soldering Flux, Journal of Occupational and Environmental Medicine 25(12) (1983) 902.

[104] C. Chelton, M. Glowatz, J. Mosovsky, Chemical hazards in the semiconductor industry, IEEE Transactions on Education 34(3) (1991) 269-288.

[105] W.J. Ready, L.J. Turbini, A comparison of hourly versus daily testing methods for evaluating the reliability of water soluble fluxes, IEEE transactions on advanced packaging 23(2) (2000) 285-292.

[106] J.A. Jachim, G.B. Freeman, L.J. Turbini, Use of surface insulation resistance and contact angle measurements to characterize the interactions of three water soluble fluxes with FR-4 substrates, IEEE Transactions on Components, Packaging, and Manufacturing Technology: Part B 20(4) (1997) 443-451.

[107] P. Veselý, D. Bušek, O. Krammer, K. Dušek, Analysis of no-clean flux spatter during the soldering process, Journal of Materials Processing Technology 275 (2020) 116289.

[108] D. Bušek, K. Dušek, D. Růžička, M. Plaček, P. Mach, J. Urbánek, J. Starý, Flux effect on void quantity and size in soldered joints, Microelectronics Reliability 60 (2016)

135-140.

[109] K. Dušek, D. Bušek, Problem with no-clean flux spattering on in-circuit testing pads diagnosed by EDS analysis, Microelectronics Reliability 56 (2016) 162-169.

[110] N. Koopman, S. Bobbio, S. Nangalia, J. Bousaba, B. Piekarski, Fluxless soldering in air and nitrogen, Proceedings of IEEE 43rd Electronic Components and Technology Conference (ECTC'93), IEEE, 1993, pp. 595-605.

[111] T. Nishikawa, M. Ijuin, R. Satoh, Y. Iwata, M. Tamura, M. Shirai, Fluxless soldering process technology, 1994 Proceedings. 44th Electronic Components and Technology Conference, IEEE, 1994, pp. 286-292.

[112] C.C. Lee, Y.-C. Chen, G. Matijasevic, R. Metzler, A fluxless oxidation-free bonding technology, 1994 Proceedings. 44th Electronic Components and Technology Conference, IEEE, 1994, pp. 595-599.

[113] C.C. Dong, A. Schwarz, D.V. Roth, Feasibility of fluxless reflow of lead-free solders in hydrogen and forming gas, Nepcon Malaysia 97 (1997) 03-32.

[114] S.-M. Hong, C.-S. Kang, J.-P. Jung, Fluxless Sn-3.5 mass% Ag solder bump flip chip bonding by ultrasonic wave, Materials Transactions 43(6) (2002) 1336-1340.

[115] S.P.-S. Lim, M.Z. Ding, J.K. Lin, V.S. Rao, Development of fluxless flip chip reflow process for high density flip chip interconnect, Electronics Packaging and Technology Conference (EPTC), 2015 IEEE 17th, IEEE, 2015, pp. 1-6.

[116] M. Samson, V. Oberson, I. Paquin, C. Fortin, J.-C. Raymond, C. Bureau, M. Barnes, X. Zhao, D. Wright, Fluxless chip join process using formic acid atmosphere in a continuous mass reflow furnace, Electronic Components and Technology Conference (ECTC), 2016 IEEE 66th, IEEE, 2016, pp. 574-579.

[117] N. Koopman, S. Nangalia, V. Rogers, Fluxless no-clean assembly of solder bumped flip chips, 1996 Proceedings 46th Electronic Components and Technology Conference, IEEE, 1996, pp. 552-558.

[118] S. Nangalia, N. Koopman, V. Rogers, M. Beranek, H. Hager, E. Ledbury, V. Loebs, E. Miao, C. Tang, C. Pico, Fluxless, no clean assembly of optoelectronic devices with

PADS, 1997 Proceedings 47th Electronic Components and Technology Conference, IEEE, 1997, pp. 755-762.

[119] J. Kwon Moon, Y. Zhou, J. Pil Jung, Fluxless plasma bumping of lead-free solders and the reliability effects of under bump metallization thickness, Soldering & surface mount technology 17(2) (2005) 3-9.

[120] K. Sakuma, N. Nagai, J. Mizuno, S. Shoji, Vacuum ultraviolet (VUV) surface treatment process for flip chip and 3-D interconnections, 2009 59th Electronic Components and Technology Conference, IEEE, 2009, pp. 641-647.

[121] K. Sakuma, K. Toriyama, H. Noma, K. Sueoka, N. Unami, J. Mizuno, S. Shoji, Y. Orii, Fluxless bonding for fine-pitch and low-volume solder 3-D interconnections, 2011 IEEE 61st Electronic Components and Technology Conference (ECTC), IEEE, 2011, pp. 7-13.

[122] N. Ozawa, T. Okubo, J. Matsuda, T. Sakai, Sn-and Cu-oxide reduction by formic acid and its application to power module soldering, 2018 IEEE 30th International Symposium on Power Semiconductor Devices and ICs (ISPSD), IEEE, 2018, pp. 248-251.

[123] S. Hu, L. Scudiero, S. Ha, Electronic effect on oxidation of formic acid on supported Pd–Cu bimetallic surface, Electrochimica Acta 83 (2012) 354-358.

[124] F. Conti, A. Hanss, O. Mokhtari, S.K. Bhogaraju, G. Elger, Formation of tin-based crystals from a SnAgCu alloy under formic acid vapor, New Journal of Chemistry 42(23) (2018) 19232-19236.

[125] S. He, H. Nishikawa, Effect of substrate metallization on the impact strength of Sn-Ag-Cu solder bumps fabricated in a formic acid atmosphere, Electronics Packaging (ICEP), 2017 International Conference on, IEEE, 2017, pp. 381-385.

[126] R. Gao, S. He, Y.-A. Shen, H. Nishikawa, Effect of Substrates on Fracture Mechanism and Process Optimization of Oxidation–Reduction Bonding with Copper Microparticles, Journal of Electronic Materials 48(4) (2019) 2263-2271.

[127] C.C. Dong, R.E. Patrick, R.A. Siminski, T. Bao, Fluxless soldering in activated

hydrogen atmosphere, 2016 China Semiconductor Technology International Conference (CSTIC), IEEE, 2016, pp. 1-3.

[128] A.K. Singh, S. Singh, A. Kumar, Hydrogen energy future with formic acid: a renewable chemical hydrogen storage system, Catalysis Science & Technology 6(1) (2016) 12-40.

[129] S. He, R. Gao, J. Li, Y.-A. Shen, H. Nishikawa, In-situ observation of fluxless soldering of Sn-3.0 Ag-0.5 Cu/Cu under a formic acid atmosphere, Materials Chemistry and Physics (2019) 122309.

[130] W. Yang, Y. Lu, C. Zhou, J. Zhang, T. Suga, Study of Cu Film Surface Treatment Using Formic Acid Vapor/Solution for Low Temperature Bonding, Journal of The Electrochemical Society 165(4) (2018) H3080-H3084.

[131] F. Conti, A. Hanss, O. Mokhtari, S.K. Bhogaraju, G. Elger, Formation of tin-based crystals from SnAgCu alloy under formic acid vapor, New Journal of Chemistry (2018).

[132] C. Dong, G. Arslenian, Fluxless soldering of flip chip assemblies, Nepcon West, 1996, pp. 96-112.

[133] W. Yang, C. Zhou, J. Zhou, Y. Lu, Y. Lu, T. Suga, Cu film surface reduction through formic acid vapor/solution for 3-D interconnection, 2018 19th International Conference on Electronic Packaging Technology (ICEPT), IEEE, 2018, pp. 1378-1381.

[134] P.-W. Chou, J.-M. Song, Z.-Y. Xie, M. Akaike, T. Suga, M. Fujino, J.-Y. Lin, Low temperature de-oxidation for copper surface by catalyzed formic acid vapor, Applied Surface Science 456 (2018) 890-898.

[135] Z. Jiang, P. Qin, T. Fang, Decomposition mechanism of formic acid on Cu (111) surface: A theoretical study, Applied Surface Science 396 (2017) 857-864.

[136] J. Liu, H. Chen, H. Ji, M. Li, Highly Conductive Cu–Cu Joint Formation by Low-Temperature Sintering of Formic Acid-Treated Cu Nanoparticles, ACS applied materials & interfaces 8(48) (2016) 33289-33298.

[137] T. Suga, A. Masakate, W. Yang, N. Matsuoka, Formic acid treatment with Pt

catalyst for Cu direct bonding at low temperature, Electronics Packaging (ICEP), 2014 International Conference on, IEEE, 2014, pp. 644-647.

[138] J.S. Yoo, F. Abild-Pedersen, J.K. Nørskov, F. Studt, Theoretical analysis of transition-metal catalysts for formic acid decomposition, Acs Catalysis 4(4) (2014) 1226-1233.

[139] W. Yang, M. Akaike, T. Suga, Effect of formic acid vapor in situ treatment process on Cu low-temperature bonding, IEEE Transactions on Components, Packaging and Manufacturing Technology 4(6) (2014) 951-956.

[140] M. Monta, K. Okiyama, T. Sakai, N. Imaizumi, Formation of solder cap on Cu pillar bump using formic acid reduction, 2012 IEEE 14th Electronics Packaging Technology Conference (EPTC), IEEE, 2012, pp. 602-607.

[141] S. Koyama, Y. Aoki, I. Shohji, Effect of formic acid surface modification on bond strength of solid-state bonded interface of tin and copper, Materials transactions 51(10) (2010) 1759-1763.

[142] T. Youngs, S. Haq, M. Bowker, Formic acid adsorption and oxidation on Cu (1 1 0), Surface Science 602(10) (2008) 1775-1782.

[143] S. Poulston, E. Rowbotham, P. Stone, P. Parlett, M. Bowker, Temperature-programmed desorption studies of methanol and formic acid decomposition on copper oxide surfaces, Catalysis letters 52(1-2) (1998) 63-67.

[144] S. Poulston, R.A. Bennett, A.H. Jones, M. Bowker, STM study of formic acid adsorption on Cu (110), Physical Review B 55(19) (1997) 12888.

[145] M. Bowker, E. Rowbotham, F. Leibsle, S. Haq, The adsorption and decomposition of formic acid on Cu {110}, Surface science 349(2) (1996) 97-110.

Chapter 2

In-situ observation of fluxless soldering of Sn-3.0Ag-0.5Cu/Cu under a formic acid atmosphere

2.1 Introduction

The soldering process under a formic acid (FA) atmosphere is a promising method in various fluxless soldering technologies[1-4], as mentioned in **Chapter 1**. However, most publications on soldering under a formic acid atmosphere have focused only on the soldering results[4-6], such as final contact angle results or mechanical properties; no parametric studies have been performed to identify the optimal processing conditions.

In this chapter, the effects of heating processes on the wetting behavior of Sn-Ag-Cu solder on a Cu pad under a FA atmosphere were observed in situ. The effect of FA on

the interfacial reaction between the solder and Cu substrate was also confirmed.

2.2 Experimental

2.2.1 Wettability test

For the wettability test, Sn-3.0mass% Ag-0.5mass% Cu (SAC305) solder balls (diameter: 0.76 mm) and Cu substrates (dimensions: 15 mm x 15 mm x 0.5 mm) were prepared, as shown in **Fig. 2.1(a)**. Formic acid gas (5 vol.% formic acid + 95 vol.% N_2) was used as the reduction atmosphere for the fluxless soldering process. Formic acid gas was supplied by nitrogen gas through liquid formic acid stored in a sealed beaker, as shown in **Fig. 2.2**. The formic acid gas flow was initiated 5 min prior to heating and was continued throughout the heating process at a flow rate at 2 L/min. To investigate the effect of heating condition on the wettability of the solder balls on the Cu solid substrate under a formic acid atmosphere, five fluxless heating processes were tested under a FA atmosphere with different peak heating times and temperatures, as shown in **Table 2.1**. As a reference heating process using liquid rosin mildly activated (RMA) flux (without formic acid) was used, as shown in **Fig. 2.3**.

The contact angle and spreading rate are important parameters in characterizing the wettability of a liquid on a solid. The contact angle formed at the interface between the solder and substrate was measured using a three-dimensional laser scanning confocal microscope (VK-9710, KEYENCE), as shown in **Fig. 2.4**. The blue section in **Fig. 2.4(a)** represents the center of the wetted solder. Because the contact angle formed at the interface between the solder and substrate plus this angle is equal to 180° (see **Fig. 2.4(b)**), the contact angle could be calculated as:

$$\theta = 180° - \theta_m \quad (1)$$

Where θ_m is the measured angle. Three samples for each condition were prepared for the wettability test. The front, rear, left, and right side of each sample were all measured. Thus, the average contact angle was determined using a total 12 sides. The spreading rate of each solder was calculated according to the Japanese Industrial Standard (JIS Z

3198–3, 2003), as per the following equation:

$$S_R = \frac{D-H}{D} \times 100\% \quad (2)$$

where S_R is the spreading rate (%), H is the height of spread solder (mm), D is the diameter when the solder sample used for the test is considered spherical (mm), and V is the volume of the solder used for the test. However, because of the shallow depth of field of the side view optical charge-couple device camera, the height of the solder cannot be measured accurately. Hence, the change of spread area radius of solder was used to evaluate the spreading rate. The solder spreading area, which needs to be measured to calculate the radius during the wetting process, was recorded in situ at a frame rate of 1 s^{-1} in the top view using a video camera to evaluate the wetting rate of solder on the Cu substrate. The spreading area of the wetting solder ball was measured using ImageJ software. Elemental compositions were identified by field-emission electron probe micro-analysis (EPMA, JEOL JXA-8530F).

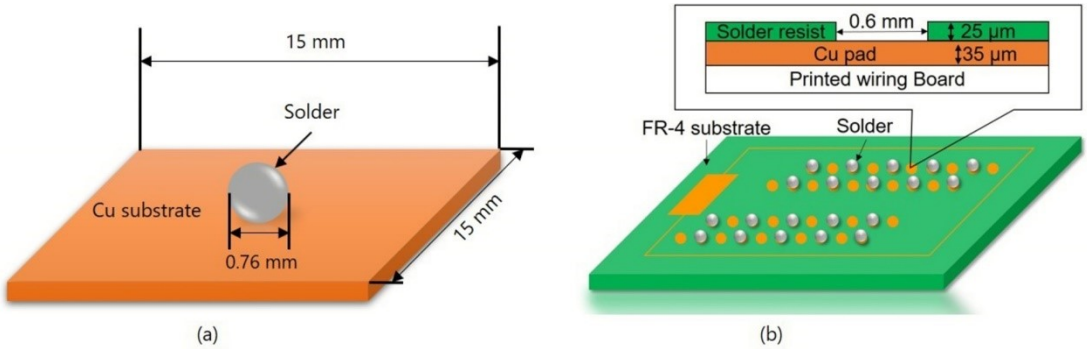

Fig. 2.1 *Schematic diagram of (a) Cu substrate using for wettability test and (b) FR-4 substrate with Cu pads for soldering process.*

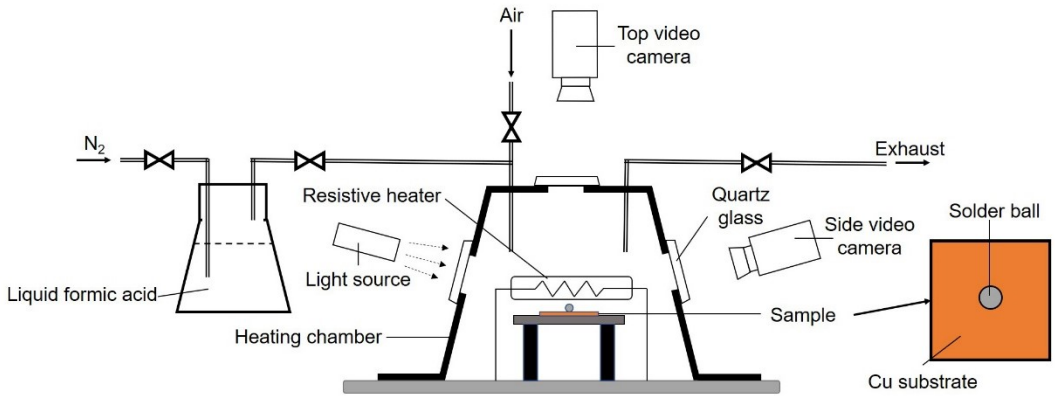

Fig. 2.2 *Schematic diagram of heating equipment for wettability test.*

Table 2.1 *Summary of heating processes using formic acid atmosphere*

Heating process	**1**	**2**	**3**	**4**	**5**
Pre-heat temperature (°C)	110	110	110	110	110
Pre-time (s)	60	60	60	60	60
Peak heating temperature (°C)	250	250	250	270	290
Peak heating time (s)	120	300	600	120	120
Heating rate (°C/s)	2.5	2.5	2.5	2.5	2.5

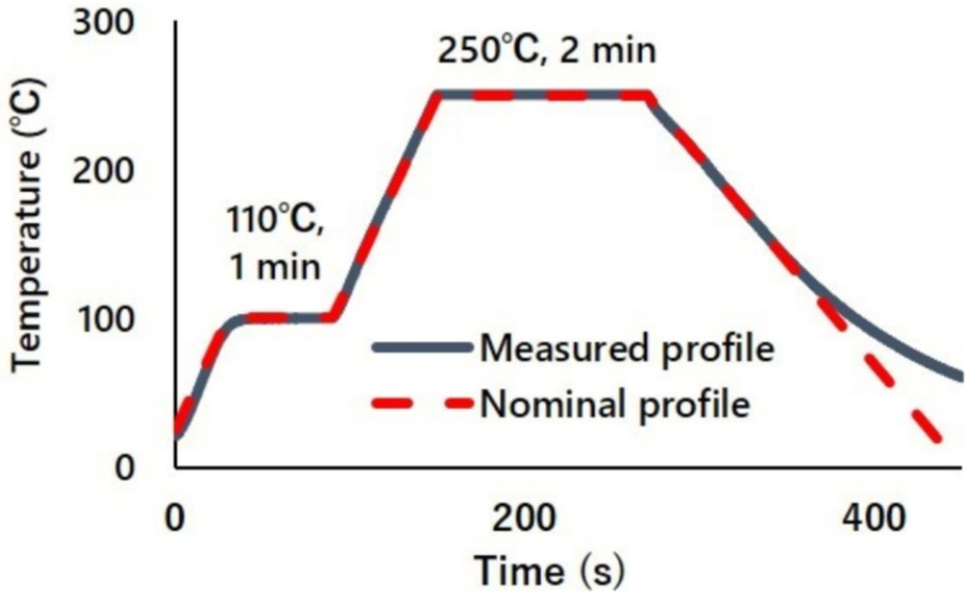

Fig. 2.3 *Heating process for soldering using liquid RMA flux.*

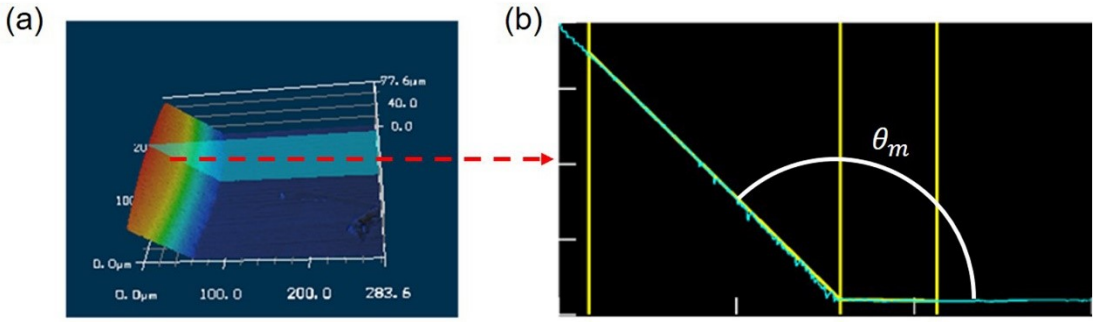

Fig. 2.4 *Schematic graph of (a) typical three-dimensional scan result of solder surface forming an angle with substrate surface and (b) sectional view of the section in (a) using three-dimensional laser scanning confocal microscope.*

2.2.2 Soldering process

Cu pads with a thickness of 35 μm and diameter of 0.6 mm were fabricated on an FR-4 printed wiring board and used as the substrate for the soldering process (**Fig. 2.1 (b)**). As pre-treatment before soldering, the Cu pads were immersed in a 4% HCl solution for 120 s. Then, the solder balls and Cu pads were ultrasonically rinsed in an ethanol solution for 300 s. After that, the SAC305 balls were soldered on the Cu pads by applying a formic acid atmosphere or liquid flux under nitrogen atmosphere using the heating process shown in **Fig. 2.3** (identical to process 1). A morphological study of the microstructure was performed using field-emission scanning electron microscopy (FE-SEM, Hitachi SU-70).

2.3 Results and discussion

2.3.1 Wettability test

2.3.1.1 Contact angle analysis

The equilibrium contact angle was determined by balancing the surface tensions according to Young's equation[5]:

$$\gamma_{SG} - \gamma_{SL} - \gamma_{LG} \cos\theta = 0 \qquad (3)$$

where γ_{SG} is the surface tension at the interface of the solid and vapor phases, γ_{SL}

is the surface tension at the solid and liquid phases, γ_{LG} is the surface tension at the liquid and vapor phases, and θ is the contact angle, as shown in **Fig. 2.5**. In this study, the solder was the liquid phase, the Cu substrate was the solid phase, and the atmosphere (formic acid or nitrogen) was the vapor phase.

Young's equation is based upon the hypothesis of an ideal surface(smooth, homogeneous, rigid and insoluble) under thermodynamic equilibrium. The process of wetting and spreading involves the flow of liquid on the surface of the substrate. This flow is affected by a number of factors such as the viscosity of the molten solder and the reaction between the solder and substrate.

Table 2.2 presents the contact angles of the SAC305 solders on the Cu substrates with different peak heating times and temperatures. The results indicate that both the solders by the fluxless FA process and reference solder by liquid flux process (denoted as FA and RMA solders, respectively) were able to wet on the Cu substrate within 2 min at 250 °C. Under the same heating conditions, the contact angle of the FA solder was similar than that of the RMA solder.

For the FA solders, the contact angle decreased as the heating peak time. The wetting of a molten solder on solid Cu is a typical reactive wetting process, in which an IMC usually forms. However, the Cu substrate is vulnerable to oxidation, forms a high melting point Cu oxide film, which unable to be wetted by the solder[5, 7, 8]. Therefore, reduction of the Cu oxide film is critical for wetting.

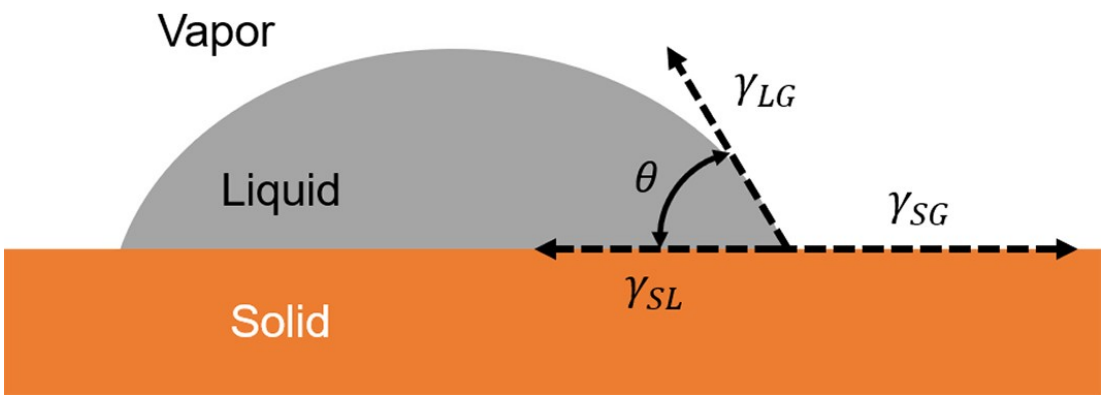

Fig. 2.5 *Schematic of a sessile-drop contact angle system.*

Conti et al.[9] suggested a possible two-step reaction for a general metal oxide (MO) in the presence of formic acid vapor. In the first step, MO reacts with formic acid (HCOOH) to produce a metal formate (**Eq. 4**):

$$HCOOH_{(g)} + MO_{(s)} \longrightarrow M(COOH)_{(s)} + H_2O_{(g)} \quad (4)$$

In the second step, the metal formate decomposes (**Eq.5**):

$$M(COOH)_{(s)} \longrightarrow M_{(s)} + CO_{2(g)} + H_{2(g)} \quad (5)$$

Oxidized Cu require temperatures range from 215 °C to 256 °C to reduce by FA[9], the temperature latter is higher than the melting point of the SAC305 solder. The results suggest that the decomposition of Cu formate is a continuous process instead of an instantaneous one[10, 11]. Therefore, the increase in peak heating time promotes the reduction of the Cu oxide film and the decomposition of Cu formates. It is a common observation that increasing the system temperature improves wettability[12], because the viscosity and surface tension of the liquid solder decrease with increasing temperature, unless the temperature is extremely high[13, 14]. Hence, even in reactive wetting systems, the diffusion rate increases with temperature[15]. As indicated in **Table 2.2**, the contact angles obtained by process 1 (250 °C), process 4 (270 °C), and process 5 (290 °C) indicate that the contact angle decreases as the peak temperature increases under a formic acid atmosphere, which matches the literature well.

Table 2.2 *Summary of contact angle results*

	Process 1	**Process 2**	**Process 3**	**Process 4**	**Process 5**	**Flux**
Contact angle (°)	43.34	42.05	39.66	36.33	35.37	41.24

2.3.1.2 Spreading rate analysis

As mentioned in **Section 2.3.1.1**, Young's equation assumes an ideally smooth, homogeneous and isotropic surface, while for practical surfaces, a range of contact angles exist along the contact line of a static drop[16-21]. This phenomenon, known as contact angle hysteresis[22], can affect the average contact angle in some conditions[17]. Contact angle hysteresis usually results from substrate roughness and heterogeneity, impurity adsorption onto the substrate, swelling of the substrate, etc.[17, 22-25]. It has been shown that formic acid adsorbs onto the Cu surface by chemisorption before decomposition of the formate[11], which may result in modification of the Cu surface. Moreover, formic acid has been reported to dissociate into formate[7, 8, 26-29], which has been widely confirmed by other researchers[30-32]. Therefore, the spreading rate should be considered in addition to the average contact angle to better evaluate the wetting behavior of SAC solder/Cu systems under a formic acid atmosphere[33].

Fig. 2.6(a) shows how the spreading area of the FA and RMA solders on Cu substrates changed during the heating process between 218 and 226 °C (heating rate: 2.5 °C/s). The FA solder had a notably spreading area during the initial wetting compared to the RMA solder. The spreading areas are evaluated statistically in **Fig. 2.6(b)**. As shown, the slope of the RMA solder was much higher than that of the FA solders until 1 s later when the maximum spreading area was reached. However, the spreading area of the FA solders increased slowly for the first 60 s and continued increasing at a slower rate for the rest of the process, eventually exceeding that of the RMA solder. This phenomenon may be caused by the continual reduction of the Cu oxide film by formic acid[9, 10]. The FA solders exhibited extremely similar radius-time curves regardless of peak heating time, suggesting that the peak-time conditions barely affect the rate of spreading of the FA solder. **Fig. 2.7** shows the spreading area radius of the FA and RMA solders on the Cu substrate under different peak-temperature conditions and different profiles. As shown, the spreading areas were similar for the

first 13 s at 250, 270, and 290 °C; subsequently, a higher peak-temperature processes had larger spreading areas. The spreading areas were very close at first because the different profiles had similar temperature curves in the beginning, as shown in **Fig. 2.7**. The profiles show that it took approximately 13, 21, and 29 s for the temperature to increase from 218 to 250, 270, and 290 °C, respectively. This suggested that the spreading area of solders increased with increasing peak-temperature under a formic acid atmosphere.

2.3.1.3 Sn steaming phenomenon

In situ observation of the wetting process revealed the formation of residues around the FA solders after reflowing; the substrate color turned to gray, as shown in **Fig. 2.8(a)-(c)**. In contrast, the substrate remained clean when using the RMA solder, as shown in **Fig. 2.8(d)**. The residues are believed to be precipitates of Sn formate, which has been found to evaporate under some condition in previous studies[1, 9, 34]. Specific analysis of Sn steaming phenomenon under a FA atmosphere is shown in **Chapter 4**.

2.3.2 Interfacial reaction

Fig. 2.9 shows the interfaces between the Cu substrate and FA or RMA solders. Scallop-shaped IMCs, which are believed to be Cu_6Sn_5[35, 36], were found at the interface with both type of solder. This suggests that the formic acid atmosphere barely changes the interfacial reaction between the Cu substrate and SAC305 solder. However, some pores were observed near the IMC layer in the FA solders, as shown in **Fig. 2.10**. These pores were caused by the generation of gas from the decomposition of Cu formate during the soldering process. The main reaction between Cu and formic acid and the decomposition of Cu formate are as follows[37]:

$$Cu_{(s)} + 2HCOOH_{(g)} \rightarrow Cu(COOH)_{2(s)} + H_{2(g)} \quad (6)$$

$$CuO_{(s)} + 2HCOOH_{(g)} \rightarrow Cu(COOH)_{2(s)} + H_2O_{(g)} \quad (7)$$

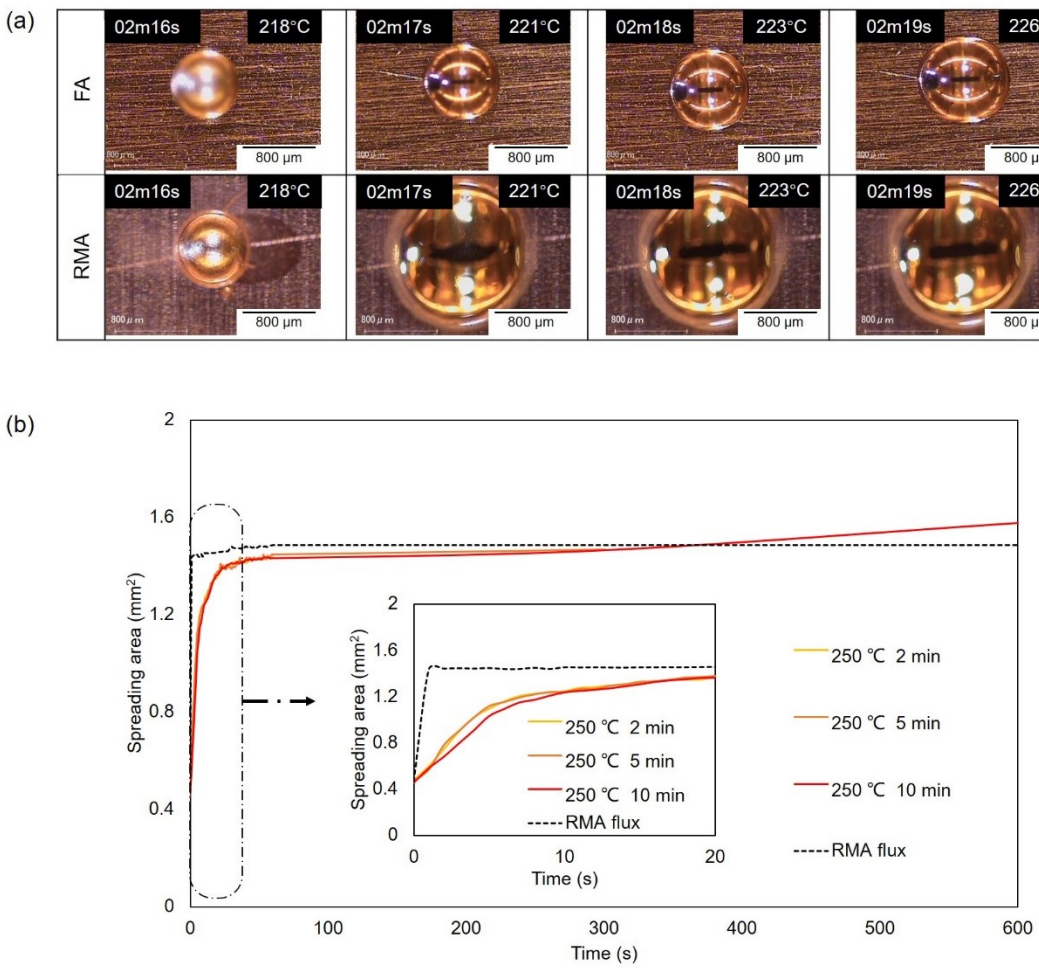

Fig. 2.6 *(a) In situ observation and (b) the statistical data of spreading area of FA and RMA solders wetting Cu substrates.*

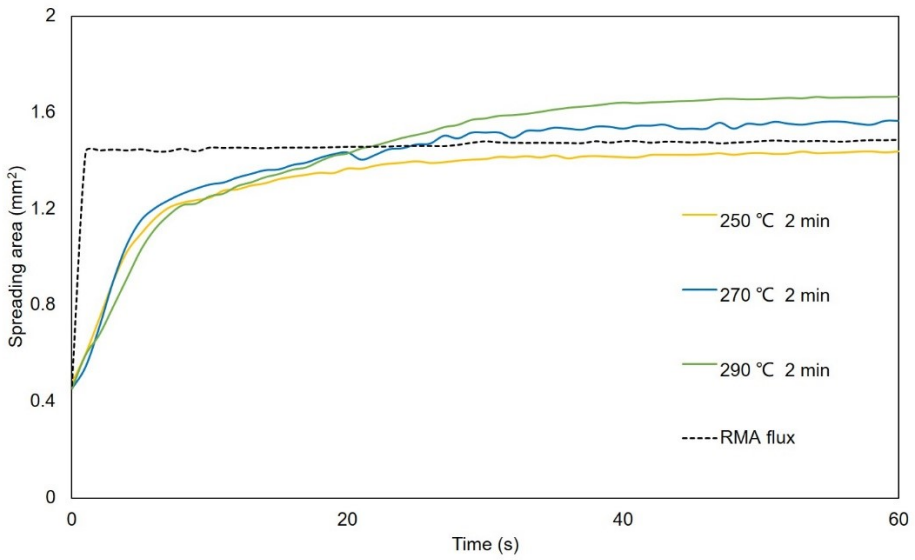

Fig. 2.7 *Effect of peak heating temperature on spreading area of FA and RMA solders on Cu substrate.*

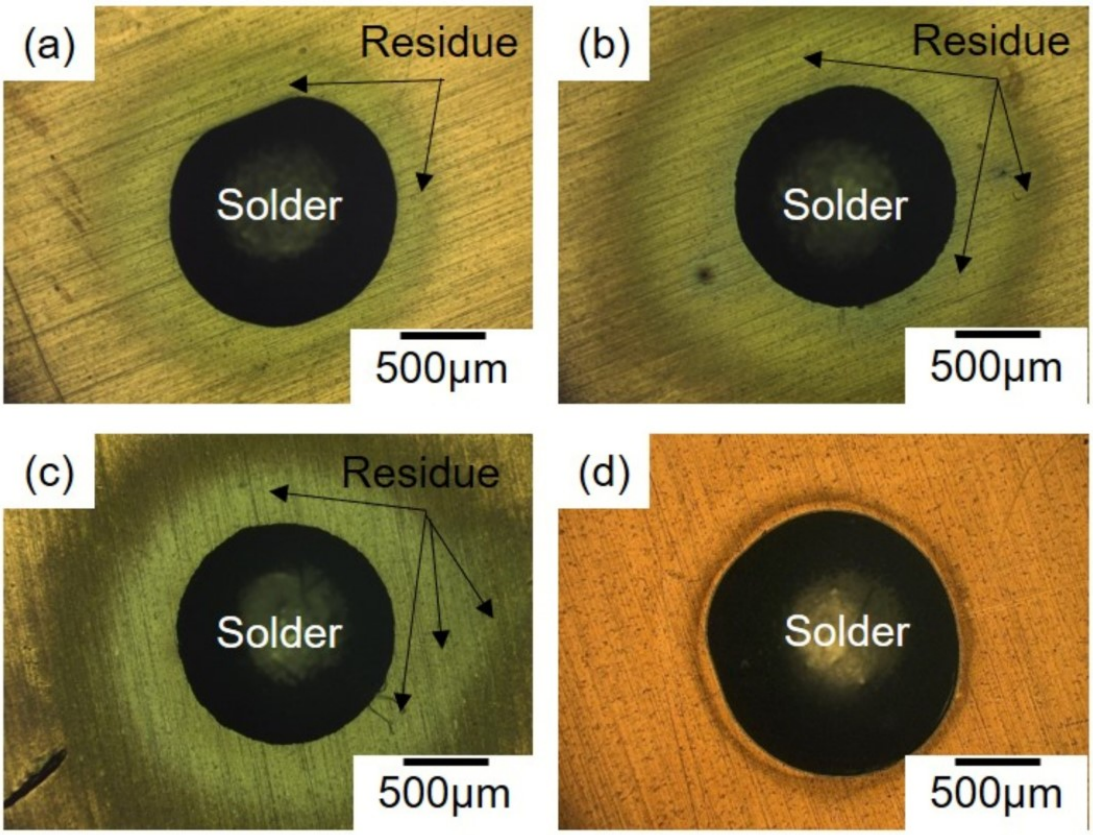

Fig. 2.8 *OM image of residues on Cu substrate at 250 °C heating temperature using FA and RMA solders: (a) 2 min using FA solder; (b) 5 min using FA solder; (c) 10 min using FA solder; (d) 2 min using RMA solder.*

$$CuO_{2(s)} + 2HCOOH_{(g)} \rightarrow Cu(COOH)_{2(s)} + H_{2(g)} + O_{2(g)} \quad (8)$$

$$Cu(COOH)_{2(s)} \rightarrow Cu_{(s)} + H_{2(g)} + CO_{2(g)} \quad (9)$$

To investigate the effects of different heating processes on the pores near the interface, we counted the number of pores in the samples obtained under formic acid with different peak heating times and temperatures (see **Fig. 2.11**). The number of pores barely changed upon extending the peak heating time (process 2 and process 3), whereas a significant decrease was observed when the peak temperature reached 290 °C (process 5). Rozhitsina et al.[38] found that the activation energy of viscous flow of SAC305 eutectic melts decreased when the temperature increased. Therefore, the viscosity of the molten SAC solder decreases at higher peak temperatures, allowing the gas to easily escape.

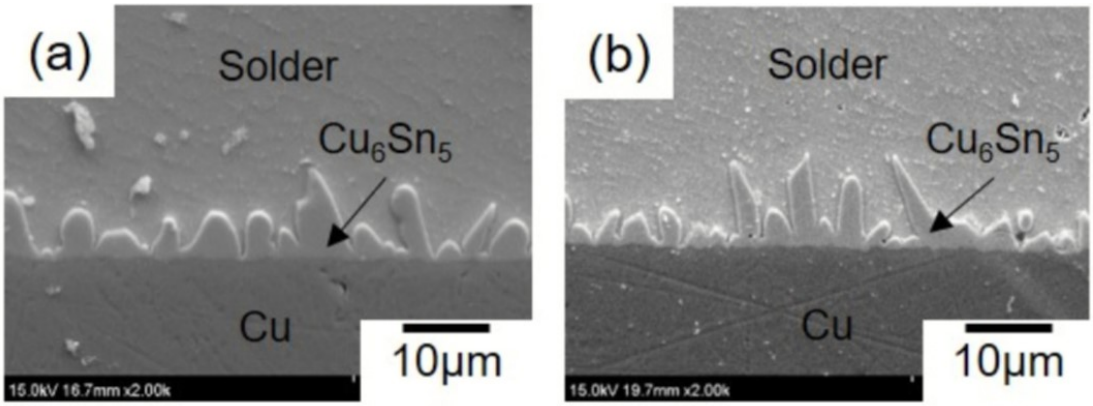

Fig. 2.9 Cross-sectional microstructure of as-reflowed solder bumps on Cu substrate: (a) FA solder and (b) RMA solder.

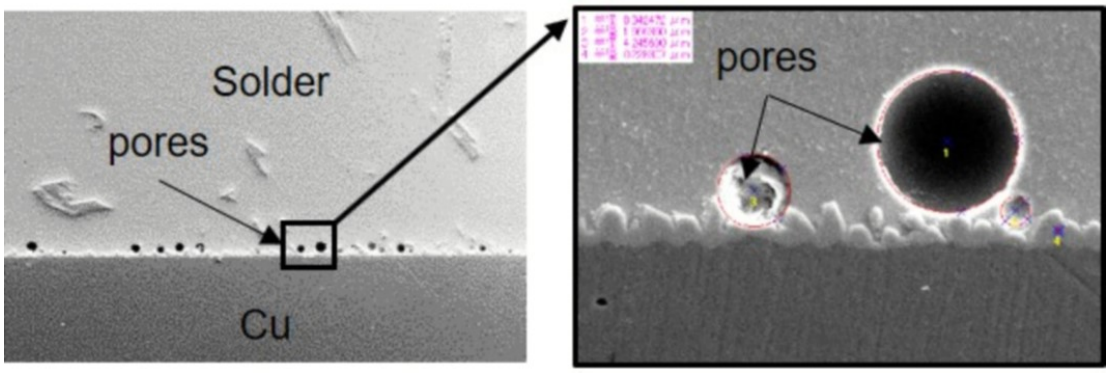

Fig. 2.10 *Cross-sectional SEM image of FA solder bumps.*

2.4 Conclusion

In this chapter, the effects of heating processes on the wettability of SAC305 solders on Cu pads and the interfacial reaction of SAC305 solder bumps on Cu substrates formed under a formic acid atmosphere were investigated.

Under the same heating conditions, the contact angle of the FA solder was similar to that of the RMA solder, whereas the spreading rate was much lower. The difference in spreading rate may be caused by the continuous reduction of the Cu oxide film by a formic acid atmosphere. The wettability of the FA solder increased as the peak heating temperature increased.

Although the substrate remained clean when using the RMA solder, some residues

were found around the FA solders after reflowing. The residues are believed to result from the precipitation of Sn formate.

Some pores were observed near the IMC layers in the FA solders. These pores were caused by the generation of gas from the decomposition of Cu formate during the soldering process. The number of pores decreased significantly when the peak temperature reached at 290 ℃.

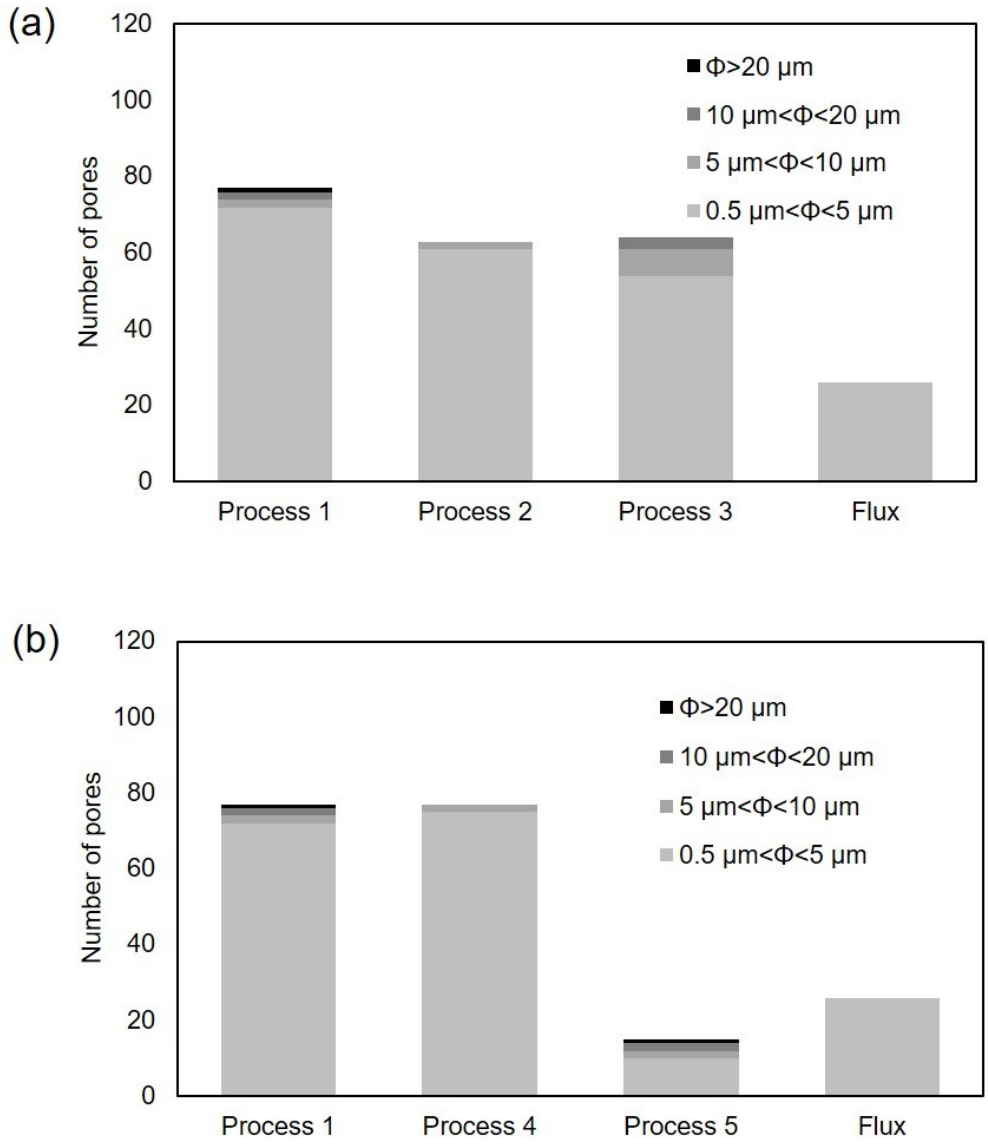

Fig. 2.11 *Effect of (a) peak heating time and (b) peak heating temperature on pore formation.*

Reference

[1] O. Mokhtari, F. Conti, S.K. Bhogaraju, M. Meier, H. Schweigart, U. Tetzlaff, G. Elger, Characterization of tin-oxides and tin-formate crystals obtained from SnAgCu solder alloy under formic acid vapor, New Journal of Chemistry (2019).

[2] N. Ozawa, T. Okubo, J. Matsuda, T. Sakai, Sn-and Cu-oxide reduction by formic acid and its application to power module soldering, 2018 IEEE 30th International Symposium on Power Semiconductor Devices and ICs (ISPSD), IEEE, 2018, pp. 248-251.

[3] F. Conti, A. Hanss, O. Mokhtari, S.K. Bhogaraju, G. Elger, Formation of tin-based crystals from SnAgCu alloy under formic acid vapor, New Journal of Chemistry (2018).

[4] W. Lin, Y. Lee, Study of fluxless soldering using formic acid vapor, IEEE transactions on Advanced Packaging 22(4) (1999) 592-601.

[5] A. Hanss, M. Hutter, J. Trodler, G. Elger, Solder process for fluxless solder paste applications, Electronic Components and Technology Conference (ECTC), 2016 IEEE 66th, IEEE, 2016, pp. 447-454.

[6] M. Monta, K. Okiyama, T. Sakai, N. Imaizumi, Formation of solder cap on Cu pillar bump using formic acid reduction, 2012 IEEE 14th Electronics Packaging Technology Conference (EPTC), IEEE, 2012, pp. 602-607.

[7] W. Yang, Y. Lu, C. Zhou, J. Zhang, T. Suga, Study of Cu Film Surface Treatment Using Formic Acid Vapor/Solution for Low Temperature Bonding, Journal of The Electrochemical Society 165(4) (2018) H3080-H3084.

[8] W. Yang, C. Zhou, J. Zhou, Y. Lu, Y. Lu, T. Suga, Cu film surface reduction through formic acid vapor/solution for 3-D interconnection, 2018 19th International Conference on Electronic Packaging Technology (ICEPT), IEEE, 2018, pp. 1378-1381.

[9] F. Conti, A. Hanss, C. Fischer, G. Elger, Thermogravimetric investigation on the interaction of formic acid with solder joint materials, New Journal of Chemistry 40(12) (2016) 10482-10487.

[10] T. Youngs, S. Haq, M. Bowker, Formic acid adsorption and oxidation on Cu (1 1 0), Surface Science 602(10) (2008) 1775-1782.

[11] Z. Jiang, P. Qin, T. Fang, Decomposition mechanism of formic acid on Cu (111) surface: A theoretical study, Applied Surface Science 396 (2017) 857-864.

[12] J.D. Bernardin, I. Mudawar, C.B. Walsh, E.I. Franses, Contact angle temperature dependence for water droplets on practical aluminum surfaces, International journal of heat and mass transfer 40(5) (1997) 1017-1033.

[13] K. Tu, T. Lee, J. Jang, L. Li, D. Frear, K. Zeng, J. Kivilahti, Wetting reaction versus solid state aging of eutectic SnPb on Cu, Journal of Applied Physics 89(9) (2001) 4843-4849.

[14] N. Zhao, X. Pan, D. Yu, H. Ma, L. Wang, Viscosity and surface tension of liquid Sn-Cu lead-free solders, Journal of electronic materials 38(6) (2009) 828-833.

[15] G. Kumar, K.N. Prabhu, Review of non-reactive and reactive wetting of liquids on surfaces, Advances in colloid and interface science 133(2) (2007) 61-89.

[16] M. Morra, E. Occhiello, F. Garbassi, Knowledge about polymer surfaces from contact angle measurements, Advances in Colloid and Interface Science 32(1) (1990) 79-116.

[17] D. Quéré, Rough ideas on wetting, Physica A: Statistical Mechanics and its Applications 313(1-2) (2002) 32-46.

[18] O. Dezellus, F. Hodaj, N. Eustathopoulos, Chemical reaction-limited spreading: the triple line velocity versus contact angle relation, Acta Materialia 50(19) (2002) 4741-4753.

[19] B. He, N.A. Patankar, J. Lee, Multiple equilibrium droplet shapes and design criterion for rough hydrophobic surfaces, Langmuir 19(12) (2003) 4999-5003.

[20] B. He, J. Lee, N.A. Patankar, Contact angle hysteresis on rough hydrophobic surfaces, Colloids and Surfaces A: Physicochemical and Engineering Aspects 248(1-3) (2004) 101-104.

[21] Y. Chen, B. He, J. Lee, N.A. Patankar, Anisotropy in the wetting of rough surfaces,

Journal of colloid and interface science 281(2) (2005) 458-464.

[22] J. Long, M. Hyder, R. Huang, P. Chen, Thermodynamic modeling of contact angles on rough, heterogeneous surfaces, Advances in colloid and interface science 118(1-3) (2005) 173-190.

[23] A.W. Adamson, A.P. Gast, Physical chemistry of surfaces, (1967).

[24] H. Kamusewitz, W. Possart, D. Paul, The relation between Young's equilibrium contact angle and the hysteresis on rough paraffin wax surfaces, Colloids and Surfaces A: Physicochemical and Engineering Aspects 156(1-3) (1999) 271-279.

[25] D.Y. Kwok, A.W. Neumann, Contact angle measurement and contact angle interpretation, Advances in colloid and interface science 81(3) (1999) 167-249.

[26] W. Yang, M. Akaike, M. Fujino, T. Suga, A combined process of formic acid pretreatment for low-temperature bonding of copper electrodes, ECS Journal of Solid State Science and Technology 2(6) (2013) P271-P274.

[27] T. Suga, A. Masakate, W. Yang, N. Matsuoka, Formic acid treatment with Pt catalyst for Cu direct bonding at low temperature, Electronics Packaging (ICEP), 2014 International Conference on, IEEE, 2014, pp. 644-647.

[28] W. Yang, M. Akaike, T. Suga, Effect of formic acid vapor in situ treatment process on Cu low-temperature bonding, IEEE Transactions on Components, Packaging and Manufacturing Technology 4(6) (2014) 951-956.

[29] J.-M. Song, S.-K. Huang, M. Akaike, T. Suga, Direct bonding for dissimilar metals assisted by carboxylic acid vapor, Japanese Journal of Applied Physics 54(3) (2015) 030217.

[30] D.H. Ying, J.M. Robert, Thermal desorption study of formic acid decomposition on a clean cu (110) surface, Journal of catalysis 61(1) (1980) 48-56.

[31] M. Bowker, R. Madix, XPS, UPS and thermal desorption studies of the reactions of formaldehyde and formic acid with the cu (110) surface, Surface Science 102(2-3) (1981) 542-565.

[32] B. Hayden, K. Prince, D. Woodruff, A. Bradshaw, An IRAS study of formic acid

and surface formate adsorbed on Cu (110), Surface science 133(2-3) (1983) 589-604.

[33] M. Hosking, F.G. Yost, The mechanics of solder alloy wetting and spreading, Springer Science & Business Media2012.

[34] F. Conti, A. Hanss, O. Mokhtari, S.K. Bhogaraju, G. Elger, Formation of tin-based crystals from a SnAgCu alloy under formic acid vapor, New Journal of Chemistry 42(23) (2018) 19232-19236.

[35] J. Wang, H. Nishikawa, Impact strength of Sn–3.0 Ag–0.5 Cu solder bumps during isothermal aging, Microelectronics Reliability 54(8) (2014) 1583-1591.

[36] H.R. Kotadia, P.D. Howes, S.H. Mannan, A review: on the development of low melting temperature Pb-free solders, Microelectronics Reliability 54(6-7) (2014) 1253-1273.

[37] S. Koyama, Y. Aoki, I. Shohji, Effect of formic acid surface modification on bond strength of solid-state bonded interface of tin and copper, Materials transactions 51(10) (2010) 1759-1763.

[38] E. Rozhitsina, S. Gruner, I. Kaban, W. Hoyer, V. Sidorov, Dynamic viscosities of pure tin and Sn-Ag, Sn-Cu, and Sn-Ag-Cu eutectic melts, Russian Metallurgy (Metally) 2011(2) (2011) 118.

Chapter 3

Effect of Thermal Aging on the Impact Strength of Sn-3.0Ag-0.5Cu Solder Bumps Soldered on Cu under a Formic Acid Atmosphere

3.1 Introduction

In **Chapter 2**, a fluxless soldering process using Cu substrate under a formic acid (FA) atmosphere was investigated. The results indicated that in the case of fluxless soldering in the FA atmosphere, a sufficient contact angle formed between the solder and Cu substrate was attained, and a typical intermetallic compound (IMC) layer was formed at the interface. However, several pores were found near the IMC layer when the FA atmosphere was used. These pores may cause long-term reliability problems.

The impact reliability of solder joints is one of the critical concerns in the electronics

industry because portable products such as cellphones can be damaged due to the impact of fall if dropped[1-3]. In this chapter, we have conducted impact tests on as-reflowed and thermally aged solder bumps on a Cu substrate, using either FA or the liquid flux, in order to investigate the impact reliability of the solder bumps.

3.2 Experimental

3.2.1 Soldering and Thermal Aging Methods

Sn-3.0 mass% Ag-0.5 mass% Cu solder balls with a diameter of 0.76 mm were used in this study. **Fig. 3.1** shows a schematic illustration of a sample solder ball on Cu pads. A Cu-pad with a thickness of 35 μm was prepared on an FR-4 printed wiring board, and the Cu pad size was set to 0.6 mm in diameter by applying the solder resist. Pre-treatment to the soldering, the Cu pads were immersed in a 4% HCl solution for 120 s. Then, the solder balls and the Cu pads were ultrasonically rinsed in an ethanol solution for 300 s. After that, Sn-Ag-Cu solder balls were soldered on Cu pads using either FA or liquid rosin mildly activated flux. The solder balls on the substrates were preheated at 110 ℃ for 60 s and the continuously heated at 250 ℃ for 120 s in an oven, as shown in **Fig.3 .2**. After reflow soldering, some solder bumps were aged in an oil bath at 150 ℃ for 168, 504, and 1008 h.

The microstructure of the interface between the solder and the substrate was observed by scanning electron microscopy (SEM) after soldering and isothermal aging. We used an electron probe microanalysis (EPMA) to confirm the element distribution. The thickness of the IMC layer was also measured.

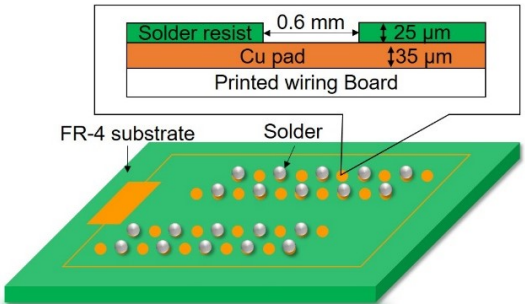

Fig. 3.1 *Schematic experimental setup of soldering with Cu pads.*

3.2.2 Impact Test

To evaluate the joint strength of soldered bumps after reflow and after thermal aging, impact tests were performed using a micro-impact tester (MI-S, Yonekura Mfg. Co., Ltd.). In the impact test, the test speed was 1 m/s, and the impact height was 0.08 mm from the solder resist, as illustrated in **Fig. 3.3**. **Fig. 3.3(b)** shows a typical impact load-displacement curve obtained from the impact tests. Ten bumps were measured for each condition, and the average value of the maximum strengths as the impact strength was used for evaluation. The strengths were calculated by the measured loads dividing by the joints area.

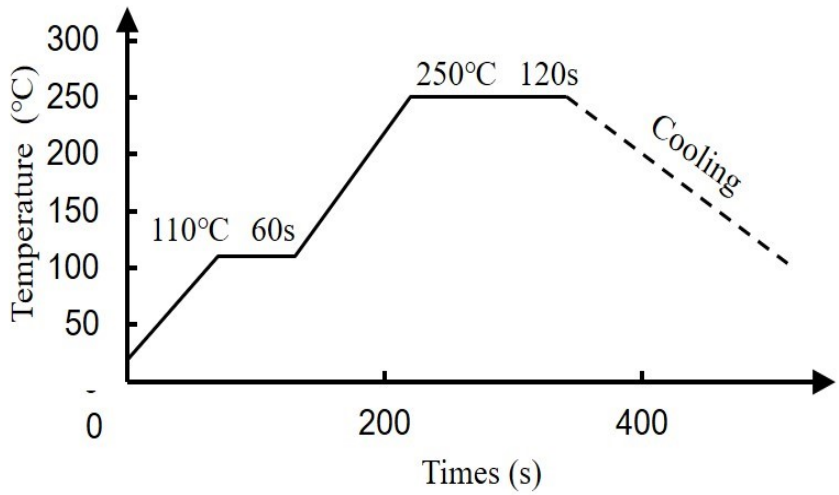

Fig. 3.2 *Heating profile of both soldering under a formic acid atmosphere and using liquid flux.*

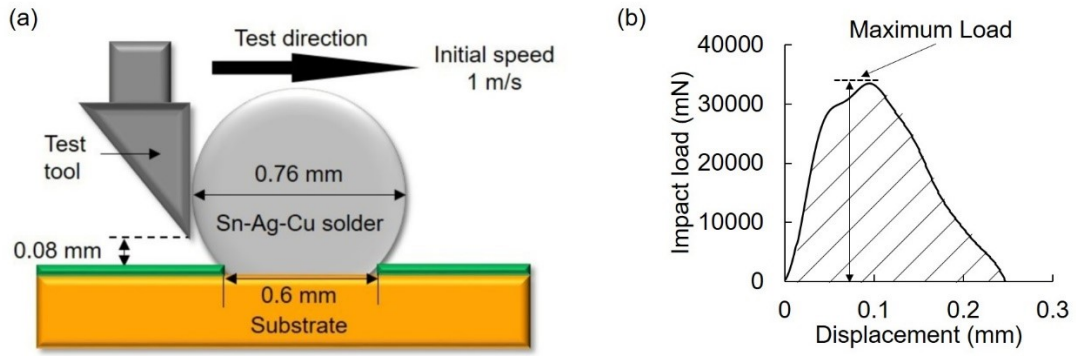

Fig. 3.3 *Schematic diagram of (a) high-speed impact test and (b) typical load-displacement curve of impact test.*

3.3 Results and Discussion

3.3.1 Microstructure after Thermal Aging

SEM images of the cross-sections at the interface between Sn-Ag-Cu solder and Cu pad are shown in **Fig. 3.4**. The morphology of the IMC layers at the interface was changed after thermal aging in the oil bath. **Figs. 3.4(a) and (b)** show a scallop-shaped IMC layer formed at the interface between the solder and the Cu pad using either FA or the liquid flux after soldering. **Fig .3.5** shows the EPMA mapping analysis results of the interface between solder and substrate under a FA atmosphere and using liquid flux. The initial formed IMC layer contained Sn and Cu (see **Fig. 3.5**), is likely to be composed of Cu_6Sn_5[4, 5]. After thermal aging for 168 h, a very thin IMC layer was newly observed between the Cu pad and the Cu_6Sn_5 layer (see **Figs. 3.4(c) and (d)** and **Fig 3.5**). This should be the Cu_3Sn phase[6, 7]. The total thickness of the IMC layer increased with the increase of the aging time for both cases. However, some pores were also observed near the IMC layers in the samples soldered under a FA atmosphere, after soldering and after thermal aging, as shown in **Fig. 3.6**. The formation of voids may be attributed to the production of the gases by the reaction of FA with solder oxide.

Fig. 3.7 shows the effect of aging time on the growth of IMC layers during the isothermal aging process at 150 °C. The total thickness of IMC layers and the thickness of the Cu_3Sn layer are shown in **Fig. 3.7**, respectively. The total IMC layer thickness and the Cu_3Sn layer thickness increase with the increase of the aging time using either the FA atmosphere or the liquid flux. The thickness is proportional to the square root of the aging time for both cases. Accordingly, the growth of the IMC layers during the thermal aging process can be considered a diffusion control process. The growth rate of the IMC layers for the samples using the FA atmosphere is similar to that for the samples using the liquid flux.

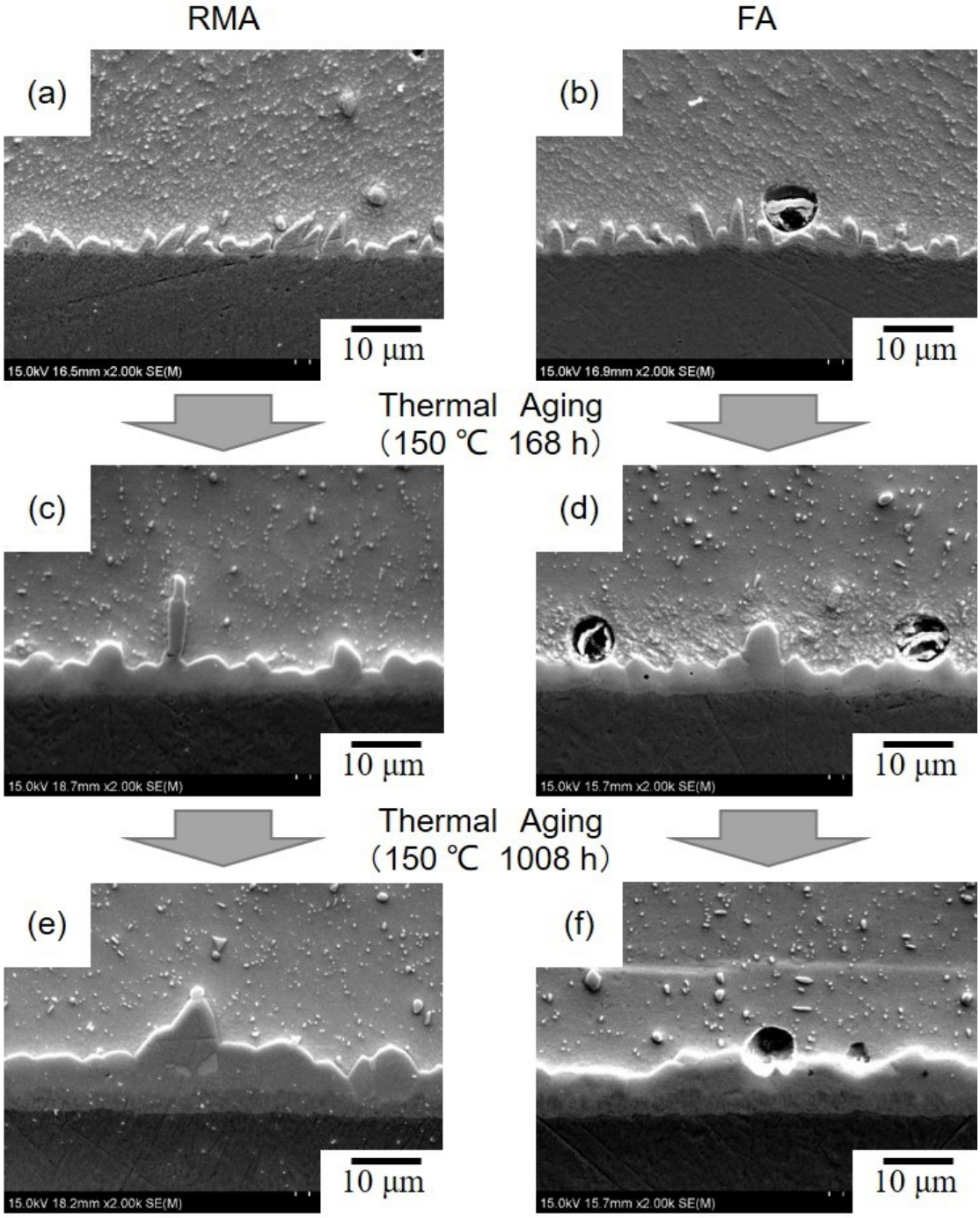

Fig. 3.4 *Cross sections of solder bumps on Cu pad using formic acid atmosphere and liquid flux: a), b) as-reflowed solder bumps; c), d) 168 h aged solder bumps; e). f) 1008 h aged solder bumps.*

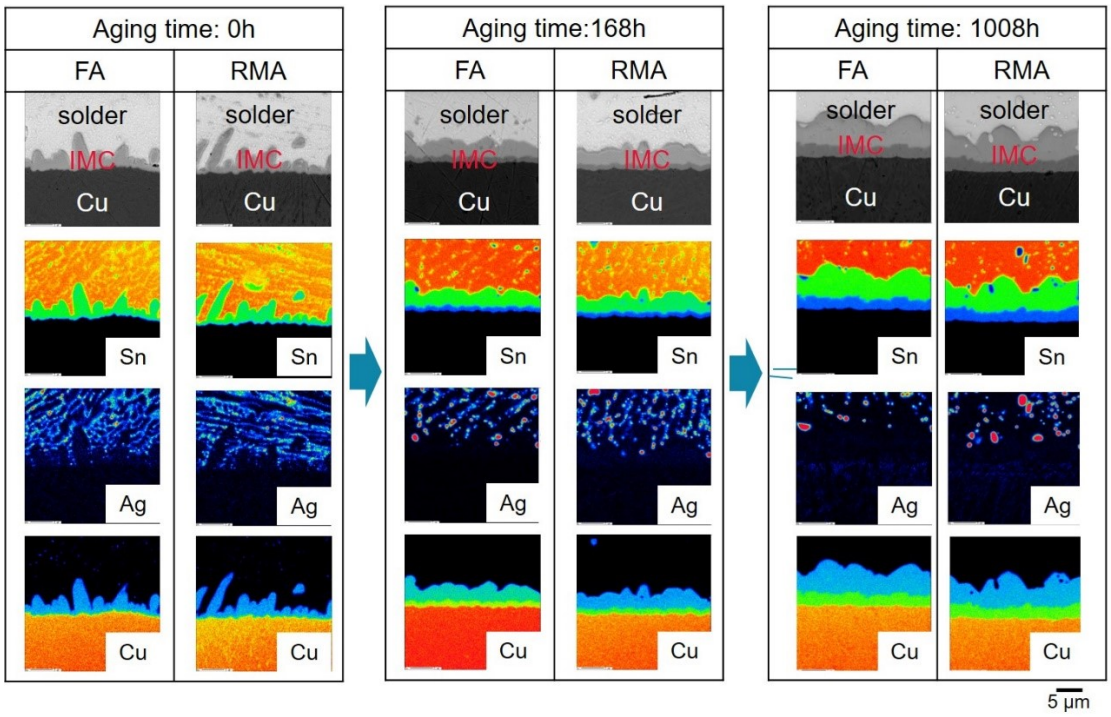

Fig. 3.5 *EPMA mapping analysis results of the interface between solder and substrate under a formic acid atmosphere and using liquid flux.*

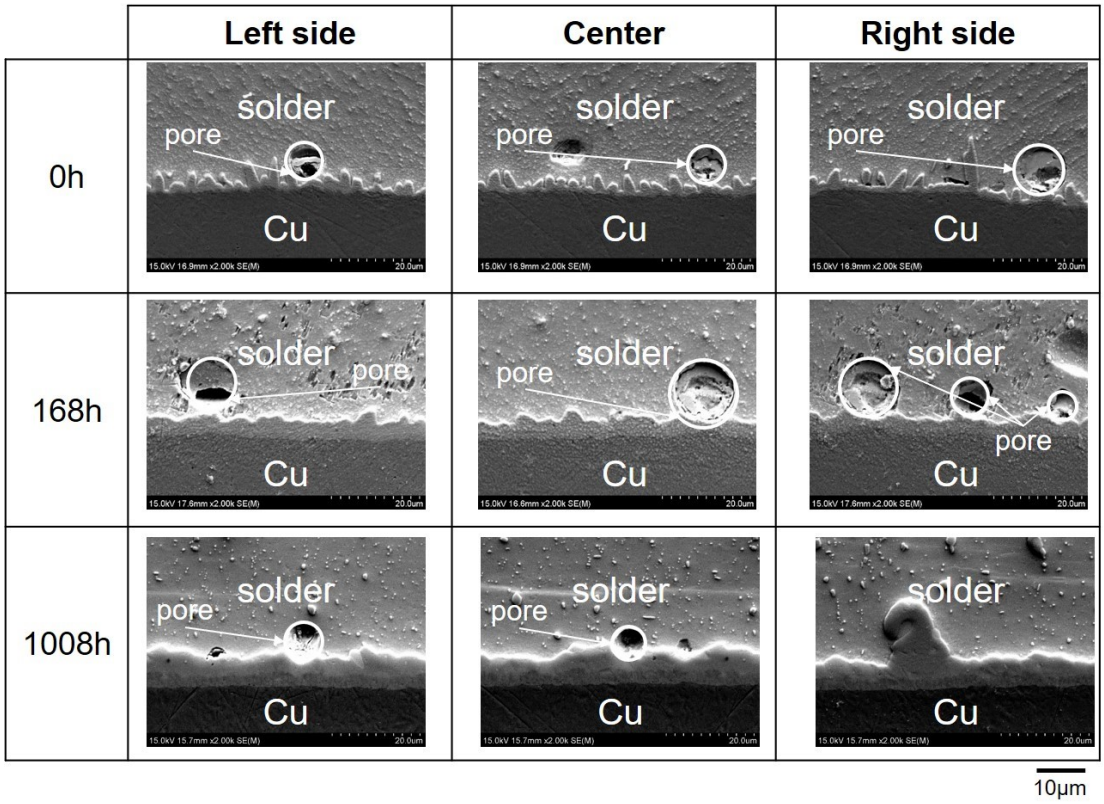

Fig. 3.6 *Pores formation near the interface under a formic acid atmosphere, after soldering and after thermal aging.*

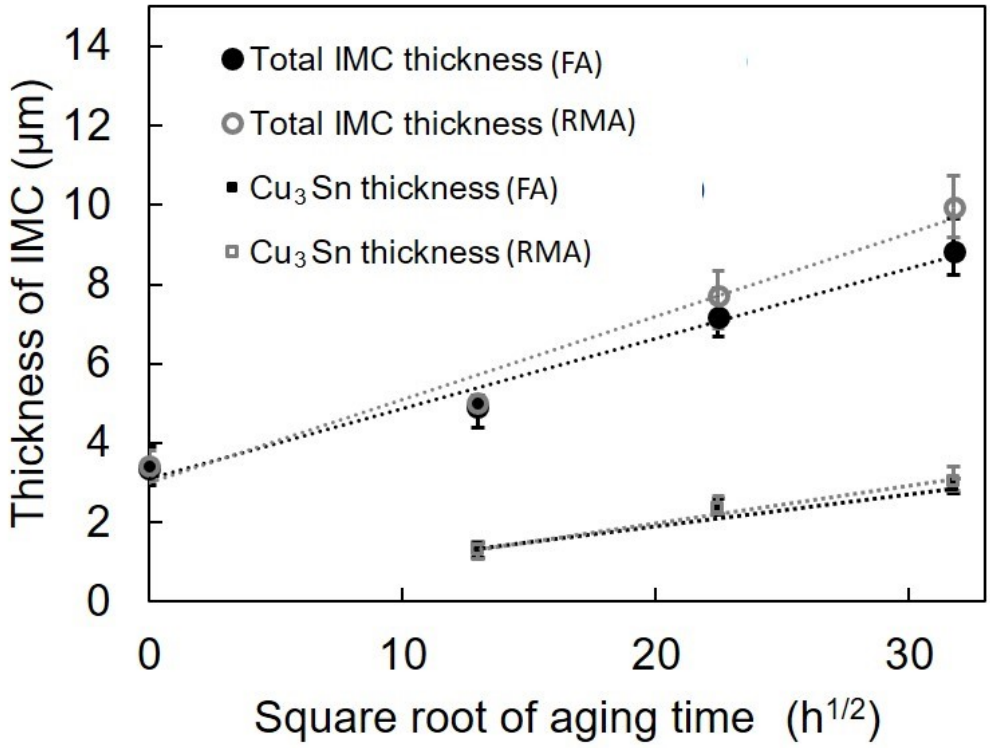

Fig. 3.7 *Effect of aging time at 150 °C on the intermetallic compound thickness at the solder/Cu pad interface.*

3.3.2 Impact strength and fracture surface before and after thermal aging

Fig. 3.8 shows the impact strength of the solder bumps, determined using the impact test. There was no significant difference between the impact strength of the as-reflowed solder bumps using FA and the liquid flux. After the aging for 168 h, the impact strength of bumps soldered by both the methods decreased significantly. For example, the average impact strength of solder bumps reflowed using the FA atmosphere decreases from 126 MPa to 105 MPa, and the average impact strength of solder bumps reflowed with the liquid flux decreases from 121 MPa to 104 MPa. The impact strength decreased with the increase of the aging time in both cases. After thermal aging for 1008 h, the impact strength of the solder bumps soldered using FA was also similar to that of solder bumps soldered using the liquid flux in a nitrogen atmosphere.

In order to further study the failure during the impact test, the fracture morphologies of

solder bumps were investigated. The composition of fracture surfaces of solder bumps was determined by EPMA analysis. **Fig. 3.9** shows the secondary electron (SE) image and the EPMA mapping analysis results of fracture surfaces of solder bumps after an impact test under as-soldered condition. Generally, each element content is shown by colors as shown in the right-hand color indicator related to the content, so the visualization in the distribution of elements of the fracture surface can be obtained. In the soldering process using the FA atmosphere, the Sn element kept high content on the entire area of the fracture surface, while there was some Cu element on the limited place. Little Ag could be measured on the entire area of the fracture surface. It seems to be that the failure was occurred predominantly in the bulk solder and partly inside the IMC layer for the soldered bumps using the FA atmosphere. However, when samples soldered with the liquid flux, Cu element was measured on almost the entire fracture surface, while Sn and little Ag element were confirmed on the entire area of the fracture surface, which suggests that a small area of residual solder and a large area of IMC layer coexist on the fracture surface. Gao et al. [8] reported that spherical porosity caused enough stress intensification around the pore. As we know, fracture occurs at stress intensification parts easily. As the pores existed near the IMC layer in the samples soldered in FA atmosphere after soldering, it suggests that the pores affect the fracture position in the impact test when using FA atmosphere， as shown in **Fig. 3.10**. However, although the typical fracture positions of the two cases are different, they exhibited similar impact strengths, as shown in **Fig. 3.8**. On the other hand, the typical strength-displacement curves of solder bumps under a FA atmosphere and the liquid flux after soldering at 250 ℃ for 120 s are shown in **Fig. 3.11**. Although the curves of the two cases were similar before reaching the maximum strengths, the curve of the sample soldered by the liquid flux dropped faster than that soldered in the FA atmosphere. It seems that the difference in the curves is caused by the afore-mentioned different fracture positions of two cases. In the future, more study about the correlation of the fracture position with the strength-displacement curves in impact test is necessary.

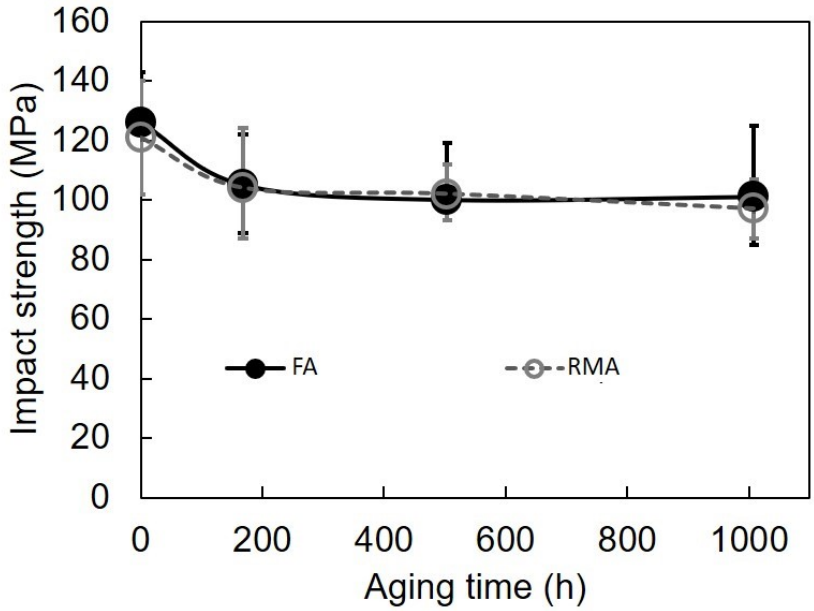

Fig. 3.8 *Effect of aging time on the impact strength of solder bumps.*

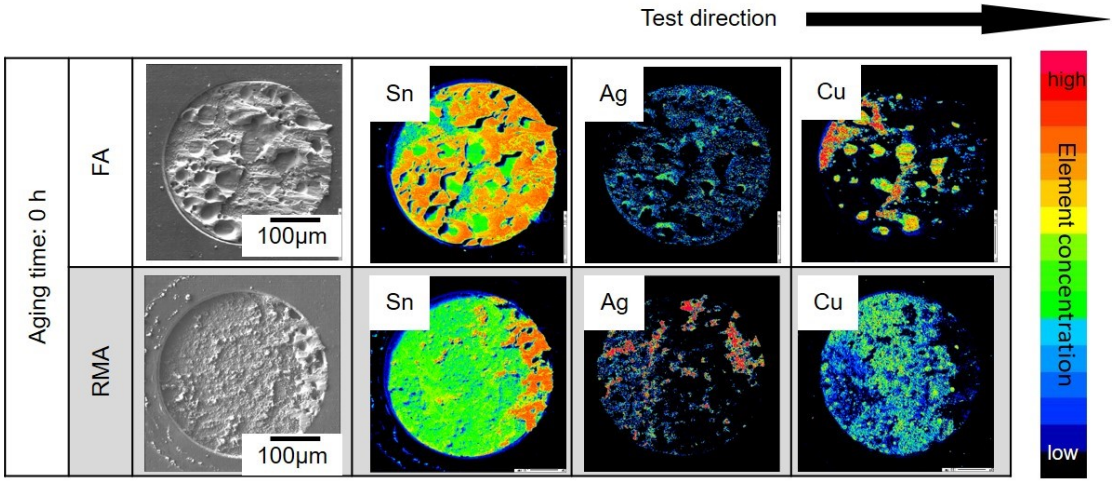

Fig. 3.9 *EPMA mapping analysis results of fracture surfaces of as-soldered bumps using formic acid atmosphere and the liquid flux in an impact test.*

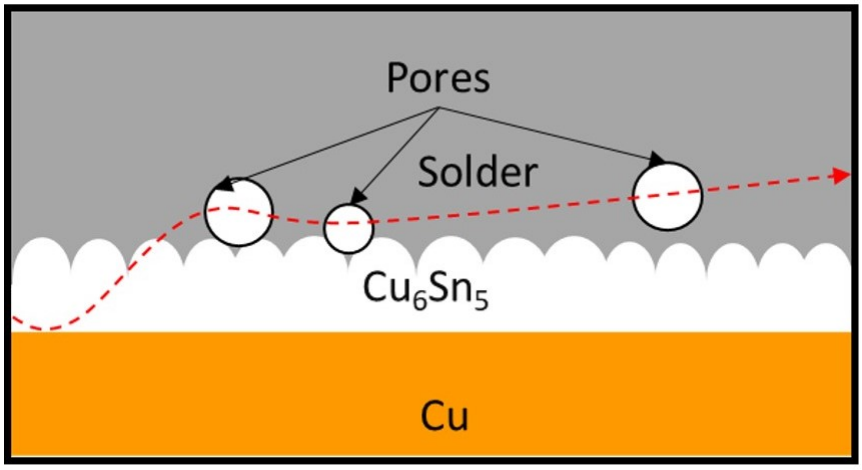

Fig. 3.10 *Effect of pores on fracture position.*

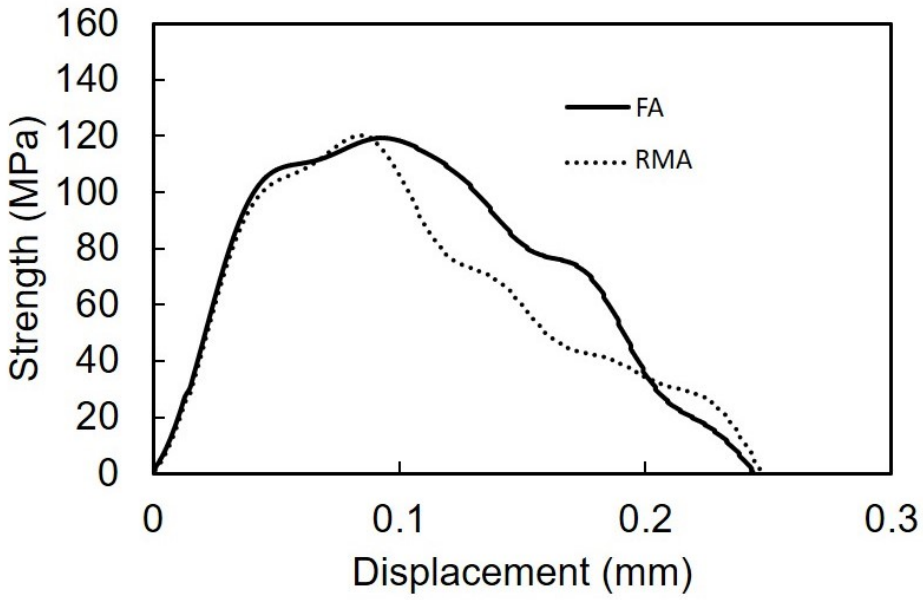

Fig. 3.11 *The load-displacement curves of as-soldered bumps using formic acid atmosphere and liquid flux in a high speed impact test.*

The fracture morphologies of thermally aged solder bumps are shown in **Fig. 3.12**. Sn element and Cu element are observed on the entire fracture surface, either using the FA atmosphere or the liquid flux. We suppose after thermal aging, as the IMC layers increased, as shown in **Fig. 3.4**, the fracture positions were at the IMC layers for both cases.

After thermal aging, two IMC phases existed at the interface between the Sn-3.0Ag-0.5Cu solder and the Cu substrate using either FA atmosphere or the liquid flux, as shown in **Fig. 3.4**. In order to investigate where the fracture happened after thermal aging, EPMA was used to do the point analysis of element distribution. **Fig. 3.13** shows the top view of fracture surfaces of Sn-3.0Ag-0.5Cu/Cu solder bump reflowed using the FA atmosphere and the liquid flux after 1008 h thermal aging. In particularly, **Figs. 3.13(a) and (c)** show the macroscopic fracture surfaces of the impacted solder bumps using the FA atmosphere and the liquid flux, respectively. **Figs. 3.13(b) and (d)** show the magnified micrographs of the corresponding square marked regions in **Figs. 3.13(a) and (c)**, respectively. In **Figs. 3.13(b) and (d)**, a number of IMC grains were observed

without any residual solder. This suggests that brittle fracture occurred inside the IMC layers, similar to the observation in **Fig. 3.9**.

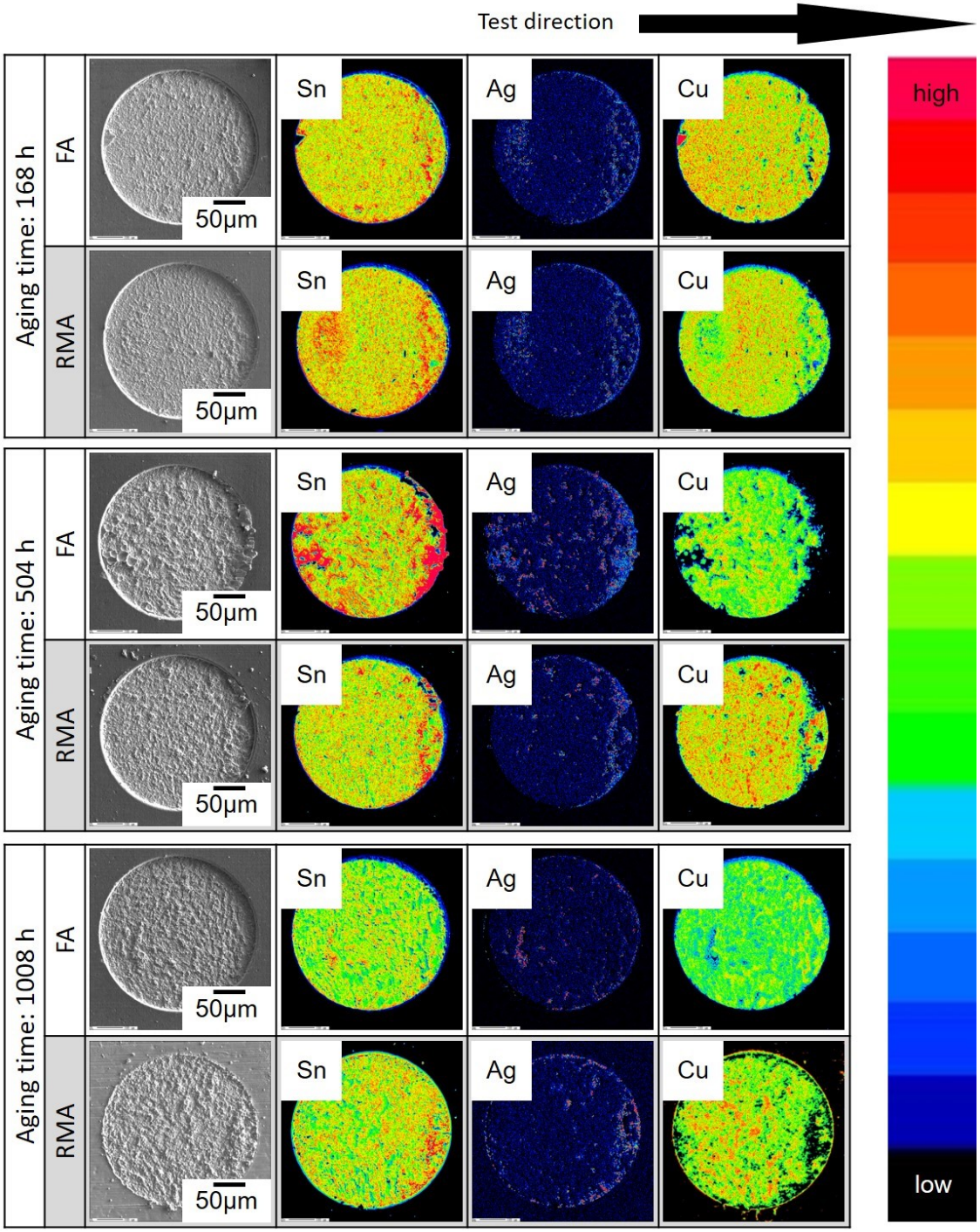

Fig. 3.12 *EPMA mapping analysis results of fracture surfaces of thermally aged bumps using FA atmosphere and the liquid flux in an impact test.*

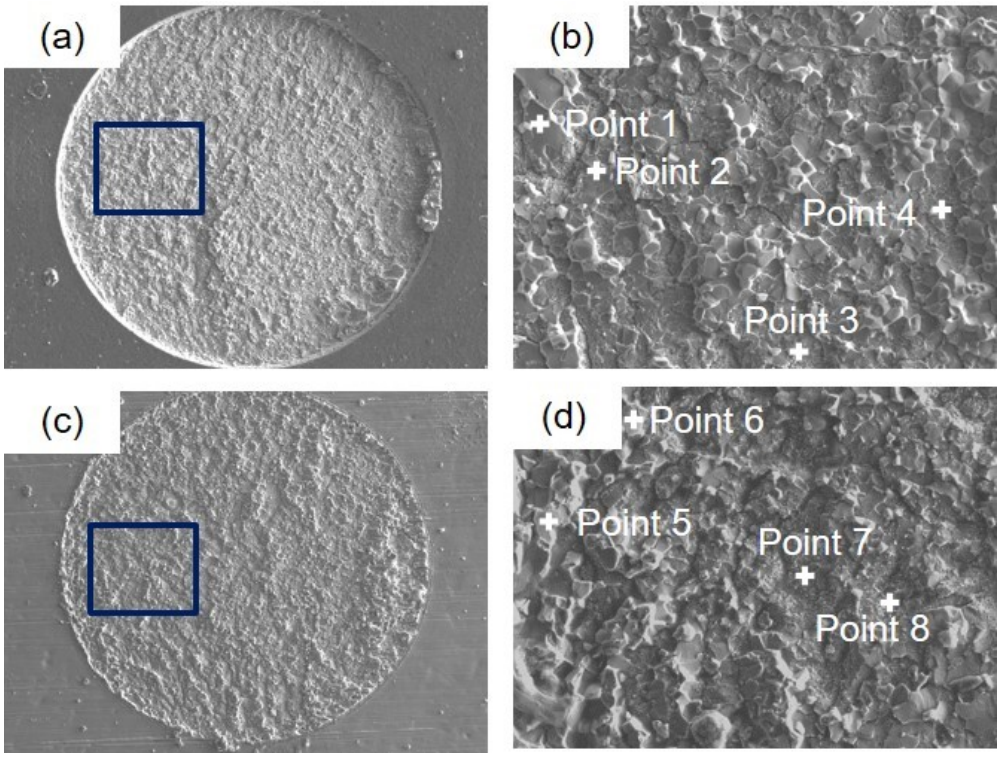

Fig. 3.13 *The top view of the impact fracture surfaces for the 1008 h aged solder bumps. (a, b) solder bump under a formic acid atmosphere; (c, d) solder bump using the RMA liquid flux.*

Table 3.1 shows the EPMA point analysis results of selected points in **Fig. 3.13**. The molar ratios of Cu to Sn in Points of 1, 2, 5, and 6 were near to 6:5, while the Points of 3, 4, 7, and 8 contained approximately 25 at.% Sn, indicating that the IMC grains were Cu_6Sn_5 and Cu_3Sn, respectively. Combining **Figs. 3.13(b), (d),** and **Table 3.1**, it is easy to infer that the fracture occurs partly at the Cu_6Sn_5 layer and partly at the Cu_3Sn layer for both cases after 1008 h thermal aging.

The typical strength-displacement curves of solder bumps under a FA atmosphere and using the liquid flux after thermal aging at 150 °C for 1008 h were also compared, as shown in **Fig. 3.14**. The tendency of the two curves were similar before reaching the maximum strengths and dropping. Associating with **Figs. 3.12** and **3.13**, it seems after 1008 h thermal aging, the fracture modes were almost the same for both cases.

In summary, failure of the solder bumps occurs as cracks propagate along with the weakest layer or interface, which determines the impact properties of the solder bumps.

As shown in **Fig. 3.15**, the failure of solder bumps occurred at different positions. When solder bumps reflowed by using the FA atmosphere, the failure occurs predominantly in the bulk solder and partly inside the IMC layer because the failure is caused by the pores existed in bulk solder. The fracture position was predominantly inside the IMC layer and partly in the bulk solder when using liquid flux. After 1008 h thermal aging, the fracture occurred partly at the Cu_6Sn_5 layer and partly at the Cu_3Sn layer for both cases.

Table 3.1 *EPMA point analysis results of selected points in* ***Fig. 3.12****.*

	Cu at.%	Sn at.%
Point 1	46.20	53.80
Point 2	52.84	47.16
Point 3	71.80	28.20
Point 4	69.93	30.07
Point 5	46.71	53.29
Point 6	46.06	53.94
Point 7	69.83	30.17
Point 8	71.21	28.79

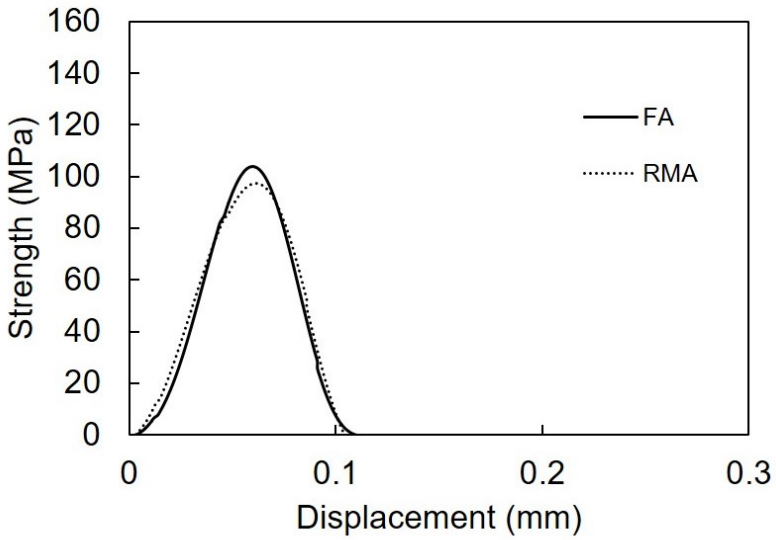

Fig. 3.14 *The load-displacement curves of bumps after 1008 h thermal aging using formic acid atmosphere and liquid flux in high-speed impact test.*

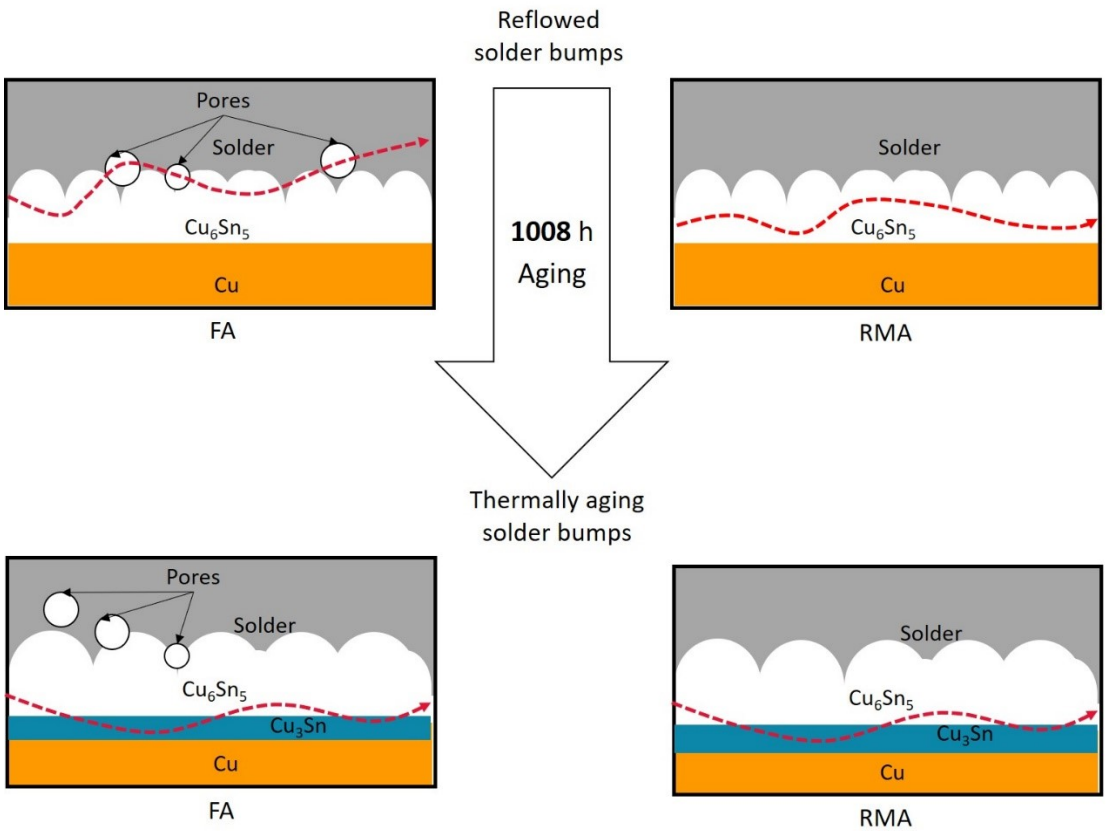

Fig. 3.15 *Schematic diagram of fracture mode of solder bumps under a FA atmosphere and using liquid flux.*

3.4 Conclusion

The impact strength of soldered bumps using FA was explored. The major conclusions can be summarized as follows:

(1) The morphology of the IMC layers in samples soldered using the FA atmosphere was similar to those soldered with the flux, after soldering and after thermal aging.

(2) After thermal aging, some pores were observed near the IMC layers in the samples soldered in the FA atmosphere.

(3) The impact strengths of the as-reflowed and thermally aged solder bumps were tested by impact tests. The fluxless solder bumps, using the FA atmosphere, have impact strengths similar to the solder bumps obtained using the liquid flux.

(4) When solder bumps reflowed by using the FA atmosphere, the failure occurs predominantly in the bulk solder and partly inside the IMC layer. However, when using the liquid flux, the fracture position was predominantly inside the IMC layer and partly

in the bulk solder. After 1008 h thermal aging, the fracture occurs partly at the Cu_6Sn_5 layer and partly at the Cu_3Sn layer for both cases.

Reference

[1] T. Daito, H. Nishikawa, T. Takemoto, T. Matsunami, Explanation of impact load curve in ball impact test in relation to thermal aging, Microelectronics Reliability 53(12) (2013) 2005-2011.

[2] J. Wang, H. Nishikawa, Impact strength of Sn–3.0 Ag–0.5 Cu solder bumps during isothermal aging, Microelectronics Reliability 54(8) (2014) 1583-1591.

[3] M. Date, T. Shoji, M. Fujiyoshi, K. Sato, K. Tu, Ductile-to-brittle transition in Sn–Zn solder joints measured by impact test, Scripta Materialia 51(7) (2004) 641-645.

[4] R.A. Gagliano, M.E. Fine, Thickening kinetics of interfacial Cu 6 Sn 5 and Cu 3 Sn layers during reaction of liquid tin with solid copper, Journal of electronic materials 32(12) (2003) 1441-1447.

[5] K. Kim, S. Huh, K. Suganuma, Effects of intermetallic compounds on properties of Sn–Ag–Cu lead-free soldered joints, Journal of Alloys and compounds 352(1-2) (2003) 226-236.

[6] H.R. Kotadia, P.D. Howes, S.H. Mannan, A review: on the development of low melting temperature Pb-free solders, Microelectronics Reliability 54(6-7) (2014) 1253-1273.

[7] L. Qu, N. Zhao, H. Zhao, M. Huang, H. Ma, In situ study of the real-time growth behavior of Cu6Sn5 at the Sn/Cu interface during the soldering reaction, Scripta Materialia 72 (2014) 43-46.

[8] Y. Gao, J. Yi, P. Lee, T. Lindley, The effect of porosity on the fatigue life of cast aluminium-silicon alloys, Fatigue & Fracture of Engineering Materials & Structures 27(7) (2004) 559-570.

Chapter 4

Thermal Effect on Sn Steaming Phenomenon Under Formic Acid Atmosphere

4.1 Introduction

As explained in **Chapter 2**, we achieved a successful soldering process using SAC solder and Cu substrate under a formic acid (FA) atmosphere. A sufficient contact angle formed between solder and Cu substrate under a FA atmosphere and a typical intermetallic compound (IMC) morphology could be observed at the interface. Nevertheless, some undesired residues were detected on the Cu substrate after the soldering process under a FA atmosphere, as shown in **Section 2.3.1.3**, the residue containing Sn was speculated from the reaction of FA with SAC solder alloy[1, 2]. We address this phenomenon Sn steaming phenomenon. The residue may lead to an increase in leakage current and affect electrical performance[3].

As we know, chemical reactions and atomic diffusion always depend on temperature and time[4]. However, to our best knowledge, the effects of heating conditions on the formation of the residue under a FA atmosphere were not directly assessed. Therefore, instead of investigating the residue formation on the substrate, this chapter aims to discuss the effect of heating conditions on the Sn steaming phenomenon under a FA atmosphere. In this chapter, the thermal effect on Sn steaming phenomenon, produced by series peak temperature and different holding times under a FA atmosphere, was investigated.

4.2 Experimental

In this study, a glass plate with a pure Sn bulk on its top surface was placed on the right side, and a Cu pad was placed at a distance of 1 mm left to the glass pad, as shown in **Fig. 4.1**. FA gas (5 vol.% formic acid + 95 vol.% N_2) was used as the reducing atmosphere. FA gas was supplied by nitrogen gas through liquid FA stored in a sealed beaker, as shown in **Fig. 4.2**. To investigate the thermal effect of the Sn steaming phenomenon under a FA atmosphere, seven heating profiles were set and performed under the FA atmosphere with various peak temperatures and heating times, as shown in **Table 4.1**. Alongside two reference heating processes using liquid rosin, mildly activated (RMA) flux with pure nitrogen and pure nitrogen atmosphere without RMA flux were set, as shown in **Fig. 4.3** corresponding to **Process 4** in **Table 4.1**. A morphological study of the microstructure of residues was performed using field-emission scanning electron microscopy (FE-SEM, Hitachi SU-70). An energy-dispersive X-ray spectroscopy (EDS) was used to detect the elemental composition of the residues. In order to observe the tendency of Sn steaming overall, a mapping of elements on the Cu pad was detected by an electron probe micro-analyzer (EPMA). The X-ray diffraction (XRD) was used to distinguish the phases on Cu pad.

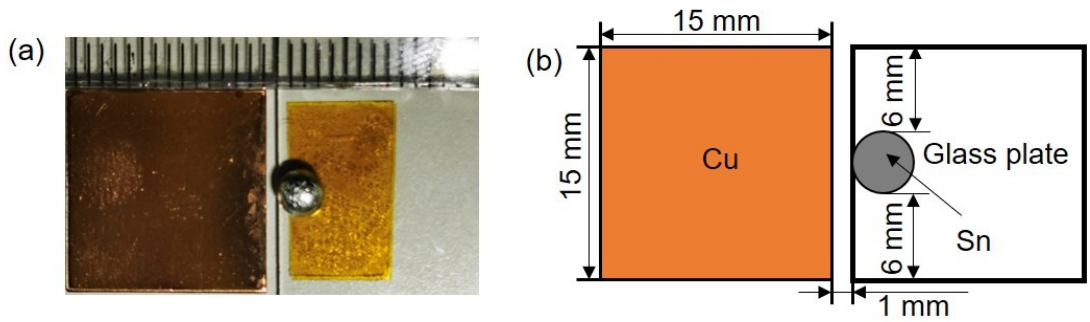

Fig. 4.1 *Sample for Sn steaming experiment: (a) sample image; (b) schematic diagram.*

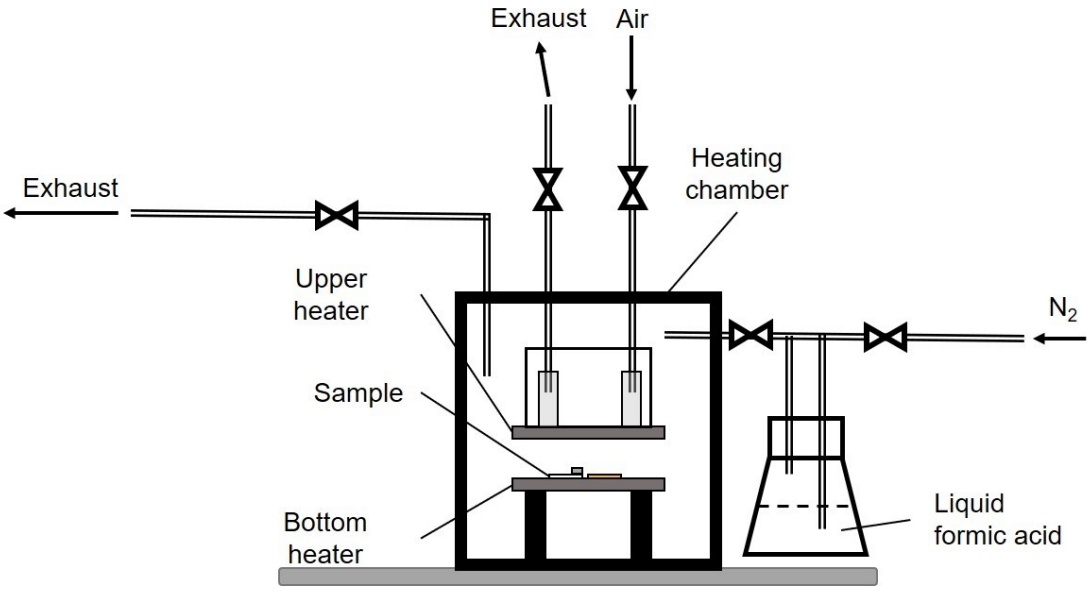

Fig. 4.2 *Schematic view of heating equipment for the Sn steaming experiment.*

Table 4.1 *Summary of heating processes under a FA atmosphere.*

Heating process	**1**	**2**	**3**	**4**	**5**	**6**	**7**
Peak heating temperature (°C)	130	170	210	250	290	250	250
Peak heating time (s)	600	600	600	600	600	60	3600
Heating rate (°C/s)	1	1	1	1	1	1	1

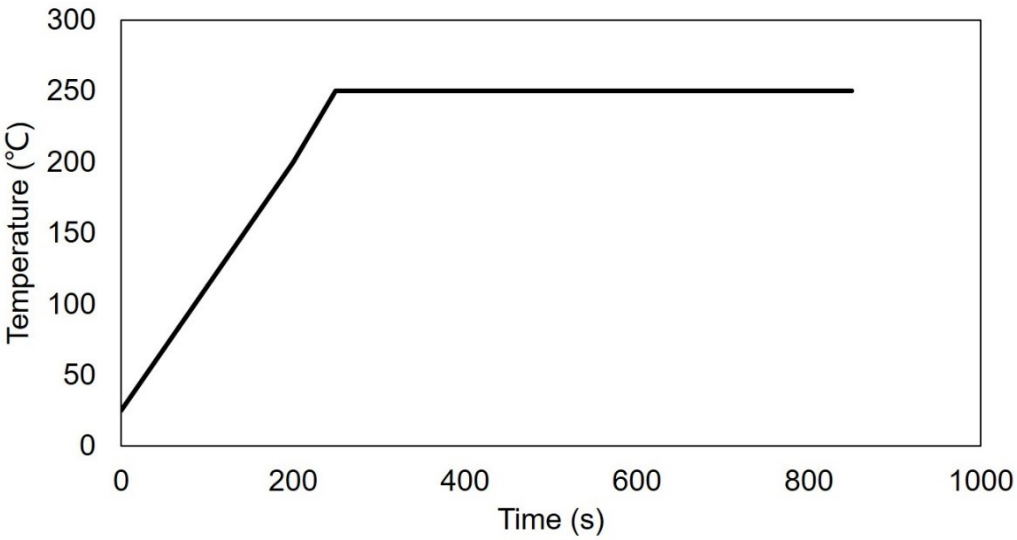

Fig. 4.3 *Heating process as reference using liquid RMA flux and pure N_2.*

4.3 Results and discussion

4.3.1 Effect of peak temperature on Sn steaming phenomenon under FA atmosphere

The residue, which occurs during a fluxless soldering process heating at 250 °C for 120 s with SAC solder under a FA atmosphere, with the intent to form the unwanted deposits on the substrate, and Sn was the main element of the residue confirmed by EPMA, as shown in **Fig. 4.4**. **Fig. 4.4 (a)** shows the optical microscopy (OM) image of the solder ball. The color of space near the solder ball on a Cu substrate turned to gray. This also could be confirmed by the naked eye.

Fig. 4.5 shows the distribution of Sn element on Cu pads using different peak temperatures by EPMA mapping. The Sn element content is shown by colors as shown in the right-hand color indicator related to the content, so the visualization in the distribution of Sn on the Cu pads surface was obtained. When the temperature below 170 °C, the Sn was hardly detected, which means the Sn steaming phenomenon was not serious under such condition, as shown in **Figs. 4.5(a) and (b)**. This situation was similar to the results observed by Conti et al. [1]. Their results suggest the Sn steaming phenomenon can be observed upon reaching 185 °C. In this study, when the temperature

reached 210 ℃ and prolonged to 290 ℃, the Sn element was able to be confirmed obviously, as shown in **Figs. 4.5(c), (d) and (e)**. And some cloudy Sn coverage in the same area on Cu pad could be observed with naked eyes under these conditions. The Sn covered area on Cu pads grew up with temperature increasing under a FA atmosphere. While the Sn signal was hardly detected on the Cu pads under a pure N_2 atmosphere at 250 ℃ for heating 600 s, as shown in **Fig. 4.5(g)**. The Sn steaming phenomenon was confirmed at 210 ºC which was below the melting temperature of Sn at 232 ºC. We considered the reaction between Sn and FA is the key to the Sn steaming phenomenon under a FA atmosphere.

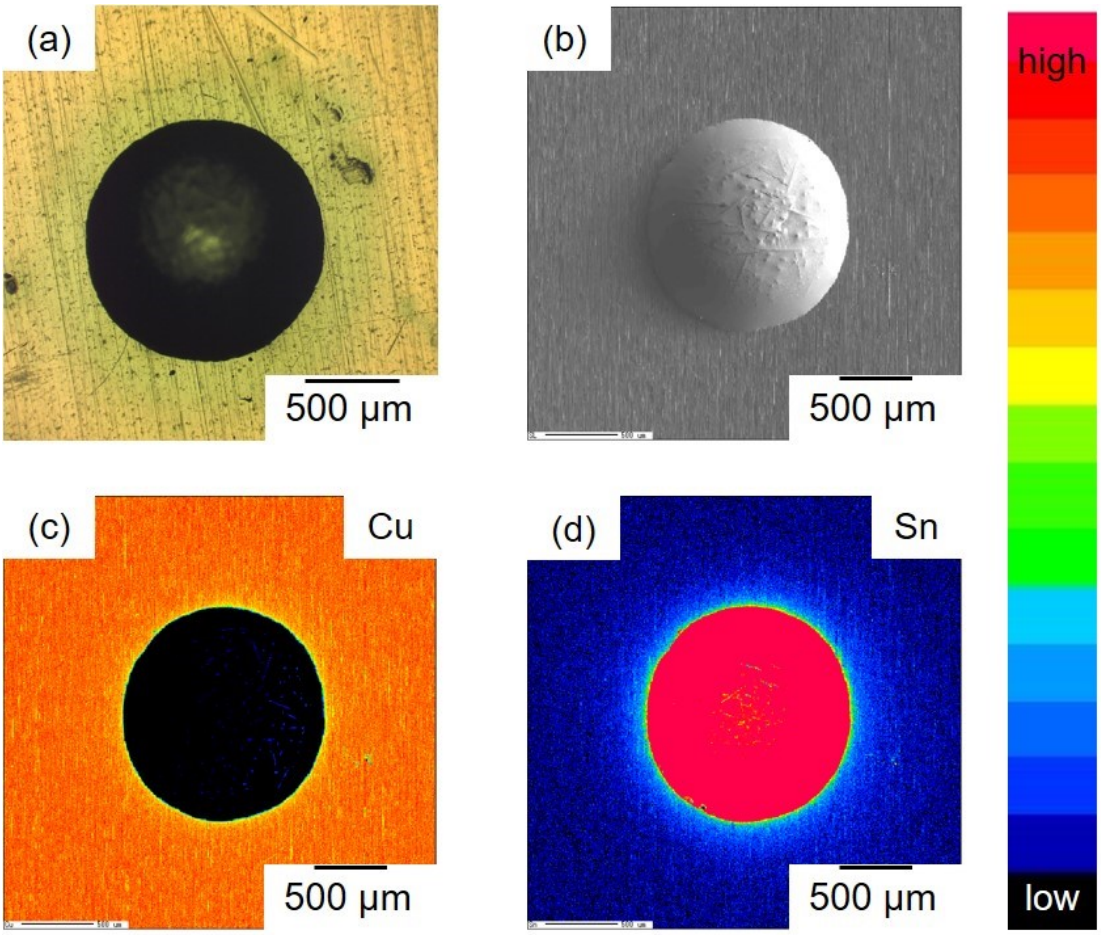

Fig. 4.4 *Sn residues confirmed after a fluxless soldering process under a FA atmosphere: (a) OM image of solder ball; (b) SEM image of solder ball; (c) distribution of Cu element detected by EPMA; (d) distribution of Sn element detected by EPMA.*

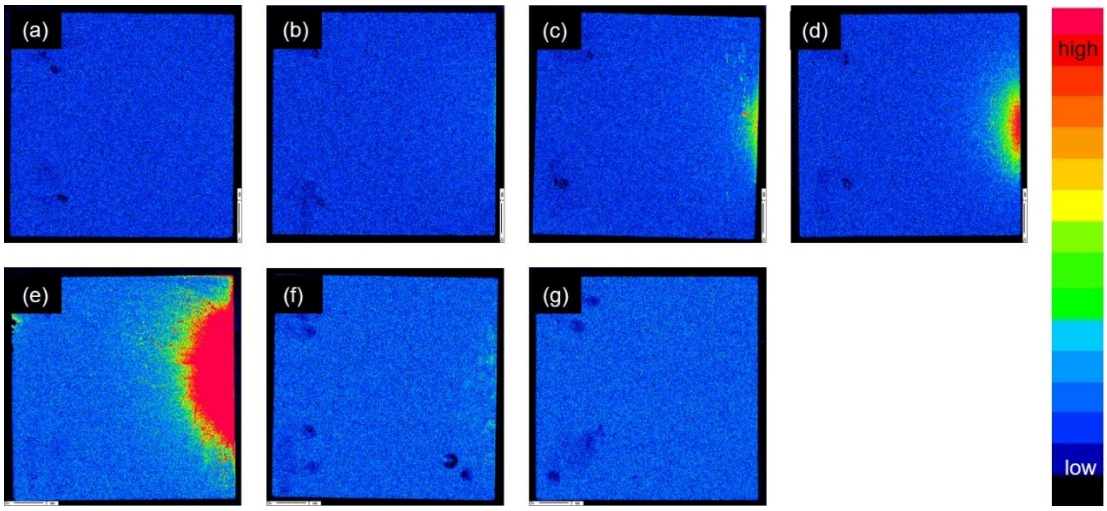

Fig. 4.5 *EMPA mapping results of Sn element on Cu pads at various temperature heating for 600 s: (a) heating at 130 ℃ under a FA atmosphere; (c) heating at 170 ℃ under a FA atmosphere; (d) heating at 210 ℃ under a FA atmosphere; (e) heating at 250 ℃ under a FA atmosphere; (f) heating at 290 ℃ under a FA atmosphere; (g) heating at 250 ℃ using RMA flux; (h) heating at 250 ℃ under N_2 atmosphere.*

Based on these results, we speculated the following hypothesis refers to **Fig. 4.6**. The formic acid was adsorbed on the surface of the metals which named Cu and Sn by chemisorption, and then metal formates which named Cu and Sn formates were generated from the reaction between formic acid and metal oxides. The Cu formate decomposed while the Sn formate evaporated first and then precipitated on the surface of the Cu substrate; then it decomposed and formed residues, as shown in **Fig. 4.6**. The main reaction between the solder and formic acid and the evaporation of the Sn formate are represented as follows:

$$SnO_{(s)} + iHCOOH_{(g)} \rightarrow Sn(COOH)_{i(s)} + H_2O_{(g)} \quad (1)$$

$$SnO_{2(s)} + iHCOOH_{(g)} \rightarrow Sn(COOH)_{i(s)} + H_{2(g)} + O_{2(g)} \quad (2)$$

$$Sn_{(s)} + iHCOOH_{(g)} \rightarrow Sn(COOH)_{i(s)} + H_{2(g)} \quad (3)$$

$$Sn(COOH)_{i(s)} \rightarrow Sn(COOH)_{i(g)} \quad (4)$$

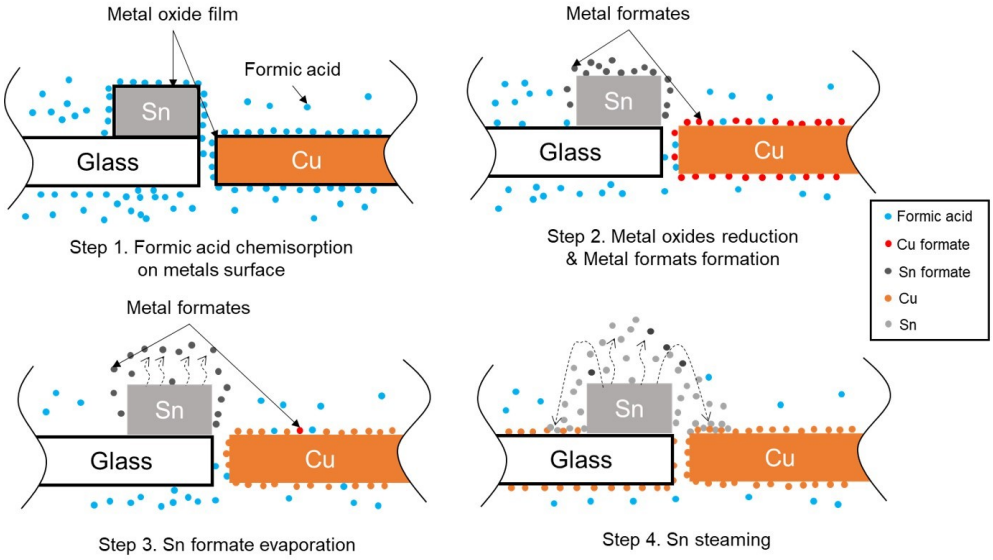

Fig. 4.6 *Diagram of Sn steaming hypothesis.*

A less content Sn was detected using RMA flux at 250 °C heating for 600 s, as shown in **Fig. 4.5(f)**. This may cause by the spattering of flux containing within molten Sn. In order to confirm the spattering of flux. The distribution of C element on Cu pads using RMA flux, under a FA atmosphere, and under the N_2 atmosphere was determined by EPMA mapping analysis, as shown in **Fig. 4.7**. **Fig. 4.7(a)** shows the SEM image of Cu pads using RMA flux. There were many stains containing C on the Cu pads when using RMA flux (see **Fig. 4.7(b)**), while the C signal was hardly detected on the Cu pads under the FA atmosphere and N_2 atmosphere, as shown in **Figs. 4.7(c) and (d)**. Because the RMA flux is organic [5], the stain was believed from a spattering of RMA flux. The spattering of RMA flux was capable of being confirmed in this study.

In order to further study the residues under a FA atmosphere, the morphologies of residues near Sn on glass pad under different conditions were observed by high magnification SEM images, as shown in **Fig. 4.8**. The micro-morphologies of the observation area schematized in **Fig. 4.8(a)** under different conditions were significantly different. Some nano-scale white particles were found when the peak temperatures reached 210 °C and 250 °C under a FA atmosphere. The composition of this particle was determined by EDS. The particle contained approximately 1.75 at.%

Sn, while no Sn element was detected in the dark area. When the temperature reached 290 °C, the nano-scale particles decreased, instead of the polyhedron-shape structure covering the whole observation area. The structure was contained approximately 10 at.% Sn. Because the set temperature (290 °C) was much higher than the melting temperature of Sn, considering the morphology of this structure[6], the structure is likely to be Cu-Sn intermetallic compounds. Unfortunately, it is hard to analyze the specific molar ratios of elements accurately by our EDS at this magnification. **Fig. 4.8(g)** shows the SEM image of the observation area on Cu pads using RMA flux. There are some irregular organic residues (containing 60 at.% C confirmed by EDS) on the surface, combining with **Figs. 4.7 (a) and (b)**, it should be flux residue.

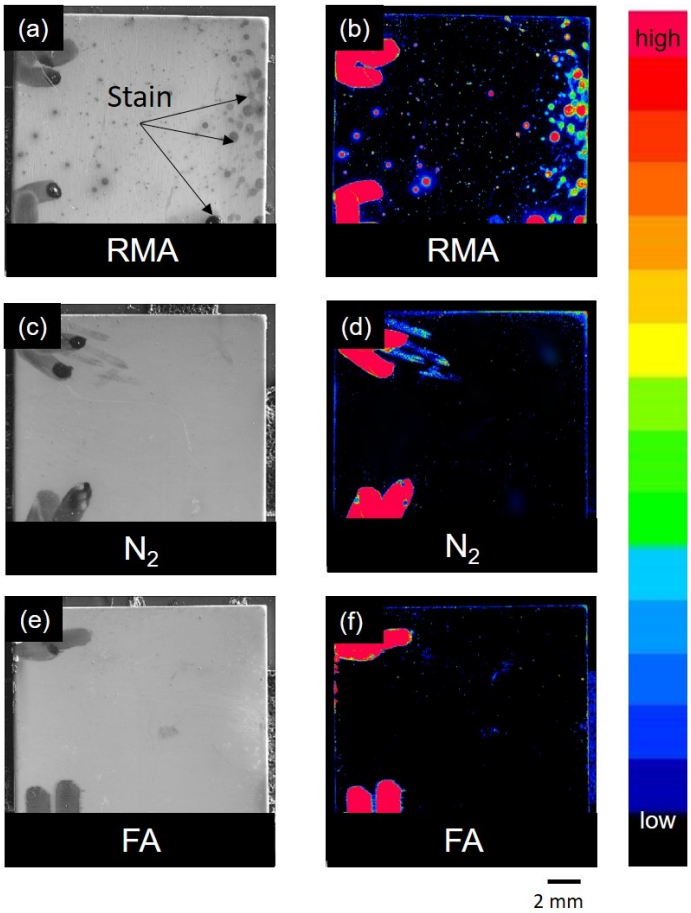

Fig. 4.7 *EMPA analysis for C element on Cu pads: (a) SEM image of Cu pad using RMA flux; (b) EPMA mapping result of C element on Cu pad using RMA flux; (c) SEM image of Cu pad under N_2 atmosphere; (d) EPMA mapping result of C element on Cu pad under N_2 atmosphere; (e) SEM image of Cu pad under FA atmosphere; (f) EPMA mapping result of C element on Cu pad under a FA atmosphere.*

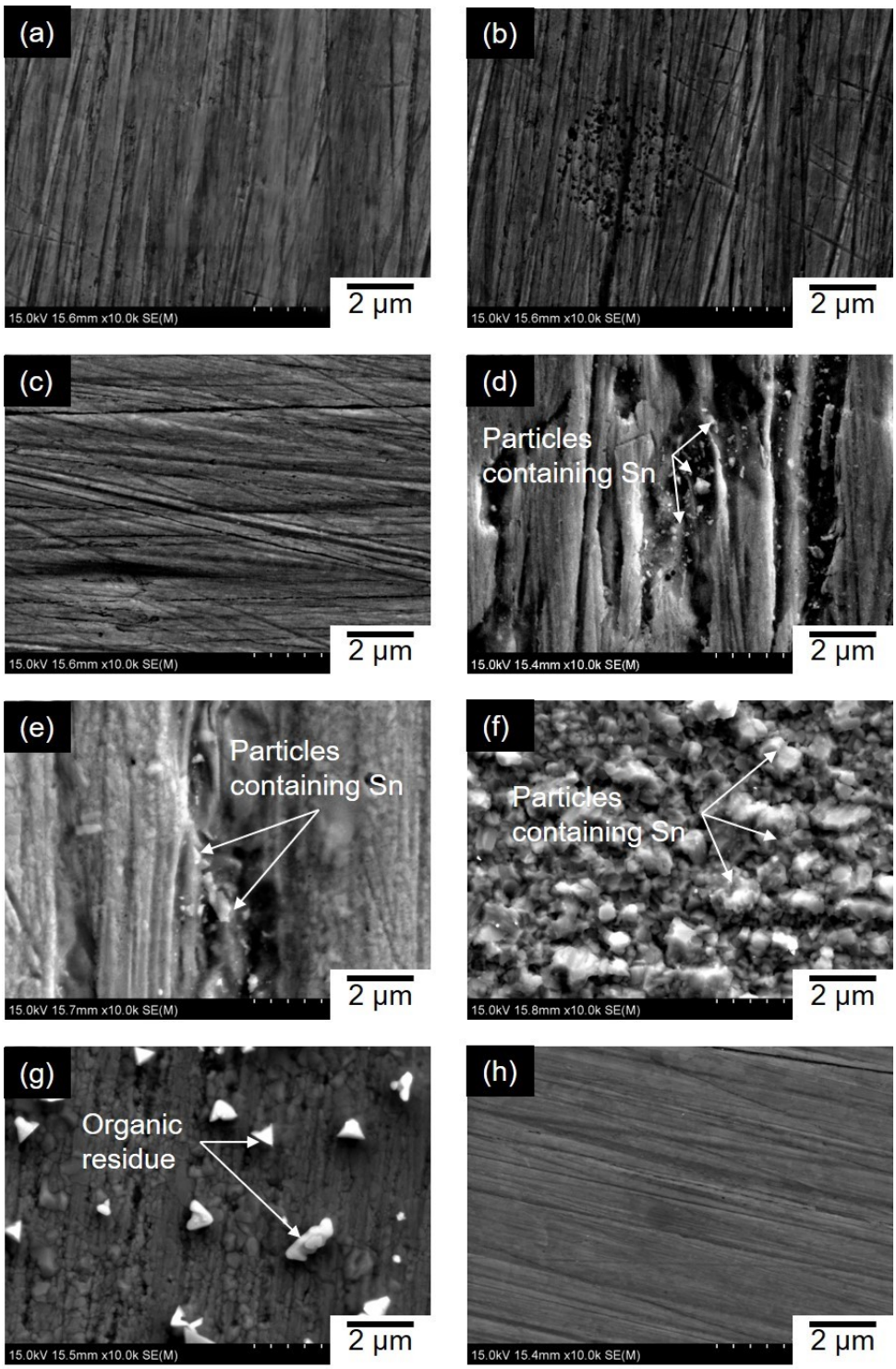

Fig. 4.8 *Morphologies of residues on Cu pads: (a) SEM image of Cu pad untreated; (b) SEM image of Cu pad under a FA atmosphere at 130 °C; (c) SEM image of Cu pad under a FA atmosphere at 170 °C; (d) SEM image of Cu pad under a FA atmosphere at 210 °C; (e) SEM image of Cu pad under a FA atmosphere at 250 °C; (f) SEM image of Cu pad under a FA atmosphere at 290 °C; (g) SEM image of Cu pad using RMA flux; (h) SEM image of Cu pad under* N_2 *atmosphere.*

In order to the further study of the residue. The XRD was used to distinguish the phases on Cu pad. The XRD results of Cu pad under a FA atmosphere is shown in **Fig. 4.9.** The Cu_6Sn_5 IMC was detected. Hence, the SAC solder will spread not only on the Cu but also on the IMCs via the Sn steaming phenomenon under FA atmosphere in **Chapter 2**. In previous studies, it was found that the final contact angle of lead-free solder on the IMC layer (Cu_6Sn_5/Cu_3Sn) was lower than that of the same solder on the Cu surface[7-9]. The final contact angle of FA solder eventually lower than that of the RMA solder may cause by the solder partly spreading on IMCs. Therefore, during soldering under FA atmosphere, Sn formate produced from solid SAC solder spread across the Cu substrate around the SAC305 solder ball and then formed IMCs at the interface. Owing to the IMC formation via the reaction between SAC solder and Cu substrate, the molten solder ball could spread across the surface of IMCs, as shown in **Fig. 4.10**.

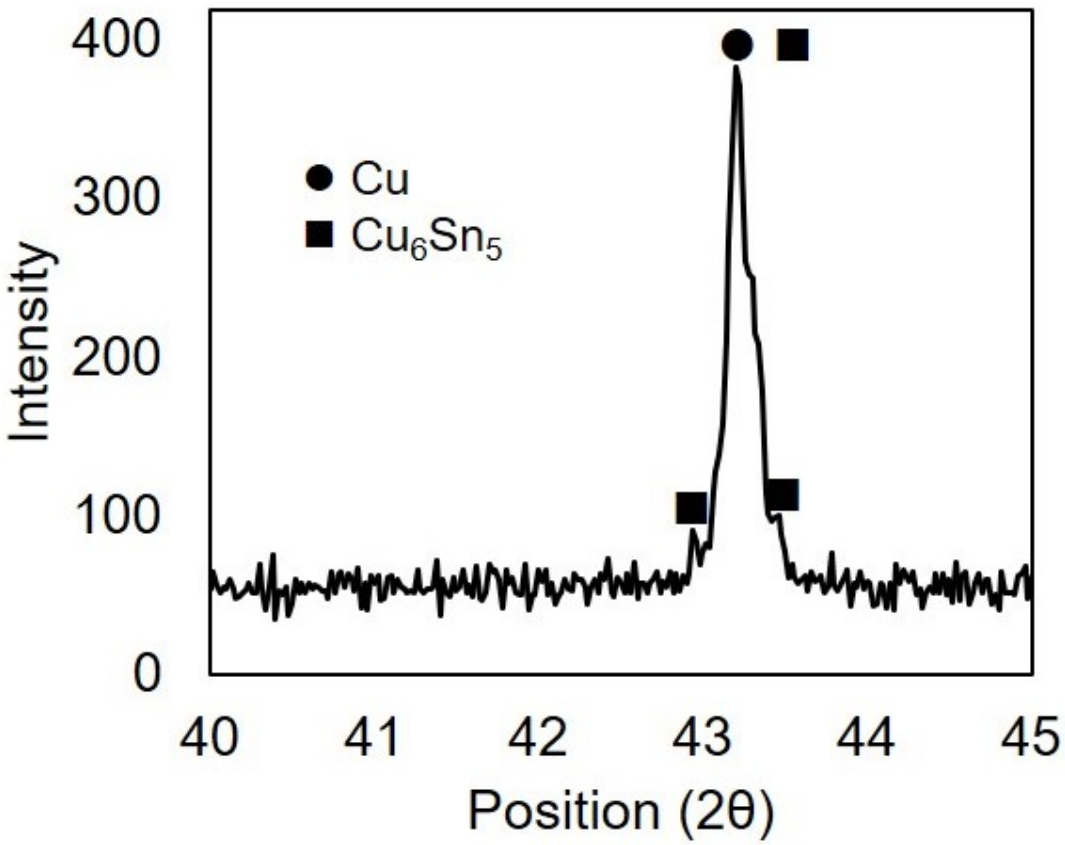

Fig. 4.9 *XRD pattern of Cu pad under a FA atmosphere after Sn steaming experiment.*

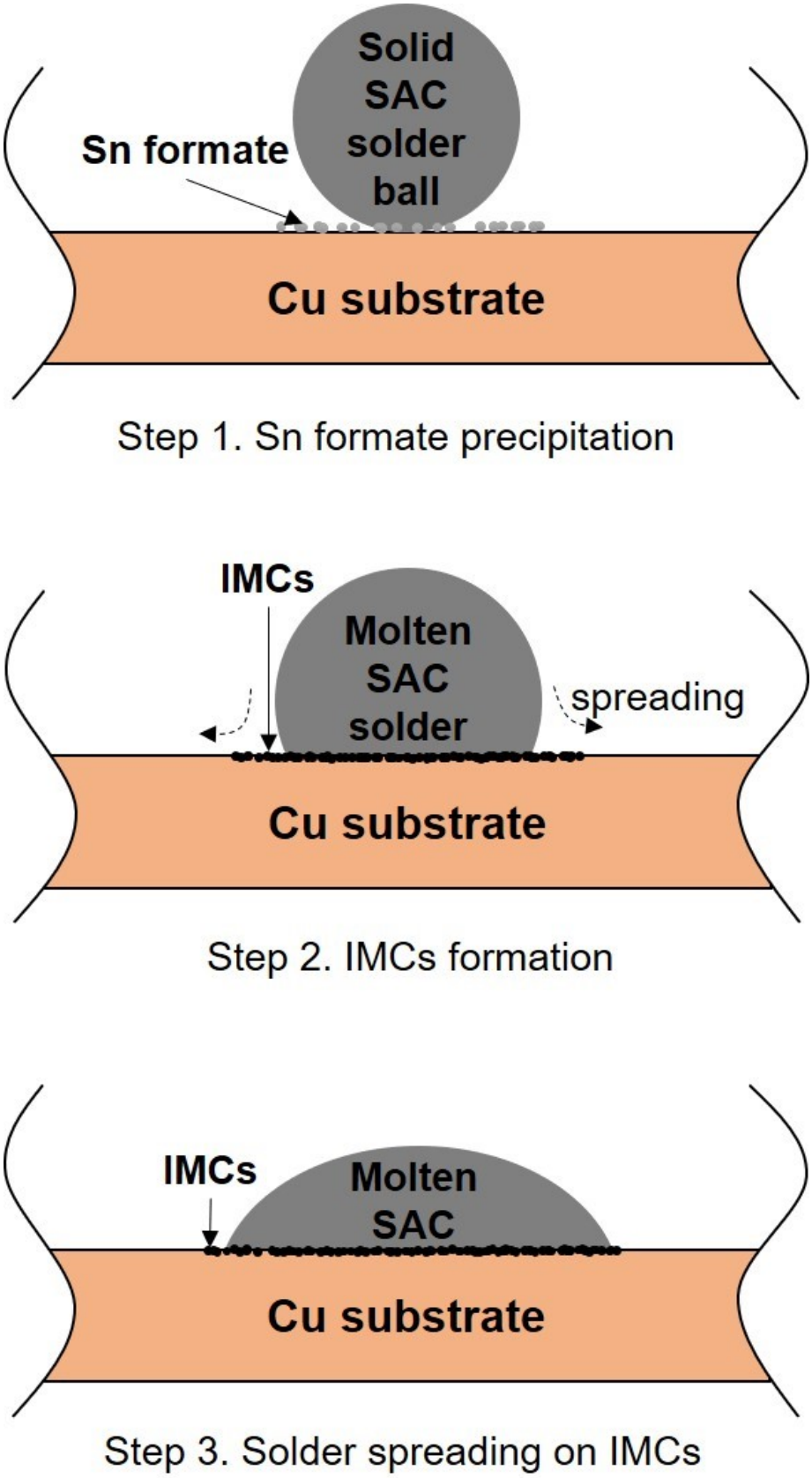

Fig. 4.10 Effect of Sn steaming phenomenon on wettability.

4.3.2 Effect of heating time on Sn steaming phenomenon under FA atmosphere

Fig. 4.11 shows the distribution of Sn element on Cu pads at 250 ℃ after 60, 600, and 3600 s heating time by EPMA mapping. When the heating time was controlled within 60 s, the Sn steaming phenomenon was not serious under a FA atmosphere. The Sn element area on the Cu pads grew up with the increasing heating time at the same temperature. Morphologies of the Sn element area on Cu pads at 250 ℃ for a various heating time under a FA atmosphere were observed by SEM, as shown in **Fig. 4.12**. The particles containing Sn (confirmed by EDS) became more and larger after heating for 3600 s. And the surface of the Cu pad became rougher after heating for 3600 s. This suggests Sn steamed more with heating time increasing, which is consistent with the EPMA results in **Fig. 4.11**.

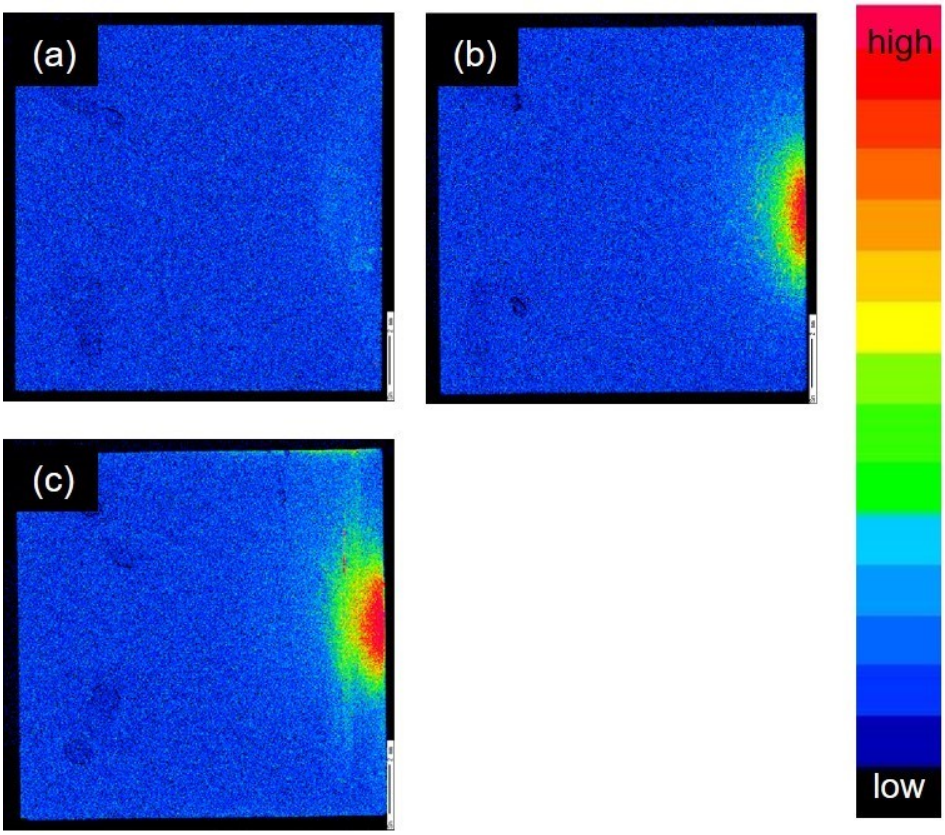

Fig. 4.11 *EMPA mapping results of Sn element on Cu pads under a FA atmosphere heating at 250 ℃ for various heating times: (a) 60 s; (b) 600 s; (c) 3600 s.*

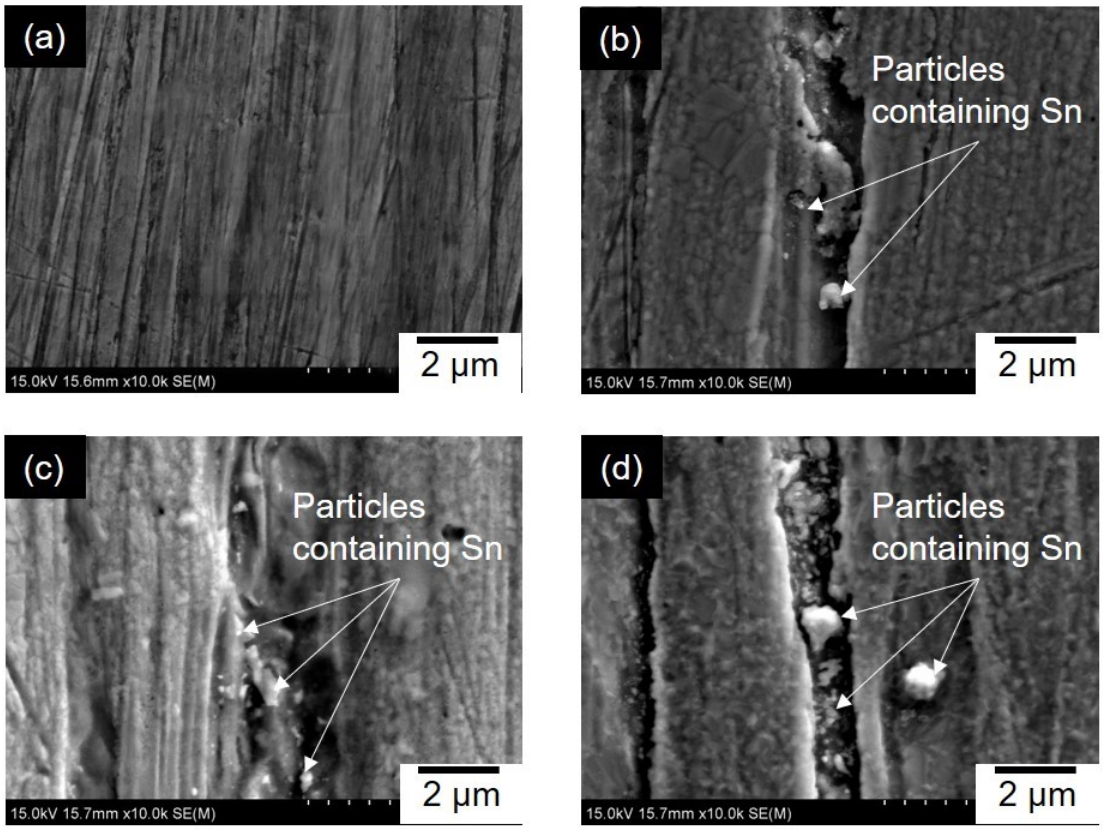

Fig. 4.12 *Morphologies of residues on Cu pads at 250 ℃ for various heating times: (a) Cu pads untreated; (b) SEM image of Cu pad heating for 60 s; (c) SEM image of Cu pad heating for 600 s; (d) SEM image of Cu pad heating for 3600 s.*

4.4 Conclusion

In this chapter, the thermal effect on the Sn steaming phenomenon under the FA atmosphere was investigated.

The Sn steaming phenomenon results from the formation of Sn formate under a FA atmosphere. When the temperature below 170 ℃, Sn steaming phenomenon was not serious. When the temperature reached 210 ℃ and prolonged to 290 ℃, the Sn steaming phenomenon was observed. The Sn steaming phenomenon under a FA atmosphere became more serious with the higher temperature and longer heating time.

The spattering of RMA flux was also confirmed in this study. The spattering not only lead to the existing of flux residues but also caused a slight Sn steaming phenomenon in this study.

Based on the thermal effect on the Sn steaming phenomenon under a FA atmosphere in this study, the process of heating time within 60 s is suggested for fluxless soldering using SAC solder.

Reference

[1] F. Conti, A. Hanss, O. Mokhtari, S.K. Bhogaraju, G. Elger, Formation of tin-based crystals from SnAgCu alloy under formic acid vapor, New Journal of Chemistry (2018).

[2] F. Conti, A. Hanss, O. Mokhtari, S.K. Bhogaraju, G. Elger, Formation of tin-based crystals from a SnAgCu alloy under formic acid vapor, New Journal of Chemistry 42(23) (2018) 19232-19236.

[3] O. Mokhtari, F. Conti, S.K. Bhogaraju, M. Meier, H. Schweigart, U. Tetzlaff, G. Elger, Characterization of tin-oxides and tin-formate crystals obtained from SnAgCu solder alloy under formic acid vapor, New Journal of Chemistry (2019).

[4] J.H. Espenson, Chemical kinetics and reaction mechanisms, McGraw-Hill New York1995.

[5] D. Bušek, K. Dušek, D. Růžička, M. Plaček, P. Mach, J. Urbánek, J. Starý, Flux effect on void quantity and size in soldered joints, Microelectronics Reliability 60 (2016) 135-140.

[6] J. Wang, H. Nishikawa, Impact strength of Sn–3.0 Ag–0.5 Cu solder bumps during isothermal aging, Microelectronics Reliability 54(8) (2014) 1583-1591.

[7] G. Kumar, K.N. Prabhu, Review of non-reactive and reactive wetting of liquids on surfaces, Advances in colloid and interface science 133(2) (2007) 61-89.

[8] P. Kim, K. Tu, Morphology of wetting reaction of eutectic SnPb solder on Au foils, Journal of Applied Physics 80(7) (1996) 3822-3827.

[9] H. Wang, H. Zhao, D.P. Sekulic, Y. Qian, A comparative study of reactive wetting of lead and lead-free solders on Cu and (Cu 6 Sn 5/Cu 3 Sn)/Cu substrates, Journal of Electronic Materials 37(10) (2008) 1640-1647.

Chapter 5

Wettability, Interfacial Reaction and Impact Strength of Sn-3.0Ag-0.5Cu Solder/ENIG Substrate by Fluxless Soldering under Formic Acid Atmosphere

5.1 Introduction

A sufficient contact angle of SAC solder on Cu substrate with a typical IMC layer formed at the interface between the solder and Cu substrate during formic acid (FA) reflow soldering is almost equal to that observed for the liquid rosin mildly activated flux (RMA solder), as mentioned in **Chapter 2**. Hence, FA is a promising reagent for fluxless soldering. However, the spreading rate of solder on a Cu substrate under a FA atmosphere was much slower compared with solder using RMA flux at the same conditions, as discussed in **Section 2.3.1.2**. On the other hand, although the solder

bumps under the FA atmosphere showed sufficient impact strength after soldering and enough reliability after thermal aging, some undesired pores were observed at the interface between the solder and Cu substrate after soldering and after thermal aging, as discussed in **Chapter 3**. These phenomena may cause by the continuous reaction between FA and Cu substrate[1, 2].

In this chapter, SAC solder balls were applied onto ENIG substrates under the FA atmosphere, and their wettability and interfacial reactions were examined. Because the mechanical reliability of solder joints is a critical parameter in the electronics industry[3-6], impact tests were conducted on these joints before and after the thermal aging at 150 °C for 168, 512, and 1008 h. Besides, RMA reflow soldering was performed for comparison purposes.

5.2 Experimental

5.2.1 Wettability test

A Sn–3.0mass%Ag–0.5mass%Cu solder (SAC solder) ball with a diameter of 0.76 mm and a Cu substrate with the dimensions 30 mm × 30 mm × 0.5 mm and ENIG finish (ENIG substrate) were prepared for wettability testing, as shown in **Fig. 5.1**. FA gas (5 vol% formic acid + 95 vol% N2) was used as a soldering reducing atmosphere for the fluxless soldering process. The thermal effect observed during the re-melting of the solder ball (reflow) on the wettability of FA-exposed solder was investigated at various temperatures ranging from 250 to 290 °C, as shown in **Table 5.1**. Spreading areas were measured by an optical microscope (OM, KEYENCE VHX-900) after soldering. In situ observations were conducted as second-by-second measurements of the spreading areas using a charge-coupled device (CCD) camera (SONY) to evaluate the corresponding spreading rates. Spreading area and spreading rate were utilized to determine the solder's wettability. The exact values of solder spreading areas were calculated using commercial software (ImageJ).

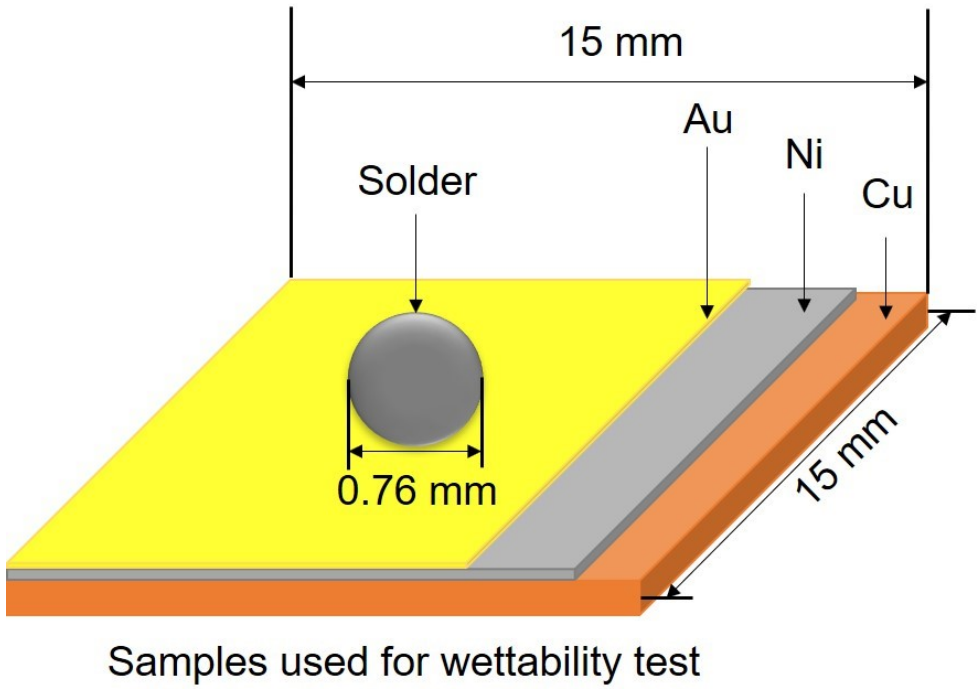

Fig. 5.1 *Schematic diagram of (a) ENIG pads using for wettability test.*

Table 5.1 *Summary of FA-exposed solder heating processes for wettability test.*

Heating process	①	②	③
Pre-heat temperature (°C)	**110**	**110**	**110**
Pre-heat time (s)	**60**	**60**	**60**
Peak-temperature (°C)	**250**	**270**	**290**
Peak-time (s)	**120**	**120**	**120**
Heating rate (°C/s)	**2.5**	**2.5**	**2.5**

5.2.2 Sn steaming phenomenon

In **Chapter 2**, some residues containing Sn on Cu substrate were observed during the fluxless soldering process under a FA atmosphere. In order to confirm the Sn precipitation phenomenon on ENIG finish, in this study, a Cu pad with a pure Sn bulk on its top surface was placed on the left side, and a Cu substrate with ENIG finish was placed at a distance of 1 mm right to the Cu pad, as shown in **Fig. 5.2**. FA gas (5 vol.% formic acid + 95 vol.% N_2) was used as the atmosphere. FA gas was supplied by nitrogen gas through liquid FA stored in a sealed beaker, as shown in **Fig. 5.3**. After introducing the FA atmosphere, the chamber was heated to 250 °C for 30 min. A mapping of the Sn element on the ENIG substrate was detected by an electron probe micro-analyzer (EPMA). The micromorphology of ENIG substrate after residue precipitation was observed by a field-emission scanning electron microscope (SEM).

5.2.3 Interfacial reactions and impact test

Solder bumps consisting of the SAC solder balls on ENIG pads embedded into a flame retardant-4 (FR-4) substrate were used for studying interfacial reactions and impact strengths via a reflow process, as shown in **Fig. 5.4**. The corresponding reflow profile is shown in **Fig. 5.5**. To obtain ENIG substrates, electroless Ni layers with thicknesses of 5 μm were deposited onto Cu pads, and the thickness of the Au flash on the Ni layer was approximately 50 nm. Before the reflow process, the SAC solder balls were immersed in a 4 vol% HCl solution for 120 s, after which both the balls and FR-4 ENIG substrates were ultrasonically cleaned in ethanol for 300 s. After the reflow, the solder bumps were aged inside an oil bath at 150 °C for 168, 512, and 1008 h.

To estimate the impact strengths of the soldered bumps, high-speed tests were conducted using a micro-impact tester (MI-S, Yonekura Mfg. Co., Ltd.). The shear rate was 1 m/s, and the impact height from the solder resist was equal to 0.08 mm (**Fig. 5.6**). Ten bumps were evaluated under each condition using the average value of the impact strength.

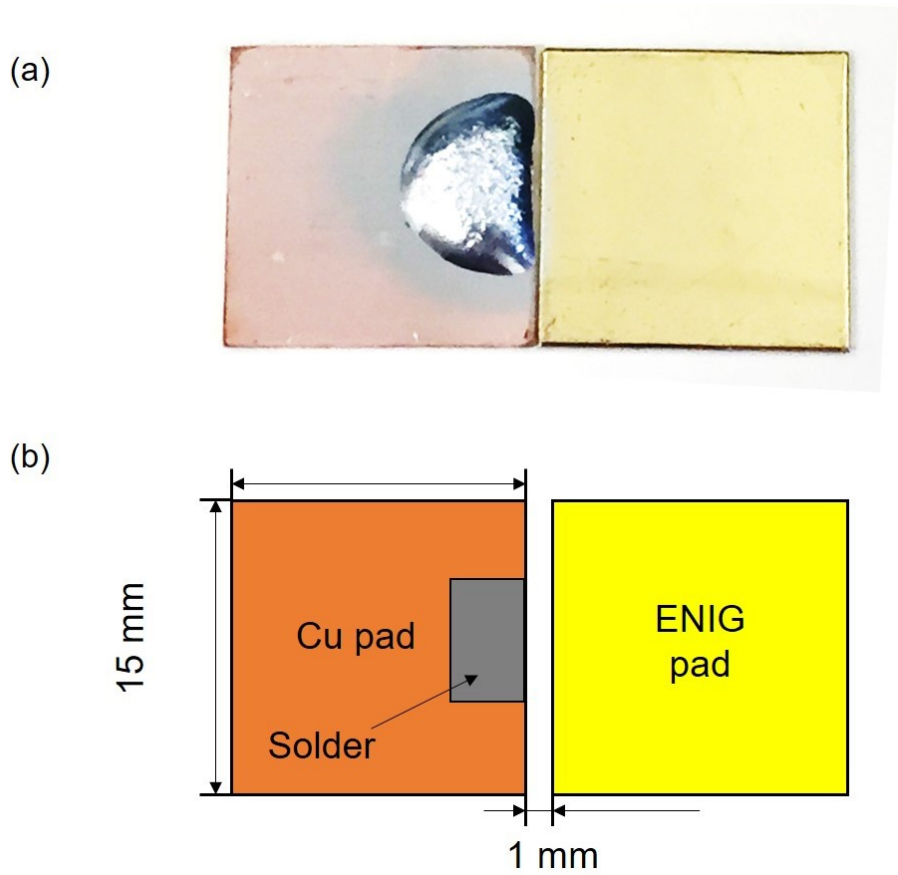

Fig. 5.2 *Sample for Sn steaming experiment: (a) sample image; (b) schematic image.*

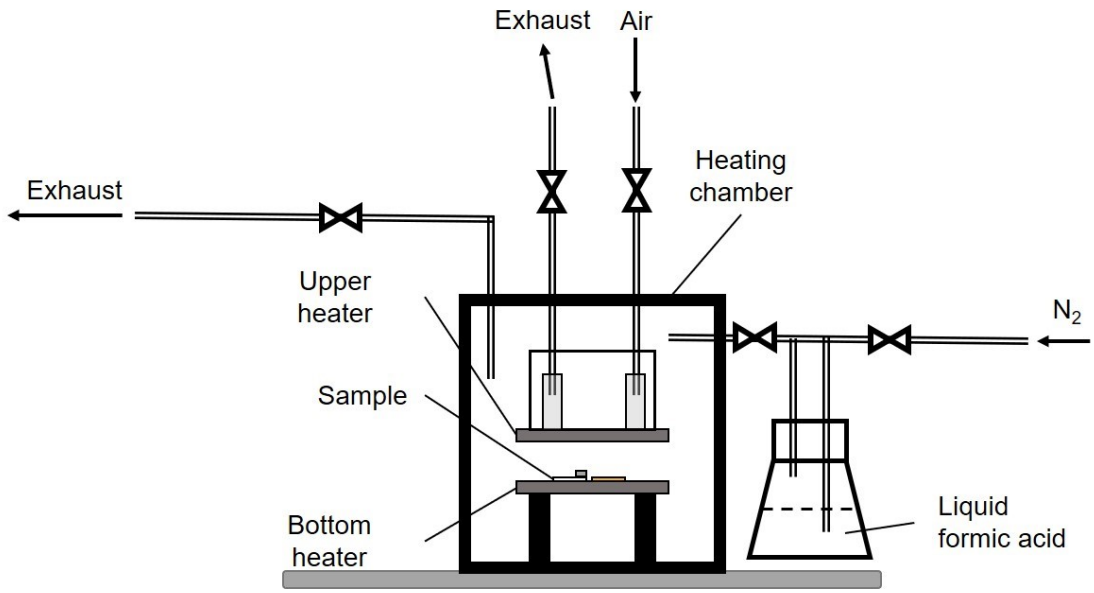

Fig. 5.3 *Schematic view of the Sn steaming experiment.*

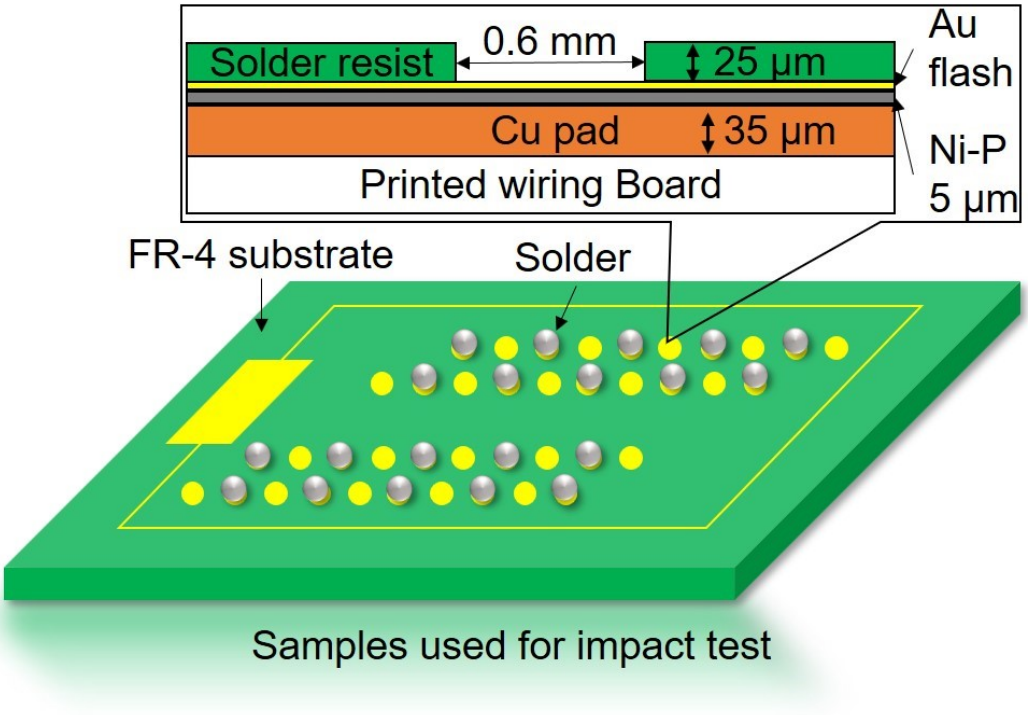

Fig. 5.4 *Schematic diagram of Cu substrate with ENIG finish using for the soldering process.*

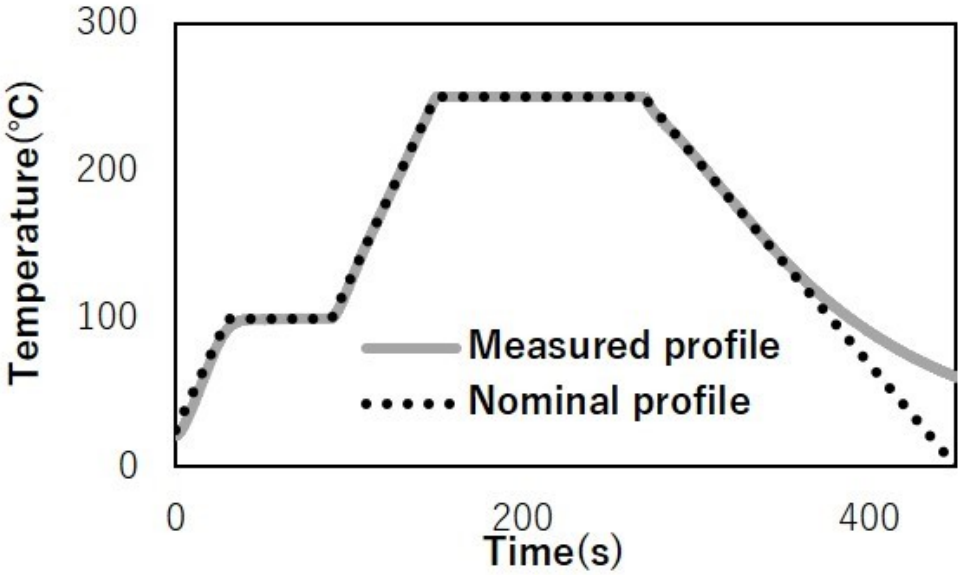

Fig. 5.5 *Soldering process of RMA solder.*

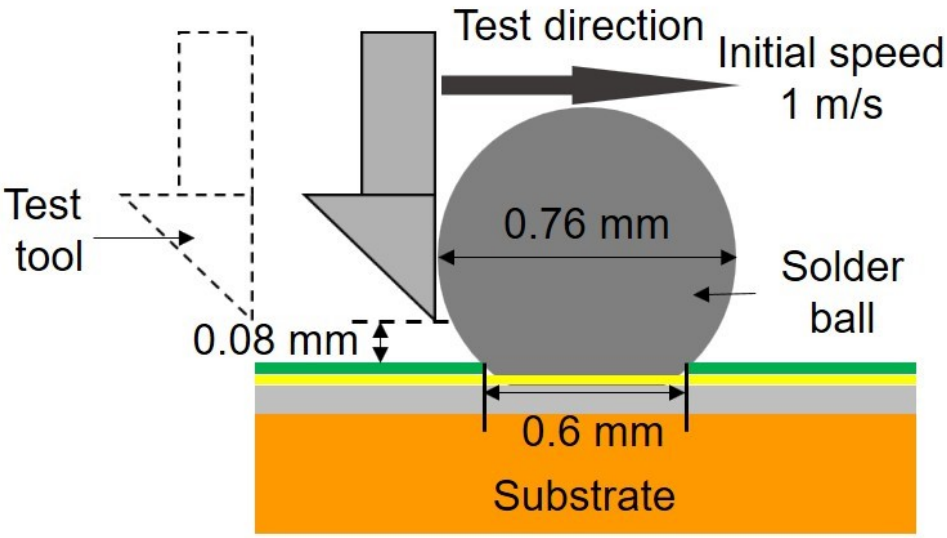

Fig. 5.6 *Schematic diagram of a high-speed impact test.*

Cross-sectional microstructures of the solder bumps were observed by a field-emission scanning electron microscope (FE-SEM, Hitachi SU-70), and their IMC thicknesses were determined. Elemental compositions of the solder bumps were identified by field-emission electron probe microanalysis (EPMA, JEOL JXA-8530F).

5.3 Results and discussion

5.3.1 Wettability test

Fig. 5.7 shows the wetting results of solders on ENIG finish under a FA atmosphere and using RMA flux. **Fig. 5.7(a)** shows the average spreading areas obtained for FA-exposed solder at 250 °C, 270 °C, and 290 °C after 2 min and for the solder containing RMA flux at 250 °C corresponding to the reflow temperature of SAC solder joints. The average spreading area in the former case was 31.2 mm^2, and that in the second case was 28.4 mm^2. Moreover, the average spreading areas of FA-exposed solder during the reflows at 270 °C and 290 °C were 37.4 and 40.8 mm^2, respectively. The obtained results show that the average spreading area of FA-exposed solder exhibits a positive correlation with the reflow temperature under the specified conditions, which significantly improves solder's wettability[7, 8] because the viscosity and surface

tension of liquid Sn-based solders typically demonstrate negative correlations with temperature unless the latter is extremely high[9, 10]. **Fig. 5.7(b)** shows the charge of the spreading area obtained for FA-exposed and RMA solders during heating of the reflow at 250 °C. The observed trends are very similar, while the spreading area of FA-exposed solder is slightly larger than that of the solder with RMA flux. The spreading areas of both solders gradually increased even at the end of the reflow process, which was in good agreement with the results of a previous study[11]. The reason for the enhanced wettability of the solder exposed to FA atmosphere is the formation of an IMC layer before solder melting.

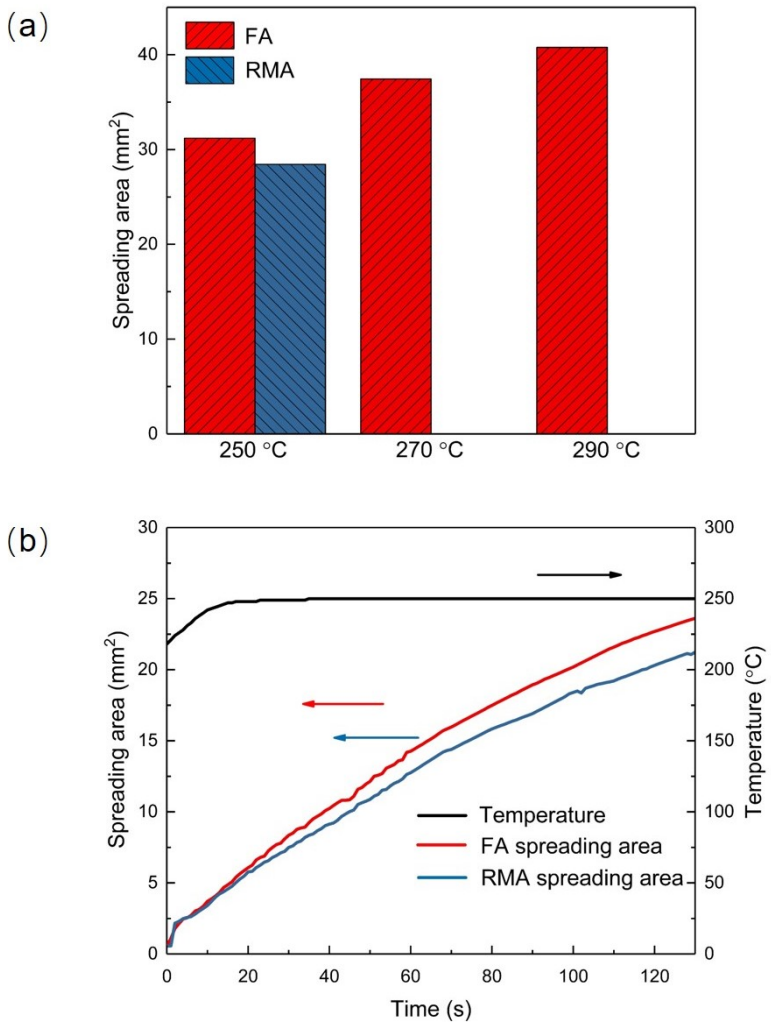

Fig. 5.7 *Spreading area of solders on ENIG pad: (a) the average spreading areas of solders under formic acid atmosphere at 250 °C, 270 °C and 290 °C for 2 mins, and that of solder using RMA flux was at 250 °C; (b) the tendency of the spreading of solder under formic acid atmosphere and solder using RMA flux of reflow at 250 °C.*

Residues containing Sn were formed on the ENIG pad near the Cu pad after heating at 250 °C for 30 min, as shown in **Fig 5.8**. **Fig .5.8 (a)** shows the SEM image of ENIG pad after heating under a FA atmosphere, while the distribution of Sn on ENIG pad by EPMA mapping is shown in **Fig. 5.8 (b)**. Because the boiling point of Sn (about 2602 °C) is much higher than 250 °C, we believe that the volatilization of Sn barely occurs under this condition. Considering with **Chapter 4**, the Sn residues were likely caused by the Sn formate steaming (Sn(COOH)i(g)) from the left side (Sn/glass) to the right side (ENIG) before the Sn phase melted on the glass surface[12] followed by the Sn formate (Sn(COOH)i(s)) decomposition on the ENIG substrate at a temperature of around 200 °C[12-14].

The formation process of Sn residues on the ENIG substrate via Sn formate steaming is illustrated in **Fig. 5.8(c)**. The SEM image of the ENIG substrate without Sn residues is shown in **Fig. 5.8 (d)**, while that with Sn residue is shown in **Fig. 5.8 (e)**. The surface modification caused by Sn melting. The modified surface with a composition determined by EPMA contained 57.39 at.% Sn, 30.68 at.% Ni, and 11.93 at.% Au. As the reflow temperature (250 °C) was greater than the Sn melting point (232 °C), we assumed that the surface modification was caused by the formation of IMCs (Ni_3Sn_4 and $AuSn_4$)[15, 16]. Therefore, during soldering under FA atmosphere, Sn formate produced from solid Sn spread across the ENIG substrate around the SAC305 solder ball (see **Fig. 5.9(a)**), and then decomposed into Sn on the ENIG substrate at approximately 200 °C (**Fig. 5.9(b)**). As the temperature increased above 232 °C, the SAC solder ball and decomposed Sn melted and formed IMCs at the interface (**Fig. 5.9(c)**). Owing to the IMC formation via the reaction between the decomposed Sn and ENIG substrate, the molten solder ball could spread across the surface of IMCs (**Fig. 5.9(d)**).

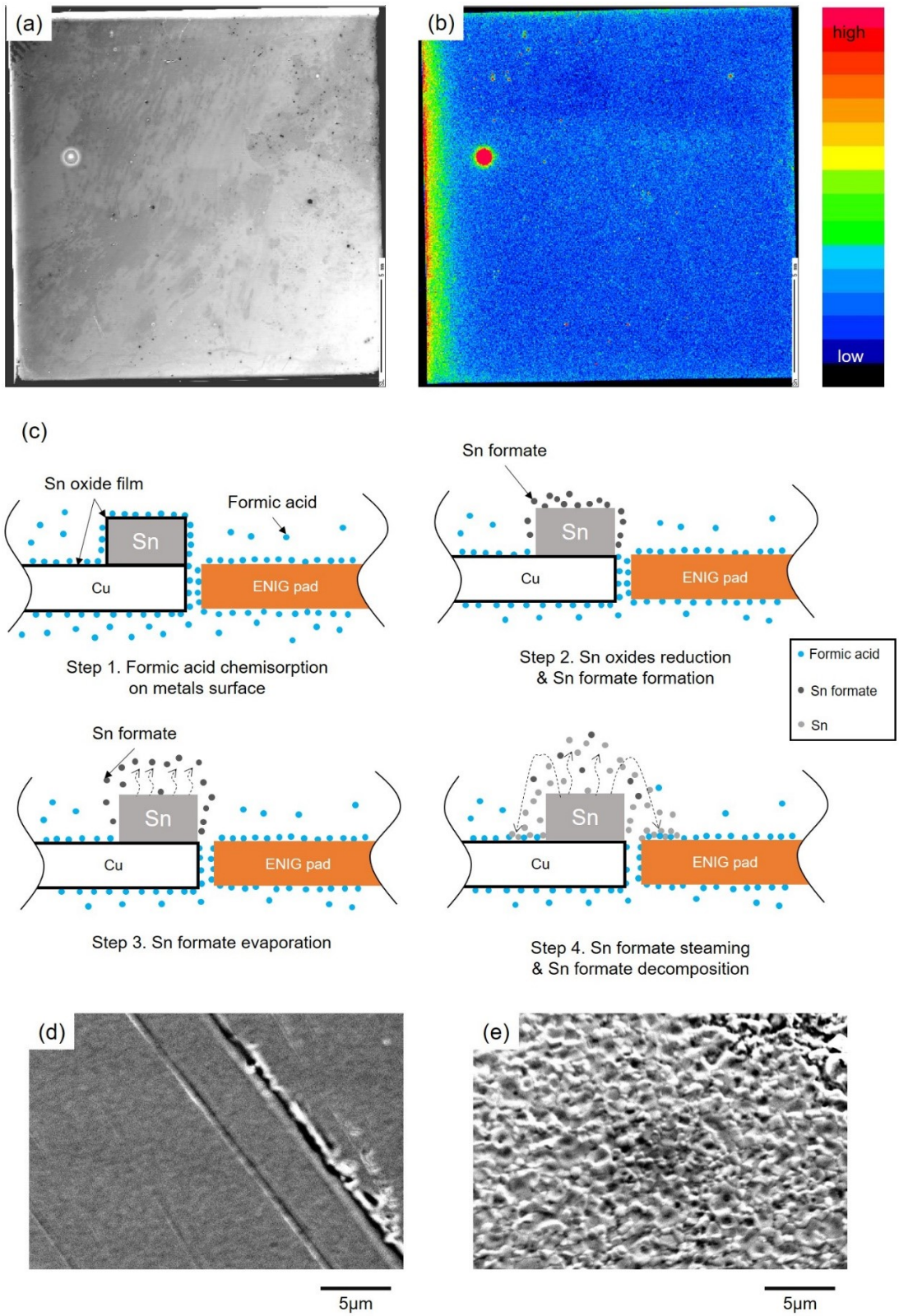

Fig. 5.8 *Diagram of Sn steaming hypothesis: (a) SEM image of ENIG pad under a FA atmosphere heating at 250 °C for 30 min; (b) EPMA mapping results of Sn steaming experiment; (c) the process of Sn residues on the ENIG substrate via Sn formate steaming hypothesis; (d) SEM image of ENIG pad without Sn residues; (e) SEM image of IMC in the area of Sn residues.*

In general, the wetting of solder on a particular substrate produces a typical reactive wetting system[17], in which IMCs precipitate at the liquid/solid interface[18]. According to the reaction product control (RPC) model, reaction products determine the ultimate solder wettability and spreading process[19]. In this study, although the same (Cu, Ni)$_6$Sn$_5$ layer was formed and contacted the liquid solder, the solder wettability under the FA atmosphere was greater than that of the solder containing RMA flux. In previous studies, it was found that the wettability of lead-free solder on the IMC layer (Cu$_6$Sn$_5$/Cu$_3$Sn) was higher than that of the same solder on the Cu surface[17, 20, 21]. Besides, the wettability of Sn on the Ag3Sn IMC surface was greater than that of Sn on an Ag substrate[22]. Thus, it can be concluded that the higher wettability of FA-exposed solder as compared with that of the solder containing RMA flux is caused by the spreading of the SAC solder ball on the IMC surface. Meanwhile, the surface roughness was also changed by the formation of IMCs under the FA atmosphere, which significantly affected the solder's wettability[16, 23-26]. Hence, a detailed study of the effects produced by the surface tension driven flow (such as Sn steaming) on the surface morphology under FA atmosphere is required.

We also compared the spreading area of the SAC solder on Cu substrate and ENIG substrate at 250 °C under a FA atmosphere, as shown in **Fig .5.10**. The wettability of the FA-exposed solder on the ENIG pad was significantly greater than that of the same solder on the Cu substrate.

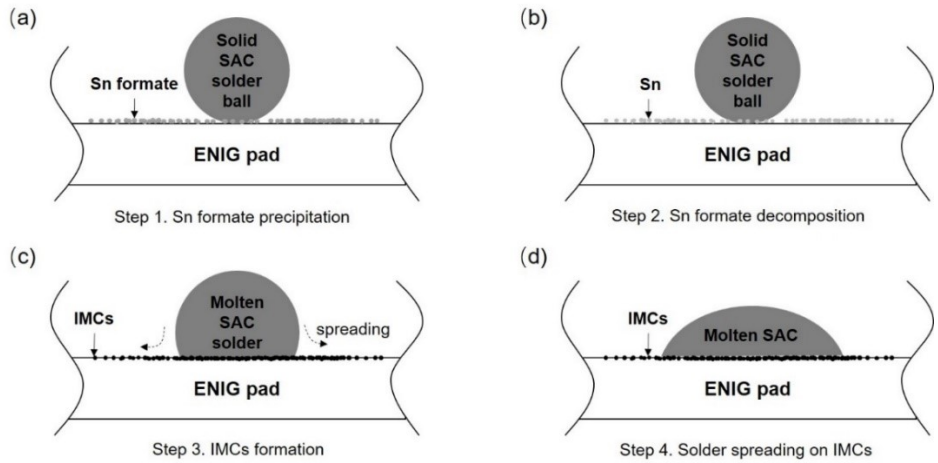

Fig. 5.9 *Effect of Sn steaming phenomenon on wettability.*

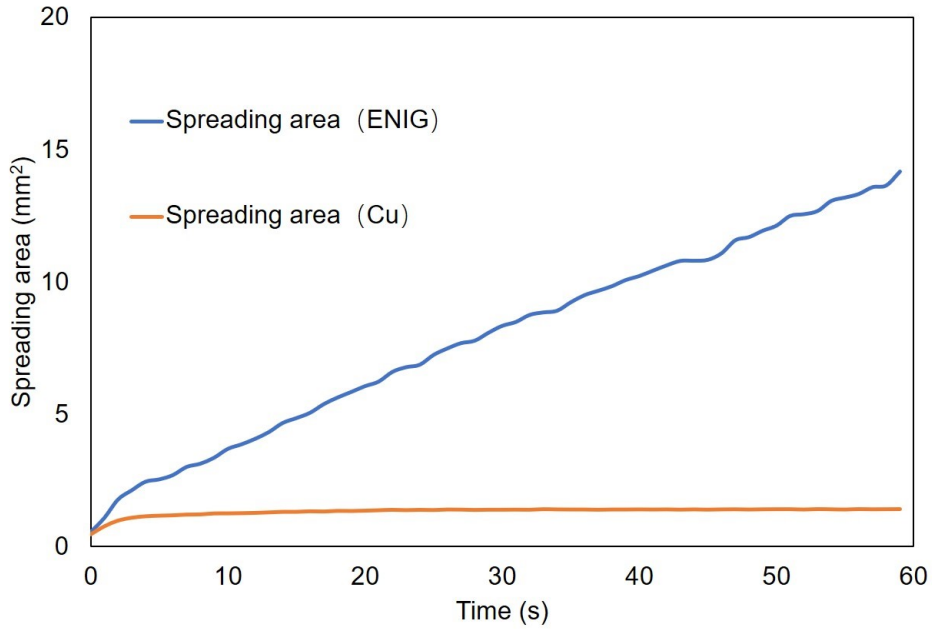

Fig. 5.10 *Tendency of the spreading of FA-exposed solder on ENIG substrate and Cu substrate reflowed at 250 °C.*

5.3.2 Interfacial reaction

Fig. 5.11(a) shows the SEM image of the joint cross-section obtained for as-reflowed FA soldering. After the reflow process, the Au flash layer dissolved into the molten SAC305 solder, leaving (Cu, Ni)$_6$Sn$_5$ IMC at the interface between SAC305 solder and the Ni(P) layer. Moreover, a thin Ni$_3$P layer was produced between the (Cu,Ni)$_6$Sn$_5$ IMC and Ni(P) layers. The Cu phase of the former layers resulted from SAC305 solder, and its composition determined by EPMA corresponded to 42.60 at.% Cu, 16.50 at.% Ni, and 40.90 at.% Sn. According to the results of thermodynamic calculations, (Cu, Ni)$_6$Sn$_5$ was formed by the dissolution of Ni in the Cu$_6$Sn$_5$ phase because the reflow time was not sufficient for the formation of a ternary compound Ni$_{26}$Cu$_{29}$Sn$_{45}$[27]. Consequently, (Cu,Ni)$_6$Sn$_5$ was produced at the interface instead of Cu$_6$Sn$_5$ or Ni$_3$Sn$_4$[28]. Furthermore, a P-rich Ni layer was also formed between the (Cu,Ni)$_6$Sn$_5$ and Ni-P layers; it contained approximately 25 at.% P suggesting Ni$_3$P as its possible composition[15]. Ni(P) species were crystallized into Ni$_3$P ones because the self-crystallization temperature of amorphous Ni(P) was 250 °C[28].

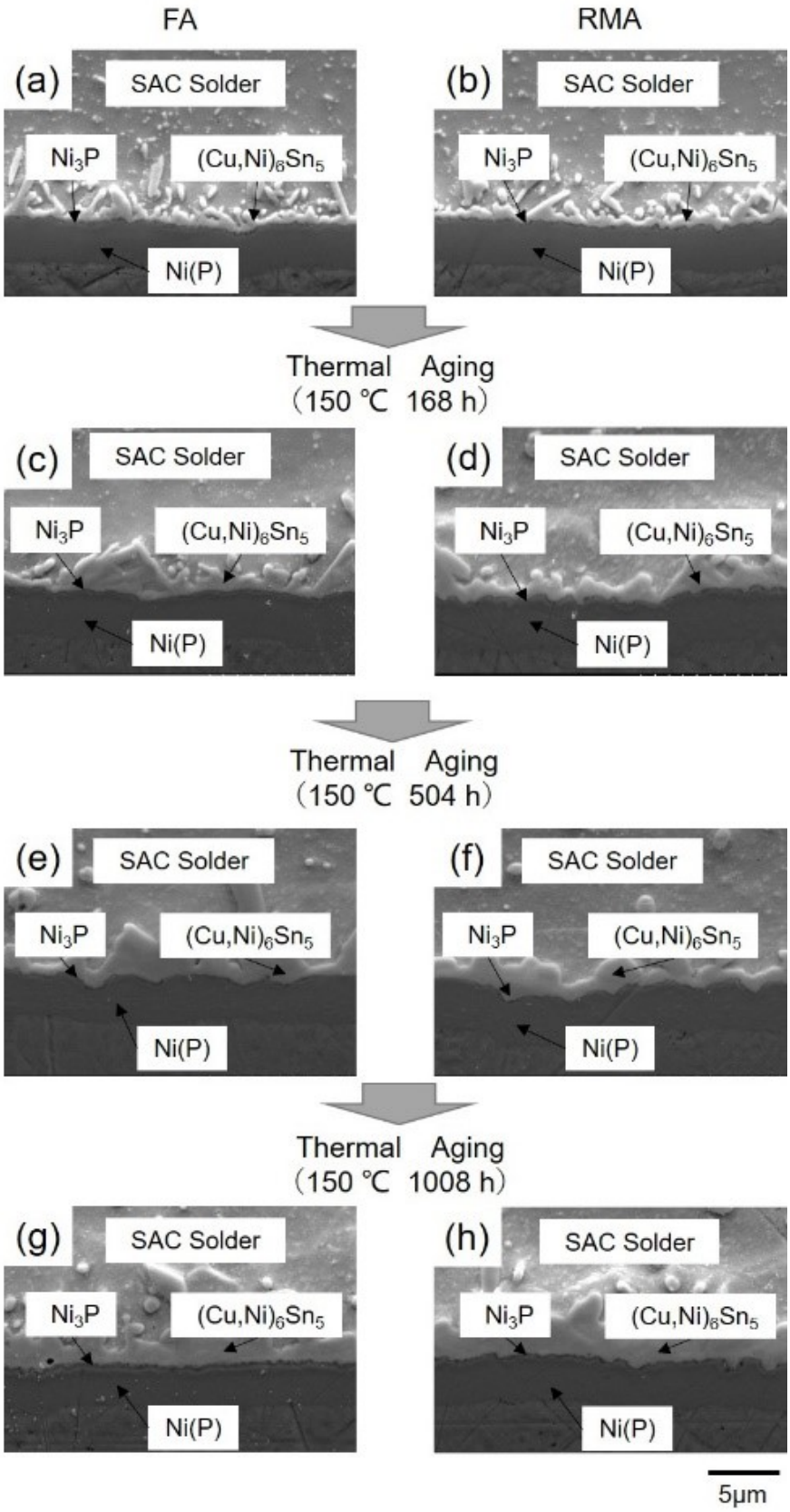

Fig. 5.11 *Cross-sectional SEM image of solder bumps on ENIG substrate for FA soldering and RMA soldering: (a), (b)as -reflowed solder bumps; (c), (d) thermally aged solder bumps for 168 h; thermally aged solder bumps for 504 h; thermally aged solder bumps for 1008 h.*

After the thermal aging for 1008 h, the thickness of the $(Cu,Ni)_6Sn_5$ layer increased (**Fig. 5.11(g)**); moreover, the presence of stable Ni_3P species strongly affected the growth of the Ni-Sn IMC phase[29]. Hung et al.[30, 31] suggested that the Ni_3P layer could act as a barrier to the diffusion of Ni and consequently suppressed the growth of the Ni_3Sn_4 layer. Additionally, the interfacial morphologies of RMA solder before (**Fig. 5.11(b)**) and after (**Fig. 5.11(h)**) thermal aging were almost identical to those of FA-exposed solder. **Fig. 5.12** shows that the IMC growth rate during FA reflow soldering was almost equal to that during RMA reflow soldering at different aging times, and that the thickness of the IMC layer was proportional to the square root of the aging time, indicating that FA atmosphere barely affected the interfacial reaction between the ENIG substrate and SAC solder. From the results presented above, it can be concluded that FA reflow soldering is a promising alternative to RMA reflow soldering in terms of performance and environmental characteristics, although no reliability testing of the former method has been conducted yet.

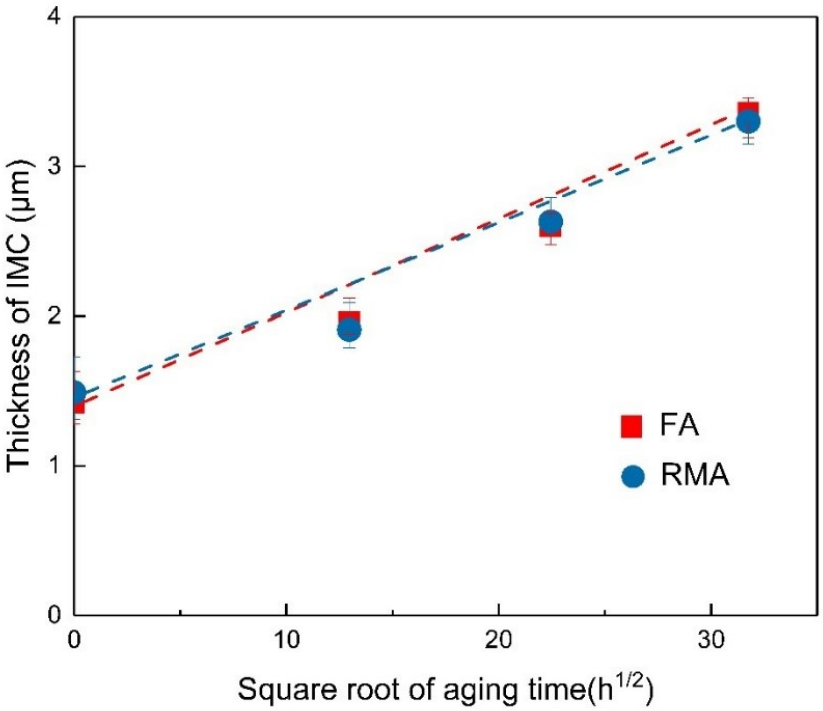

Fig. 5.12 *Statistics of IMC thickness of solder bumps for FA soldering and RMA soldering.*

5.3.3 Impact strength

The mechanical reliability of FA reflow soldering was evaluated by performing impact tests, and the obtained data were compared with the results of RMA reflow soldering (**Fig. 5.13**). During FA reflow soldering, the impact strength before the thermal aging at 150 °C was 107 MPa, and its magnitude decreased to 86, 83 and 80 MPa after the thermal aging for 168, 504, and 1008 h, respectively. All impact strengths of the samples used for FA reflow soldering were slightly higher than those of the specimens utilized for RMA reflow soldering, and their decreases were likely caused by the growth of brittle IMCs at the interface during thermal aging.

Fig. 5.14 shows the EPMA mappings corresponding to the SEM images of the fracture surfaces obtained for the FA-exposed and RMA solders before and after the thermal aging for 168, 504, and1008 h (impact direction is oriented from left to right).

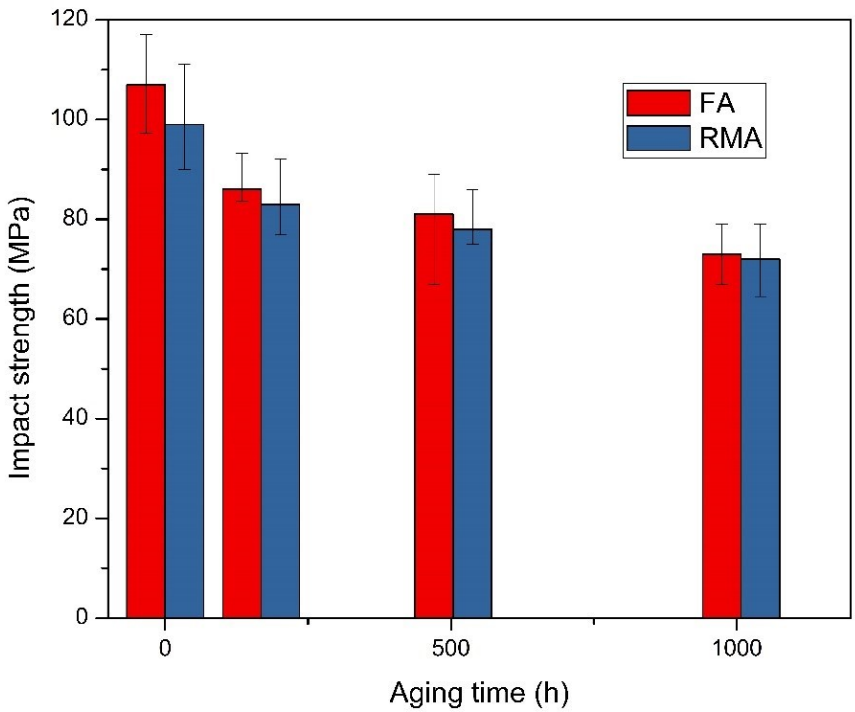

Fig. 5.13 *Effect of aging time on the impact strength of FA-exposed and RMA solder bumps.*

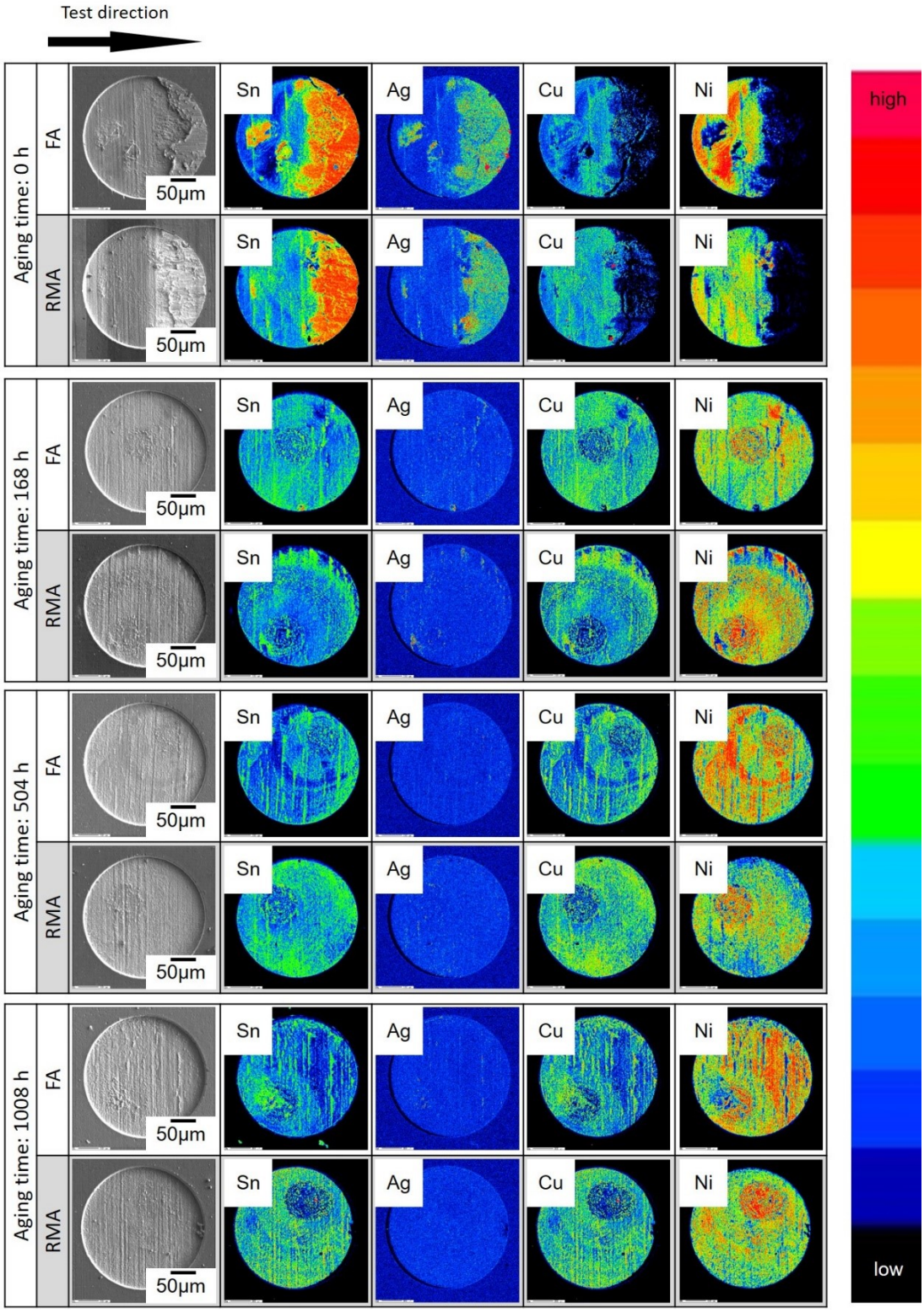

Fig. 5.14 *EPMA mapping analysis results of the fracture surface of as-reflowed and 168, 504, and 1008 h aged FA-exposed and RMA solders in an impact test.*

In the as-reflowed solders, as the high concentration of Ni remained in the left section of the fracture surface, fracture mostly occurred across the IMC layer, while the high concentrations of Sn and Ag were partially preserved in the right section. The joints of both the as-reflowed FA-exposed and RMA solders cracked along the solder/substrate interface and then propagated into the bulk solder. After the thermal aging for 168 h, high contents of Ni were observed across the entire fracture surface, while Sn and Cu species were also detected in the same areas for both cases, suggesting that the fracture occurred within the IMC layer at the solder/substrate interface after thermal aging for 168 h. It was reported previously that ductile fracture occurred in the solder bulk where brittle fracture originated in the IMC layer. Therefore, the as-reflowed solders exhibited both ductile and brittle fractures simultaneously. After 168 h of aging, the fracture mode changed to the total brittle fracture with increasing thickness of the IMC layer. Because the differences in the impact strengths and fracture modes of FA-exposed and RMA solders were very small, the FA atmosphere had almost no effect on their mechanical stabilities. Hence, the latter factor can be neglected when considering the replacement of RMA reflow soldering with FA reflow soldering.

The impact strength of solder bumps after soldering by a fluxless soldering process heating at 250 °C for 2 min under a FA atmosphere and thermal aging at 150 °C for 168, 504, and 1008 h fabricated using Cu substrate and ENIG substrate were also compared, as shown in **Fig. 5.15**. There was a significant difference between the impact strength of the as-reflowed solder bumps fabricated on the Cu and ENIG pads. Before aging, the average impact strength of the solder bumps on the Cu substrates was 126 MPa, while the solder bumps on the ENIG substrates achieved only 107 MPa. In both cases, the impact strength decreased with increasing aging time. Furthermore, after thermal aging, the impact strength of the solder bumps on the ENIG pads was also lower than that of the solder bumps on the Cu pads. These results are well consistent with reference[15, 32]. Many authors have reported that the Ni_3P layer, which forms during prolonged reactions, contributes to a weakened interface and fails easily[16, 28,

30, 31, 33].

5.4 Conclusion

In this chapter, the wettability, interfacial reactions, and impact strength of FA-exposed solder on the ENIG substrate were examined, and the obtained results were compared with the parameters of RMA reflow soldering. As indicated by in-situ observations, the spreading area of the solder exposed to FA atmosphere was 10% greater than that of the solder containing RMA flux, which demonstrated the enhancement of the solder's wettability by FA. The latter was caused by the solder spreading on the interfacial layer of $(Cu, Ni)_6Sn_5$ IMC formed by Sn residues on the ENIG substrate via Sn formate steaming before the solder ball melted during FA reflow soldering. The IMC growth rate of FA-exposed solder was nearly identical to that of RMA solder, and their interfacial reactions were very similar. Moreover, the impact strength of FA-exposed solder was approximately equal to that of RMA solder due to the same interfacial reactions. The decrease in the impact strength observed after 168, 504, and 1008 h of the thermal aging at 150 °C was induced by the growth of the brittle IMC layer at the interface with a similar pattern. The findings of this work indicate that RMA reflow soldering can be potentially replaced with FA reflow soldering for environmental protection during electronic packaging.

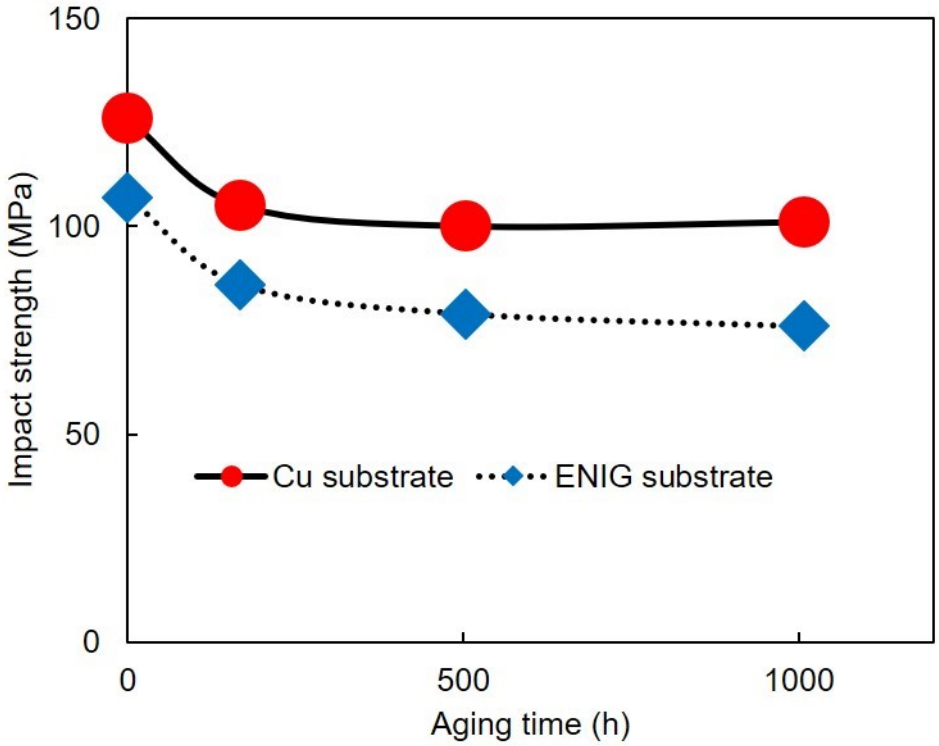

Fig. 5.15 *The impact strength of solder bumps after soldering by a fluxless soldering process heating at 250 °C for 2 min under a FA atmosphere and thermal aging at 150 °C for 168, 504, and 1008 h fabricated using Cu substrate and ENIG substrate.*

Reference

[1] T. Youngs, S. Haq, M. Bowker, Formic acid adsorption and oxidation on Cu (1 1 0), Surface Science 602(10) (2008) 1775-1782.

[2] F. Conti, A. Hanss, C. Fischer, G. Elger, Thermogravimetric investigation on the interaction of formic acid with solder joint materials, New Journal of Chemistry 40(12) (2016) 10482-10487.

[3] M. Date, T. Shoji, M. Fujiyoshi, K. Sato, K. Tu, Ductile-to-brittle transition in Sn–Zn solder joints measured by impact test, Scripta Materialia 51(7) (2004) 641-645.

[4] Y.-S. Lai, H.-C. Chang, C.-L. Yeh, Evaluation of solder joint strengths under ball impact test, Microelectronics Reliability 47(12) (2007) 2179-2187.

[5] J. Wang, H. Nishikawa, Impact strength of Sn–3.0 Ag–0.5 Cu solder bumps during isothermal aging, Microelectronics Reliability 54(8) (2014) 1583-1591.

[6] T. Daito, H. Nishikawa, T. Takemoto, T. Matsunami, Explanation of impact load curve in ball impact test in relation to thermal aging, Microelectronics Reliability 53(12) (2013) 2005-2011.

[7] T. Matsumoto, K. Nogi, Wetting in soldering and microelectronics, Annu. Rev. Mater. Res. 38 (2008) 251-273.

[8] K. Suganuma, K. Niihara, T. Shoutoku, Y. Nakamura, Wetting and interface microstructure between Sn–Zn binary alloys and Cu, Journal of Materials Research 13(10) (1998) 2859-2865.

[9] K. Tu, T. Lee, J. Jang, L. Li, D. Frear, K. Zeng, J. Kivilahti, Wetting reaction versus solid state aging of eutectic SnPb on Cu, Journal of Applied Physics 89(9) (2001) 4843-4849.

[10] N. Zhao, X. Pan, D. Yu, H. Ma, L. Wang, Viscosity and surface tension of liquid Sn-Cu lead-free solders, Journal of electronic materials 38(6) (2009) 828-833.

[11] C. Liu, H. Kim, K. Tu, P. Totta, Dewetting of molten Sn on Au/Cu/Cr thin-film metallization, Applied physics letters 69(26) (1996) 4014-4016.

[12] F. Conti, A. Hanss, O. Mokhtari, S.K. Bhogaraju, G. Elger, Formation of tin-based crystals from a SnAgCu alloy under formic acid vapor, New Journal of Chemistry 42(23) (2018) 19232-19236.

[13] O. Mokhtari, F. Conti, S.K. Bhogaraju, M. Meier, H. Schweigart, U. Tetzlaff, G. Elger, Characterization of tin-oxides and tin-formate crystals obtained from SnAgCu solder alloy under formic acid vapor, New Journal of Chemistry (2019).

[14] S. He, R. Gao, J. Li, Y.-A. Shen, H. Nishikawa, In-situ observation of fluxless soldering of Sn-3.0 Ag-0.5 Cu/Cu under a formic acid atmosphere, Materials Chemistry and Physics (2019) 122309.

[15] J.-W. Yoon, S.-B. Jung, Interfacial reactions between Sn–0.4 Cu solder and Cu substrate with or without ENIG plating layer during reflow reaction, Journal of alloys and compounds 396(1-2) (2005) 122-127.

[16] J.-W. Yoon, B.-I. Noh, S.-B. Jung, Effects of third element and surface finish on

interfacial reactions of Sn–Ag–xCu (or Ni)/(Cu or ENIG) solder joints, Journal of Alloys and compounds 506(1) (2010) 331-337.

[17] G. Kumar, K.N. Prabhu, Review of non-reactive and reactive wetting of liquids on surfaces, Advances in colloid and interface science 133(2) (2007) 61-89.

[18] Q. Lin, F. Li, J. Wang, Wetting of Sn/Cu and Sn/Cu-Sn IMCs at 623–723K, Journal of Alloys and Compounds 767 (2018) 877-882.

[19] N. Eustathopoulos, Progress in understanding and modeling reactive wetting of metals on ceramics, Current Opinion in Solid State and Materials Science 9(4-5) (2005) 152-160.

[20] P. Kim, K. Tu, Morphology of wetting reaction of eutectic SnPb solder on Au foils, Journal of Applied Physics 80(7) (1996) 3822-3827.

[21] H. Wang, H. Zhao, D.P. Sekulic, Y. Qian, A comparative study of reactive wetting of lead and lead-free solders on Cu and (Cu 6 Sn 5/Cu 3 Sn)/Cu substrates, Journal of Electronic Materials 37(10) (2008) 1640-1647.

[22] O. Liashenko, F. Hodaj, Wetting and spreading kinetics of liquid Sn on Ag and Ag3Sn substrates, Scripta Materialia 127 (2017) 24-28.

[23] B. He, J. Lee, N.A. Patankar, Contact angle hysteresis on rough hydrophobic surfaces, Colloids and Surfaces A: Physicochemical and Engineering Aspects 248(1-3) (2004) 101-104.

[24] Y. Chen, B. He, J. Lee, N.A. Patankar, Anisotropy in the wetting of rough surfaces, Journal of colloid and interface science 281(2) (2005) 458-464.

[25] D. Quéré, Rough ideas on wetting, Physica A: Statistical Mechanics and its Applications 313(1-2) (2002) 32-46.

[26] H. Nakae, R. Inui, Y. Hirata, H. Saito, Effects of surface roughness on wettability, Acta materialia 46(7) (1998) 2313-2318.

[27] K. Kim, S. Huh, K. Suganuma, Effects of intermetallic compounds on properties of Sn–Ag–Cu lead-free soldered joints, Journal of Alloys and compounds 352(1-2) (2003) 226-236.

[28] D. Kim, J.J. Pak, Micro void growth in NiSnP layer between (Cu, Ni) 6 Sn 5 intermetallic compound and Ni 3 P by higher reflow temperature and multiple reflow, Journal of Materials Science: Materials in Electronics 21(12) (2010) 1337-1345.

[29] H.R. Kotadia, P.D. Howes, S.H. Mannan, A review: on the development of low melting temperature Pb-free solders, Microelectronics Reliability 54(6-7) (2014) 1253-1273.

[30] K. Hung, Y. Chan, C. Tang, H. Ong, Correlation between Ni 3 Sn 4 intermetallics and Ni 3 P due to solder reaction-assisted crystallization of electroless Ni–P metallization in advanced packages, Journal of Materials Research 15(11) (2000) 2534-2539.

[31] K. Hung, Y. Chan, C. Tang, Metallurgical reaction and mechanical strength of electroless Ni-P solder joints for advanced packaging applications, Journal of Materials Science: Materials in Electronics 11(8) (2000) 587-593.

[32] W. Zhu, L. Xu, J.H. Pang, X. Zhang, E. Poh, Y. Sun, A.Y. Sun, C. Wang, H. Tan, Drop reliability study of PBGA assemblies with SAC305, SAC105 and SAC105-Ni solder ball on Cu-OSP and ENIG surface finish, 2008 58th Electronic Components and Technology Conference, IEEE, 2008, pp. 1667-1672.

[33] C. Ho, Y. Lin, S. Wang, Sn–Ag–Cu solder reaction with Au/Pd/Ni (P) and Au/Pd (P)/Ni (P) platings, Thin Solid Films 544 (2013) 551-556.

Chapter 6

Conclusion

6.1 Summary

In this dissertation, a fluxless soldering process under a formic acid (FA) atmosphere using Sn-3.0Ag-0.5Cu solder (SAC305) was investigated for electronic packaging, as a low cost, eco-friendly, and reliable substitution of soldering process using rosin mildly activated (RMA) flux. The motivation was to study the process parameters of fluxless soldering under a FA atmosphere and the mechanism of the FA atmosphere in the fluxless soldering process. The author focused on the wetting behavior of lead-free solder under a FA atmosphere, effect of FA atmosphere on the interfacial reaction between solder and different substrates, and long term reliability of solder bumps after fluxless soldering.

In **Chapter 1**, a brief introduction of electronic packaging, lead-free soldering

process, the role of flux in soldering, and the problems of flux were given. Consequently, fluxless soldering processes have a high market potential. Then, various fluxless soldering technologies were listed. Among the fluxless soldering processes, the soldering under a FA atmosphere was a promising process because of the low cost and effective reduction of Sn-base solder.

In **Chapter 2**, a successful fluxless soldering process using SAC305 solder and Cu substrate under a FA atmosphere was achieved. The effects of heating processes on the wettability of SAC305 solders on Cu pads and the interfacial reaction of SAC305 solder bumps on Cu substrates formed under a FA atmosphere were investigated. The results showed under the same heating conditions, the contact angle of the FA solder was similar to that of the RMA solder, whereas the spreading rate was much lower. The difference in the spreading rate may be caused by the continuous reduction of the Cu oxide film by a formic acid atmosphere. The wettability of the FA solder became better as the peak heating temperature increased. Although the substrate remained clean when using the RMA solder, some residues were found around the FA solders after reflowing. The residues are believed to result from the precipitation of Sn formate. The FA atmosphere barely changes the interfacial reaction between the Cu substrate and SAC305 solder. However, some pores were observed near the IMC layers in the FA solders. These pores were caused by the generation of gas from the decomposition of Cu formate during the soldering process. The number of pores decreased significantly when the peak temperature reached 290 °C.

In **Chapter 3**, the effect of pores discovered in the study of **Chapter 2** on long-term reliability was investigated. The impact reliability of soldered bumps using FA was explored. The morphology of the IMC layers in samples soldered using the FA atmosphere was similar to those soldered with the flux, after soldering and after thermal aging. After thermal aging, some pores were also observed near the IMC layers in the samples soldered in the FA atmosphere. The impact strengths of the as-reflowed and thermally aged solder bumps were tested by impact tests. The fluxless solder bumps,

using the FA atmosphere, have impact strengths similar to the solder bumps obtained using the liquid flux. When solder bumps reflowed by using the FA atmosphere, the failure occurs predominantly in the bulk solder and partly inside the IMC layer. However, when using the liquid flux, the fracture position was predominantly inside the IMC layer and partly in the bulk solder. After 1008 h thermal aging, the fracture occurs partly at the Cu_6Sn_5 layer and partly at the Cu_3Sn layer for both cases. In summary, the pores near the IMC layer barely affect the impact strength after soldering and after thermal aging.

In **Chapter 4**, the thermal effect on Sn steaming phenomenon, produced by series peak temperature and different holding times under a FA atmosphere, was investigated. Some residue containing Sn was found in the study of **Chapter 2**. The residue may lead to an increase in leakage current and affect electrical performance. The residue is believed to result from the Sn steaming phenomenon under a FA atmosphere. The results showed the Sn steaming phenomenon results from the formation of Sn formate under a FA atmosphere. When the temperature below 170 °C, Sn steaming phenomenon was not serious. When the temperature reached 210 °C and prolonged to 290 °C, the Sn steaming phenomenon was observed certainly. The Sn steaming phenomenon under a FA atmosphere became more serious with the higher temperature and longer heating time. Based on the thermal effect on the Sn steaming phenomenon under a FA atmosphere in this study, the process of heating time within 60 s is suggested for fluxless soldering using SAC solder.

In **Chapter 5**, based on the results in **Chapter 2**, in order to improve the spreading rate of wetting of SAC305 solder, the substrate with ENIG finish was used. The wettability, interfacial reactions, and impact strength of FA-exposed solder on the ENIG substrate were examined, and the obtained results were compared with the parameters of RMA reflow soldering. As indicated by in-situ observations, the spreading area of the solder exposed to FA atmosphere was 10% greater than that of the solder containing RMA flux, which demonstrated the enhancement of the solder's wettability by FA. The

latter was caused by the solder spreading on the interfacial layer of $(Cu, Ni)_6Sn_5$ IMC formed by Sn residues on the ENIG substrate via Sn formate steaming before the solder ball melted during FA reflow soldering. The IMC growth rate of FA-exposed solder was nearly identical to that of RMA solder, and their interfacial reactions were very similar. Moreover, the impact strength of FA-exposed solder (107 MPa) was approximately equal to that of RMA solder (99 MPa) due to the same interfacial reactions. The decrease in the impact strength observed after 168, 504, and 1008 h of the thermal aging at 150 °C was induced by the growth of the brittle IMC layer at the interface with a similar pattern.

Consequently, the RMA reflow soldering can be potentially replaced with FA reflow soldering during electronic packaging.

6.2 Environmental assessment on fluxless soldering under a FA atmosphere

The fluxless soldering process was considered environmentally friendly for one reason is considering the cleaning process. After the soldering process, the flux residues must be cleaned from the substrate after soldering, because they are corrosive and may cause long-term reliability problems[1]. The residues of no rosin flux used halogenated solvents, such as chlorofluorocarbons (CFCs). The CFCs is believed one major contribution to the depletion of ozone, as discussed in **Section 1.3.2**. In order to decrease the impact on the environment, water-soluble fluxes are developed using for soldering PCBs in electronics factories[2, 3]. However, the cleaning process is also necessary during soldering using water-soluble flux. This cleaning process would consume water, obviously. Because of the cleaning process, the cost of the soldering process using flux is higher, absolutely.

Although some Sn residue caused by Sn steaming phenomenon was observed during a fluxless soldering process under a FA atmosphere, this phenomenon was unobservable if the heating time reduced within 60 s, as we discussed in **Chapter 3**. And within the

modern soldering process using for electronic packaging, the heating time is also hold within 30 s[4, 5]. We believe the residue is scarcely detected in this situation.

The compositions of flux also have the impact on the health of creatures. There are many reports about occupational diseases among workers in the electronics industry from soldering flux[6-10]. Hence, in order to protect the workers and the environment in many electronics factories, soldering is developed to more automatic and seal. The FA, as one of the organic acids, also harms to health as a respiratory and eye irritant[11-13]. A reversible pulmonary chemical injury by formic acid inhalation was reported[14]. However, with the developing of more automatic soldering systems using for electronic packaging, the risk of formic acid inhalation becomes lower, and the handling of nitrogen-enriched with formic acid is feasible used in electronic manufacturing now[4, 15].

The qualitative environmental assessment on the soldering process using flux and fluxless soldering under a FA atmosphere, in terms of energy consumption, cost, environmental impact, and disease risk are summarized in **Table 6.1**. The soldering process using Sn-Ag-Cu solder shows no advantages in terms of economic perspective. However, the usage of Sn-Pb solder should be eliminated in order to response the environmental directive, as mentioned in **Chapter 1**. In summary, to our best knowledge, only one minor issue needs to be considered of fluxless soldering process under a FA atmosphere is the irritation to respiratory and eye. And it is not a problem in modern soldering systems.

6.3 Future work

6.3.1 Effect of FA on joint long-term reliability

In **Chapter 3**, it was shown the fluxless solder bumps, using the FA atmosphere, have impact strengths similar to the solder bumps obtained using the flux. However, the fracture mode was different: when solder bumps reflowed by using the FA atmosphere, the failure occurs predominantly in the bulk solder and partly inside the IMC layer;

when using the liquid flux, the fracture position was predominantly inside the IMC layer and partly in the bulk solder. Besides, the strength-displacement curve was analyzed, Although the curves of two cases were similar before reaching the maximum strengths, the curve of the sample soldered by the liquid flux dropped faster than that soldered in FA atmosphere. It seems that the difference in the curves is caused by the afore-mentioned different fracture positions of two cases. However, the effect of pores on the strength-displacement curve in the impact test is still unclear. And in this thesis, only the thermal aging in oil bath was used to evaluate the long-term reliability, the thermal cycle test is also a common method to evaluate the resistance to thermal shock of electronics devices. Therefore, for the practical application, the reliability of a more realistic joint fabricated with the fluxless soldering process should be further verified by long term reliability test.

6.3.2 improvement of a suitable fluxless soldering process without Sn steaming for realistic application

In **Chapter 4**, we discussed the thermal effect on Sn steaming phenomenon under a FA atmosphere. The results showed the severity of Sn steaming depended on the peak temperature and holding time of peak temperature during the fluxless soldering process. However, the pathway of Sn steaming is still unclear. For example, the sequence of the Sn formate evaporation and decomposition under a FA atmosphere. It is important to design a great process for realistic applications and to reduce the risk of short circuits. In order to investigate the pathway of the Sn steaming phenomenon, more chemical analysis is needed.

6.3.3 Improvement of wetting rate of solder on Cu substrate under FA atmosphere

In **Chapter 2**, the wetting behavior of SAC solder on Cu substrate under FA atmosphere and using RMA flux was compared. The results indicated under the same heating conditions, the contact angle of the FA solder was similar to that of the RMA

solder, whereas the spreading rate was much lower. We considered the difference in spreading rate may be caused by the continuous reduction of the Cu oxide film by a FA atmosphere. At that time, we ignored the effect of FA amount on reduction rate of Cu oxides. As we know, the reaction also relates to the amounts of reactants. Hence, the dynamic amount of FA should also be considered as one parameter of fluxless soldering process.

Table 6.1 *Environmental assessment on the soldering process using flux and fluxless soldering under a FA atmosphere.*

	Soldering using fluxes	**Fluxless soldering (under a FA atmosphere)**
Energy consumption (Process temperature)	△ Process temperature higher than Sn-Pb solder[16]	△ Process temperature higher than Sn-Pb solder[16]
Resource consumption	△ Consumption of water (water used in the cleaning process)	○ No cleaning process
Environmental impact	× Ozone depletion (CFCs used in cleaning process) [17-21]	○ No cleaning process
Cost	△ Need cleaning process[22-25]	○ No cleaning process
Disease risk	× Compositions detrimental to creatures: allergy, dermatitis, irritation of respiratory, carcinogenic in animals, etc., (aminoethyl ethanolamine, colophony, hydrazine, etc., in fluxes)[6, 8-10, 26-32]	△ Respiratory and eye irritant (formic acid)[12, 13]

○ Good △ Not bad × Bad

Reference

[1] W. Lin, Y. Lee, Study of fluxless soldering using formic acid vapor, IEEE transactions on Advanced Packaging 22(4) (1999) 592-601.

[2] W.J. Ready, L.J. Turbini, A comparison of hourly versus daily testing methods for evaluating the reliability of water soluble fluxes, IEEE transactions on advanced packaging 23(2) (2000) 285-292.

[3] J.A. Jachim, G.B. Freeman, L.J. Turbini, Use of surface insulation resistance and contact angle measurements to characterize the interactions of three water soluble fluxes with FR-4 substrates, IEEE Transactions on Components, Packaging, and Manufacturing Technology: Part B 20(4) (1997) 443-451.

[4] N. Ozawa, T. Okubo, J. Matsuda, T. Sakai, Sn-and Cu-oxide reduction by formic acid and its application to power module soldering, 2018 IEEE 30th International Symposium on Power Semiconductor Devices and ICs (ISPSD), IEEE, 2018, pp. 248-251.

[5] M. Samson, V. Oberson, I. Paquin, C. Fortin, J.-C. Raymond, C. Bureau, M. Barnes, X. Zhao, D. Wright, Fluxless chip join process using formic acid atmosphere in a continuous mass reflow furnace, Electronic Components and Technology Conference (ECTC), 2016 IEEE 66th, IEEE, 2016, pp. 574-579.

[6] P. Burge, M. Harries, I. O'brien, J. Pepy, Respiratory disease in workers exposed to solder flux fumes containing colophony (pine resin), Clinical & Experimental Allergy 8(1) (1978) 1-14.

[7] D. Koh, I. Foulds, T. Aw, Dermatological hazards in the electronics industry, Contact Dermatitis 22(1) (1990) 1-7.

[8] H.-H. Tan, M.T.-L. Chan, C.-L. Goh, Occupational skin disease in workers from the electronics industry in Singapore, American Journal of Contact Dermatitis 8(4) (1997) 210-214.

[9] T. Keira, Y. Aizawa, H. Karube, M. Niituya, S. Shinohara, A. Kuwashima, H. HARADA, T. TAKATA, Adverse effects of colophony, Industrial health 35(1) (1997)

1-7.

[10] J.K. Morris, N.J. Wald, A.L. Springett, Occupational exposure to hydrazine and subsequent risk of lung cancer: 50-year follow-up, PloS one 10(9) (2015) e0138884.

[11] A. Hanss, G. Elger, Residual free solder process for fluxless solder pastes, Soldering & Surface Mount Technology 30(2) (2018) 118-128.

[12] G.D. Nielsen, Sensory irritation of vapours of formic, acetic, propionic and butyric acid, Regulatory Toxicology and Pharmacology 99 (2018) 89-97.

[13] P. Saavalainen, E. Turpeinen, L. Omodara, S. Kabra, K. Oravisjärvi, G.D. Yadav, R.L. Keiski, E. Pongrácz, Developing and testing a tool for sustainability assessment in an early process design phase–Case study of formic acid production by conventional and carbon dioxide-based routes, Journal of cleaner production 168 (2017) 1636-1651.

[14] J.A. Yelon, R.L. Simpson, O. Gudjonsson, Formic acid inhalation injury: a case report, The Journal of burn care & rehabilitation 17(3) (1996) 241-242.

[15] W. Yang, C. Zhou, J. Zhou, Y. Lu, Y. Lu, T. Suga, Cu film surface reduction through formic acid vapor/solution for 3-D interconnection, 2018 19th International Conference on Electronic Packaging Technology (ICEPT), IEEE, 2018, pp. 1378-1381.

[16] O. Deubzer, H. Griese, T. Suga, Lead-free soldering-future aspects of toxicity, energy and resource consumption, Proceedings Second International Symposium on Environmentally Conscious Design and Inverse Manufacturing, IEEE, 2001, pp. 952-957.

[17] P. Newman, L. Oman, A. Douglass, E. Fleming, S. Frith, M. Hurwitz, S. Kawa, C. Jackman, N. Krotkov, E. Nash, What would have happened to the ozone layer if chlorofluorocarbons (CFCs) had not been regulated?, Atmospheric Chemistry and Physics 9(6) (2009) 2113-2128.

[18] Q.-B. Lu, L. Sanche, Effects of cosmic rays on atmospheric chlorofluorocarbon dissociation and ozone depletion, Physical Review Letters 87(7) (2001) 078501.

[19] P.M. Haas, Banning chlorofluorocarbons: epistemic community efforts to protect stratospheric ozone, International organization 46(1) (1992) 187-224.

[20] F.S. Rowland, Stratospheric ozone in the 21st century: the chlorofluorocarbon problem, Environmental science & technology 25(4) (1991) 622-628.

[21] F.S. Rowland, Chlorofluorocarbons and the depletion of stratospheric ozone, American Scientist 77(1) (1989) 36-45.

[22] D. Bušek, K. Dušek, D. Růžička, M. Plaček, P. Mach, J. Urbánek, J. Starý, Flux effect on void quantity and size in soldered joints, Microelectronics Reliability 60 (2016) 135-140.

[23] K.S. Hansen, M.S. Jellesen, P. Moller, P.J.S. Westermann, R. Ambat, Effect of solder flux residues on corrosion of electronics, 2009 Annual Reliability and Maintainability Symposium, IEEE, 2009, pp. 502-508.

[24] V. Lopez, A. Kennedy, Flux-assisted wetting and spreading of Al on TiC, Journal of colloid and interface science 298(1) (2006) 356-362.

[25] D. Peebles, H. Peebles, J. Ohlhausen, Kinetics of the isothermal spreading of tin on the air-passivated copper surface in the absence of a fluxing agent, Colloids and Surfaces A: Physicochemical and Engineering Aspects 144(1-3) (1998) 89-114.

[26] C. Foti, D. Bonamonte, G. Mascolo, G. Tiravanti, L. Rigano, G. Angelini, Aminoethylethanolamine: a new allergen in cosmetics?, Contact Dermatitis 45(3) (2001) 129-133.

[27] T. Mathias, Contact Allergy to Colophony in Soldering Flux, Journal of Occupational and Environmental Medicine 25(12) (1983) 902.

[28] I. Fawcett, A. Taylor, J. Pepys, Asthma due to inhaled chemical agents--fumes from'Multicore'soldering flux and colophony resin, Clinical Allergy 6(6) (1976) 577-585.

[29] H. Akhter, J. Murshed, M.A. Rashed, Y. Oshima, Y. Nagao, M.M. Rahman, A.M. Asiri, M. Hasnat, M.N. Uddin, I.A. Siddiquey, Fabrication of hydrazine sensor based on silica-coated Fe2O3 magnetic nanoparticles prepared by a rapid microwave irradiation method, Journal of Alloys and Compounds 698 (2017) 921-929.

[30] P. Wang, T. Yan, Q. Ma, D. Hu, L. Wang, Preparation of hydrazine-modified

CMC/Fe3O4 hybrid magnetic particles for adsorption of Reactive Blue 21 from water, Desalination and Water Treatment 57(32) (2016) 14986-14996.

[31] K. Yokota, T. Minami, H. Michitsuji, T. Fujio, S. Yamada, Occupational dermatitis from soldering flux, Industrial health 42(3) (2004) 383-384.

[32] C. Goh, Occupational dermatitis from soldering flux among workers in the electronics industry, Contact Dermatitis 13(2) (1985) 85-90.

Research achievement

I List of publication

i Peer-reviewed journal articles

- **He, S.**, Gao, R., Shen, Y-A., Li, J. and Nishikawa, H., Wettability, Interfacial reactions, and Impact Strength of Sn-3.0Ag-0.5Cu Solder/ENIG Substrate Used for Fluxless Soldering under Formic Acid Atmosphere. *Journal of Materials Science (2020),* Volume 55, Issue 7, pp 3107–3117. Doi:10.1007/s10853-019-04153-9
- **He, S**. and Nishikawa, H., Effect of Thermal Aging on the Impact Strength of Soldered Bumps under Formic acid Atmosphere. *Quarterly Journal of The Japan Welding Society 35(2017),* pp.127-131.
- **He, S.**, Gao, R., Li, J., Shen, Y-A. and Nishikawa, H., In-situ observation of fluxless soldering of Sn-3.0Ag-0.5Cu/Cu under a formic acid atmosphere. *Materials chemistry and Physics 239 (2020)122309.* Doi:10.1016/j.matchemphys.2019.122309

- Zhou, S., **He, S**. and Nishikawa, H., Effect of Zn addition on interfacial reactions and mechanical properties between eutectic Sn58Bi solder and ENIG substrate. *Journal of Nanoscience and Nanotechnology, 20 (1), (2020),* pp.106-112
- Jin, Z., Shen, Y-A., **He, S.**, Zhou, S., Chan, Y, C. and Nishikawa, H. Novel Polarity Effect on Intermetallic Compound Thickness Changes during Electromigration in Cu/Sn- 3.0Ag - 0.5Cu/Cu Solder Joints. *Journal of Applied Physics (Accepted).*
- Shen, Y-A., Lin, C.M., Li, J., **He, S.** and Nishikawa, H., 2019. Effect of FeCoNiCrCu 0.5 High-entropy-alloy Substrate on Sn Grain Size in Sn-3.0 Ag-0.5 Cu Solder. *Scientific Reports 9(1) (2019)*, pp.3658.
- Gao, R., **He, S.**, Shen, Y-A and Nishikawa, H., Effect of Substrates on Fracture Mechanism and Process Optimization of Oxidation–Reduction Bonding with Copper Microparticles. *Journal of Electronic Materials: Materials 48(4) (2019)*, pp.2263-2271.
- Liu, X., **He, S**. and Nishikawa, H., Low temperature solid-state bonding using Sn-coated Cu particles for high temperature die attach. *Journal of Alloys and Compounds 695 (2017),* pp.2165-2172.
- Liu, X., **He, S**. and Nishikawa, H., Thermally stable Cu3Sn/Cu composite joint for high-temperature power device. *Scripta Materialia*, *110 (2016)*, pp.101-104.
- Nishikawa, H., Alhazaa, A.N., **He, S.,** Almajid, A.A and Soliman, M.S., Interfacial reaction between Sn-Ag-Cu-Mg solder and ENIG substrate. *Key Engineering Materials 701 (2016)*, pp.216-219.
- Gao, R., **He, S.**, Li, J., Shen, Y-A and Nishikawa, H., Mechanism of reliable all-cu bonding using pressure-less sintering of pre-oxidized cu microparticle under formic acid atmosphere. (In preparation for *ACS applied materials & interfaces).*
- **He, S.**, Liu, X., Kim, M-S., Gao, R., and Nishikawa, H., Surface modification of microscale Cu particles by an oxidation-reduction process for low-temperature sintering bonding. (In preparation for *Acta Materialia).*

- **He, S.**, HUO, F., Gao, R., Li, J., Shen, Y-A., HUANG, S., and Nishikawa, H., Thermal effect on Sn steaming phenomenon on Cu under formic acid atmosphere. (In preparation for *Scripta Materialia).*

ii Conference Proceedings

- **He, S.,** Gao, R., Li, J. and Nishikawa, H., Sn steaming phenomenon under formic acid atmosphere. In *The 5th International Symposium on Visualization in Joining & Welding Science through Advanced Measurements and Simulation (Visual-JW2019), 2019*
- **He, S.** and Nishikawa, H., Effect of substrate metallization on the impact strength of Sn-Ag-Cu solder bumps fabricated in a formic acid atmosphere. In *International Conference on Electronic Packaging (ICEP), 2017* (pp. 381-385). IEEE.
- **He, S.** and Nishikawa, H., Effect of Thermal Aging on the Impact Strength of Soldered Bumps under formic acid atmosphere. In *The international Symposium on visualization in Joining & Welding Science through Advanced Measurements and Simulation (Visual-JW2016), 2016* (pp. 27-28).
- Liu, X., **He, S**. and Nishikawa, H. Low temperature bonding using microscale Cu particles coated with thin Sn layers at 200° C. In *International Conference on Electronic Packaging (ICEP), 2016* (pp. 306-309). IEEE.
- Zhang, Y., **He, S.** and Nishikawa, H. Impact strength of Sn-Ag-Cu/Cu solder bumps formed by an induction heating method. In *2017 12th International Microsystems, Packaging, Assembly and Circuits Technology Conference (IMPACT), 2017* (pp. 50-53). IEEE.
- Nishikawa, H., Liu, X. and **He, S.** Effect of bonding conditions on shear strength of joints at 200° C using Sn-coated Cu particle. In *2017 21st European Microelectronics and Packaging Conference (EMPC), 2017* (pp. 1-4). IEEE.
- Nishikawa, H., Liu, X. and **He, S.** Effect of isothermal aging at 250° C on shear strength of joints using Sn-Coated Cu particle paste for high-temperature application. In

proceeding of iMAPS International Conference on High Temperature Electronics Network (HiTEN2017), 2017 (pp.202-206) IEEE.

iii Domestic conference proceedings

- 何 思亮, 西川 宏. ギ酸雰囲気を用いた無電解 Ni/Au めっき上へはんだバンプ形成. 第 23 回エレクトロニクスにおけるマイクロ接合・実装技術シンポジウム論文集, 2017
- 何 思亮, 西川 宏. リフローはんだ付におけるフラックスとギ酸雰囲気の比較. 第 26 回マイクロエレクトロニクスシンポジウム論文集, 2016.
- 何 思亮, 西川 宏. ギ酸雰囲気を用いたはんだ付でのボイド形成及ぼす加熱条件の影響. 溶接学会平成２８年度春季全国大会, 2016.
- 何 思亮, 西川 宏, 菊池 大地, 上島 稔. はんだ濡れ性および界面反応におけるギ酸雰囲気の影響. 溶接学会平成２７年度秋季全国大会, 2015.

II List of conference

- *(Poster) The 5th International Symposium on Visualization in Joining & Welding Science through Advanced Measurements and Simulation (Visual-JW2019), 2019, Osaka, Japan*
- *(Poster) 2019 Taiwan-Japan Workshop on Electronic-Interconnection III, 2019, Taichung, Taiwan, China*
- *(Oral) International Conference on Electronic Packaging (ICEP-IAAC- IEEE), 2017, Tendo, Yamagata, Japan*
- *(Oral) 23rd Symposium on "Micro-joining and Mounting Technology in Electronics", 2017, Yokohama, Kanagawa, Japan*
- *(Oral) The 4th international Symposium on visualization in Joining & Welding Science through Advanced Measurements and Simulation (Visual-JW2016), 2016, Osaka, Japan*
- *(Oral) The 26th Microelectronics Symposium, 2016, Nagoya, Japan*
- *(Oral) National Meeting of Japan Welding Society, 2016, Osaka, Japan*
- *(Oral) National Meeting of Japan Welding Society, 2015, Sapporo, Hokkaido, Japan*

Acknowledge

I would like to express my deepest gratitude to all those who helped me during my doctoral course study.

Firstly, I would like to give my sincere gratitude to my supervisor, Professor Hiroshi Nishikawa, for offering me the opportunity to do research and providing me invaluable guidance throughout the research and writing this thesis. Prof. Nishikawa has offered me many valuable suggestions in the academic studies. Truly, without his painstaking efforts in revising and polishing my drafts, the completion of this thesis would not have been possible. I do appreciate his patience, encouragement, and professional instruction during my doctoral study. His dynamism, vison, kindness and motivation have deeply inspired me.

Besides my supervisor, I would like to thank the rest of my thesis committee: Assoc. Prof. Hiraoki Muta and Prof. Soshu Kirihara, for their insightful comments and encouragement, but also for the hard question which incented me to widen my research from various perspectives. My thanks also go to staff of Joining and Welding Research Institute, Mr. Kenji Asano, Mr. Takuya Ogura, and staff of SANYOSEIKO., LTD (Japan), Mr. Masashi Nishimuro for technical supports.

I thank members and alumni of Nishikawa Lab, especially, Ms. Sachiko Sakata, Dr. Omid Mokhtari, Dr. Myonghoon Roh, Dr. Min-Su Kim, Dr. Yu-An Shen, Dr. Xiangdong Liu, Dr. Shiqi Zhou, Dr. Sanghun Jin, Mr. Runhua Gao, Mr. Zhi Jin, Mr. Fupeng Huo, Mr. Jiahui Li, Mr. Sijie Huang and Mr. Laizhou Zhou. Without their support and advices, it would be impossible to finish this research.

I am grateful to Ms. Li Peng for her invaluable support, patience, and love.

Last but not the least, I would like to thank my parents for inspiring me to realize my own potential, for supporting me spiritually throughout my life. Without them, I would not pursue my dream.